A Teacher's Guide To Classroom Demonstrations in Transport Phenomena

David T. Leighton, Jr.

Department of Chemical & Biomolecular Engineering

University of Notre Dame

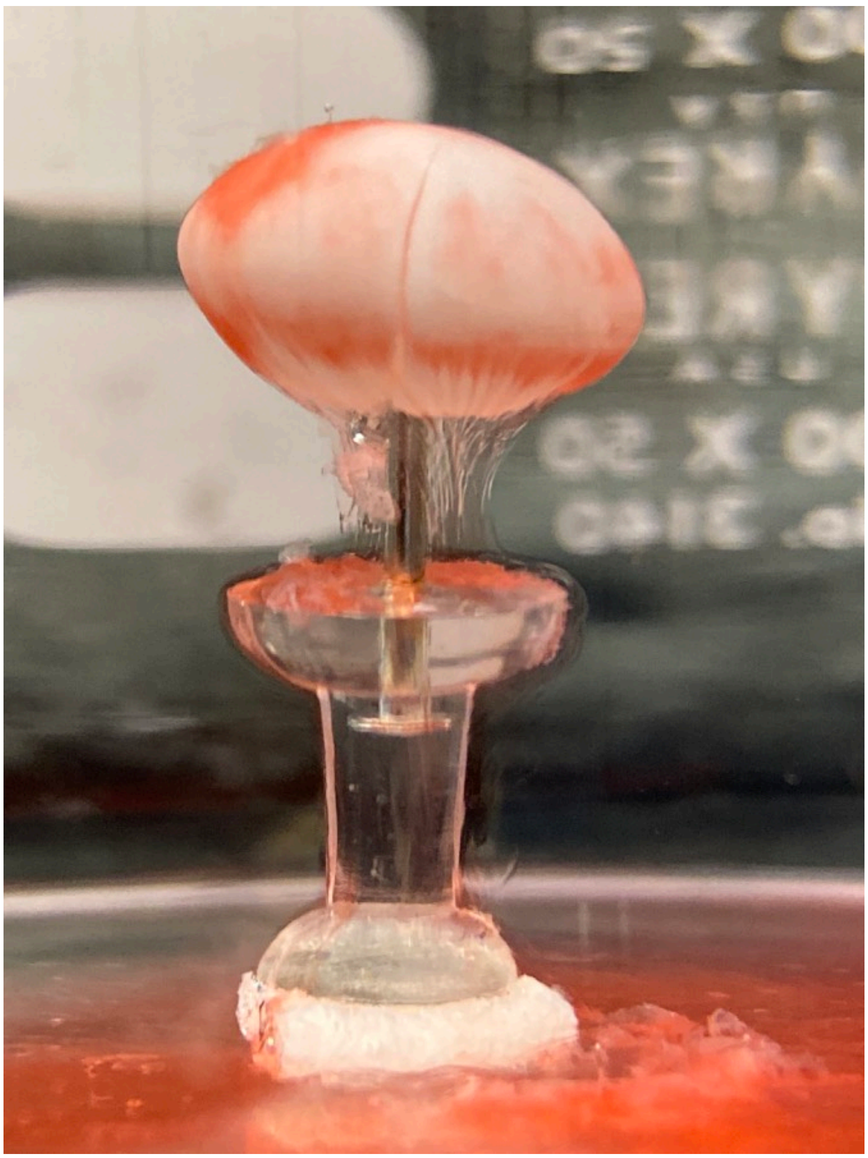

Published by **Diffusive Press**
First Edition
ISBN: Assigned by Amazon KDP

For permissions or inquiries, contact: info@diffusivepress.org

Acknowledgements

First, I would like to acknowledge the contribution of the thousands of students it has been my privilege to introduce to the fascinating world of transport over my four decades at Notre Dame. Student led demonstrations added immeasurably to the class: everything from antibubbles (which I hadn't previously known of) to the "meter high raging tornado of fire" (for which they had to get written pre-approval from Risk Management) and a Blue Man Group Drumbone (with resonance equations presented in blue face and mime). Their inquisitiveness and desire to master this difficult subject has always been an inspiration to me.

In addition to undergraduate students, of course, the help of my graduate assistants and graduate students over the years has been invaluable. An early version of this guide was initiated many years ago by my grad students so that we would have "materials on hand" for the demonstrations when they came around each year and has been periodically updated as new ones were added.

These demonstrations are, of course, not completely original to me. While a few arose directly from our research, many more came from the research of colleagues around the world or other historical or literature sources and are simply repackaged here for ease of use in a classroom setting.

Finally, I would like to acknowledge the contribution of the early readers of this guide whose enthusiasm has helped motivate me to put this document over the finish line. In particular, the enthusiastic reception and helpful comments of my first external reader Howard Stone (and who adopted several of the demonstrations for his course at Princeton) was very encouraging and convinced me of the value of this project.

A Teacher's Guide To Classroom Demonstrations in Transport Phenomena

D. T. Leighton

Department of Chemical & Biomolecular Engineering

University of Notre Dame

Introduction

At Notre Dame it has become a tradition to perform in-class demonstrations of phenomena related to transport. While innumerable YouTube videos of such demonstrations can be found on the web, there is something different about a physical demonstration that is actually done "in person" in the classroom itself, particularly when students can be volunteered to actively participate. This is somewhat akin to the difference between watching a movie and attending a live theatre performance: the "production values" of the movie are generally much higher, but the live performance is special in its own way. In my courses (Transport I focusing on Fluid Mechanics and Transport II focusing on Heat & Mass Transport) I conduct the demonstrations for the first half of the semester and students do the demonstrations for the second half. In the latter case, students are divided up into groups and propose their demonstration topic sufficiently far in advance so that a safety review and "reality check" can be performed. Students have generally found the demonstration process to be an excellent learning experience, and a lot of fun too.

In this guide I will describe demonstrations which are relatively easy to prepare using equipment which is (usually) readily found in the laboratory or which can be easily constructed, borrowed, or otherwise acquired. We also do other demonstrations which involve more specialized equipment (e.g., the "Singing Water Bowl", Taylor-Couette vortices, etc.), and these are not included in this list. There are, of course, far more possible demonstrations than could be included in this guide, however hopefully the three dozen included here will serve as a starting point for creating demonstrations tailored to specific course needs. In each case I try to describe the demonstration in sufficient detail that it should be possible to construct the demo. The demonstrations are designed to take about 10 to 15 minutes of class time, maximum, so they provide a nice break in a longer 75 minute class period.

Most of the demonstrations are tied to the subject of the lecture and are designed to illustrate concepts, equations, and derivations that are otherwise rather "dry". For those which are tied into class, I have provided some notes and derivations relevant to the demo. I have also provided references for further information. For many of these references I have provided the DOI link for convenience which should remain stable. For a few cases I have provided a general web link. These are less stable, of course, however searching on the "Way Back Machine" (web.archive.org) should yield the relevant page if the cited version has vanished. Some of the key references are in German, however ChatGPT is actually quite good at translating the text to English (less so for the equations, however it does try).

The audience for this guide is primarily faculty instructing students in transport at the undergraduate level, however many of the examples are suitable for secondary school physics classes (e.g., Magnus lift and the Coanda effect) while others are significantly more advanced (e.g., Jeffery Orbits and Moffatt eddies). In the latter cases the phenomena can still be demonstrated (Moffatt eddies are rather pretty), however the detailed mathematics behind the effects may not be appropriate for most undergraduates.

One issue, particularly for smaller and more intricate demonstrations, is the ability to project what is going on to a large screen. At Notre Dame all classrooms are equipped with a computer and a projection system, and have a designated "zoom room" for the class (a legacy of the remote teaching required during the pandemic). In my class I take advantage of this by "zooming in" with an iPod (or iPhone) set to its back camera and "pin" the image to the first screen. The iPod is usually held with a clamp to visualize the phenomenon being demonstrated, although it can be moved about as necessary. It is easy to switch the projection from the demonstration to other material (such as notes or a web page) on the classroom computer.

A second issue is illumination. For many of the demonstrations room lighting is sufficient, however for some a "light box" is useful. In my case the box is constructed by encasing a small fluorescent light in a box with an interior painted white. The top of the box is glass with a thin sheet of white plastic underneath to provide uniform light intensity. Now, however, LED light pads are readily available for under $20 and may provide a superior option.

A final (and important) issue is safety: what precautions are necessary in a classroom demonstration. In most cases there is no hazard at all (e.g., Bernoulli suction, or squeeze flows), however in others PPE should be used as appropriate (e.g., gloves and safety glasses for can crushing or whenever heating liquids). Some demonstrations (such as a fire tornado) are fun and instructive, but aren't really suitable for a classroom environment and are not included in this guide.

There are many ways to use the demonstrations described here. Most simply, a subset of the demonstrations can be turned over to a graduate TA for use in a weekly tutorial or review session. This is likely to increase attendance (particularly if the review sessions are optional) and if chosen to align with that week's assignments can be a very useful instructional tool. Many of the demonstrations described here are easily adapted to such assignments. If done in a regular class by the faculty member (or a TA assistant) the demonstrations can be a break in a longer lecture - and something students always look forward to. Ideally, individual demonstrations can be chosen to tie into a particular day's lecture, illustrating the mathematical concepts involved. This is the way I use most of them, such as Archimedes' Law, hydrostatics, dynamic similarity of vortices, etc. Others have a level of mathematics which is a bit involved for a lecture, but make a nice problem for homework (e.g., sedimentation of a body of revolution). Still others are interesting to look at, but the mathematics are beyond what I cover in the class such as Benard-Marangoni instabilities, Jeffery Orbits, the fractal breakup of a drop on a surfactant, or double-diffusive convection.

One way in which the demonstrations can be employed is to demonstrate the effect and then challenge the class to explain the underlying mechanism. Simple examples of this would be Hero's Fountain (How long will it last? What is the discharge coefficient?), Torricelli's Fountain (Which stream travels the farthest?), or egg spinning (What is the effect of viscosity?). More complicated examples would include Bernoulli suction (What is an estimate of the equilibrium gap width and flow rate?), the tea-leaf paradox (How long does it take to spin up?), or the Boycott effect (How does the settling time depend on angle?). Other demonstrations could involve students taking data and analyzing their results in class or as a homework assignment, such as the Persian water clock, squeeze flow of a Newtonian fluid or suction from rotation. For example, students could observe how long it takes a thermochromic rod to completely turn color - and then develop the equation necessary for relating that time to the physical property of the thermal diffusivity. The key is to get students to think about how mathematics can be used to develop a quantitative physical understanding of observable phenomena, something which is both very important (particularly in transport), but is also very difficult for many of them to grasp.

While intended as a complement to a basic course in transport, these demonstrations could also be used as the basis for an elective experiential learning in transport course. An appropriate subset of the demonstrations could be used to illustrate key concepts, students would be assigned to develop complementary original demonstrations, and as a "deliverable" student led demonstrations could be used as K-12 outreach in the local community or recorded for wider dissemination. The possibilities are only limited by student and faculty creativity.

Egg Spinning

Materials:

1. A dozen eggs, some of which are hard boiled
2. A turkey baster bulb
3. Water, corn oil, & corn syrup
4. A candle
5. A glass dish

A useful demonstration of the time scale associated with momentum diffusivity is differentiating between raw and cooked eggs by spinning. Because the kinematic viscosity of a raw egg is fairly small (and it is viscoelastic as well), it is impossible to impart a significant angular momentum to the egg by spinning on end with your hand. Thus, the egg topples over. For a hard-boiled egg, however, simply twisting it imparts a large angular momentum and it stays spinning. Student volunteers are called up to try to identify which eggs are raw and which are hardboiled. The glass dish is needed in case they get it wrong!

It is useful to use scaling analysis to quantitatively demonstrate why the uncooked egg "topples over". A hen's egg has a typical radius of 2.3cm. During the "spinning" process your hand typically exerts torque over about a quarter of a rotation. For cooked eggs this results in a spin of about 6 rev/s, thus the torque is exerted only over approximately 0.04s. The internal structure of the egg is complex, primarily consisting of the central yolk surrounded by the egg white. The portion near the yolk is quite viscous, however the egg white near the shell is much thinner, with a viscosity of about 0.04 cm^2/s (e.g., Lang & Rha, 1982). Since it is the portion near the shell which matters in this problem, the penetration depth of the momentum transfer is about $(0.04*0.04)^{1/2}$ = 0.04cm. Since this is much less than the radius of the egg, only a thin layer of fluid near the shell is accelerated and little momentum transfer occurs. It would be necessary to apply the spin over a period of O(10s) in order to approach equilibrium, or for the albumen to be replaced with a fluid some two orders of magnitude more viscous.

Spinning the raw egg on its side breaks the symmetry, and thus some angular momentum is transferred. If the spinning egg is "stopped" with a finger and released it will resume rotation (slowly) due to the fluid motion inside. The solid hard-boiled egg will not move after stopping, so this is another way of discriminating between the two.

The effect of fluid viscosity on spinning can be further demonstrated by replacing the contents with fluids of different viscosity. This is actually fairly easy to do. Using a drill (1/8″ bit in a drill press) or dremel tool, drill out a small hole at the top of the egg and the side (leave the bottom undisturbed for spinning). Insert a toothpick or wire to break up the yolk membrane. Using the bulb of a turkey baster, blow out the contents of the egg into a cup (for later consumption if done in your kitchen!). By filling the bulb with water, the interior of the egg can be thoroughly rinsed. Filling the egg with other fluids (using the turkey baster bulb) allows testing of the effect of kinematic viscosity on the spinning process. Fluids available in the kitchen with useful viscosities are water (0.01 cm^2/s), corn oil (0.7 cm^2/s) and corn syrup (25 cm^2/s). The behavior of these filled eggs can be compared to a raw egg, an empty egg, and a hard boiled egg. Water and corn oil are easy to load using the baster, however to fill the egg with corn syrup it is helpful to heat the syrup in a microwave first (about 10s) to reduce the viscosity. The holes can be sealed by dripping a bit of wax from a lit candle onto the dried egg. In practice, an empty egg spins very nicely (all of the inertia is in the shell which acquires the angular momentum from spinning), the water filled egg behaves like a raw one, and the corn syrup filled egg is similar to the hard boiled one, depending on the temperature (if cold, it is indistinguishable). Since the kinematic viscosity of room temperature corn syrup is about 25 cm^2/s, the penetration depth is 1cm, comparable to the radius of the egg. For corn oil, while it is a much more viscous fluid than water, the viscosity is still low enough that the penetration depth is only 0.16 cm and it is essentially indistinguishable from the water filled egg for axisymmetric motion. Interestingly, if the eggs are rotated on their sides (e.g., not in axisymmetric position), the corn oil egg rotates more readily than the water filled egg and is readily distinguishable. In class, the three filled eggs are labeled with a letter and students are asked to identify which egg is which by their spinning behavior. Votes are collected, and then the identities are revealed.

An interesting extension of this demonstration is spinning the hard-boiled egg very rapidly on its side. It is a little tricky to do, but it should "pop up" like a top to spin on its end. The mathematics of this counter-intuitive process (popping up on the end increases the center of gravity of the egg) were described in the 2002 paper by H. K. Moffat and Y. Shimomura.

Another application of the "spinning" process and the internal dynamics for a raw egg is the relationship to concussions (Lang, et al., 2021). In fact, it is possible to liquefy the interior of a raw egg via spinning and induced internal circulation. Such "egg liquefiers" are available for under $20 and are used as a pretreatment to make "golden" hard-boiled eggs.

References:

Lang, E.R. and Rha, C., "Apparent shear viscosity of native egg white." International Journal of Food Science & Technology, 17: 595-606 (1982).
https://doi.org/10.1111/j.1365-2621.1982.tb00219.x

Moffatt, H., Shimomura, Y., "Spinning eggs — a paradox resolved." Nature 416, 385–386 (2002).
https://www.nature.com/articles/416385a

J. Lang, R. Nathan, and Q. Wu, "How to deform an egg yolk? On the study of soft matter deformation in a liquid environment," Phys. Fluids 33, 011903 (2021).
https://doi.org/10.1063/5.0035314

A Hydraulic Scale

Materials:

1. A milk jug with two holes drilled into its cap.
2. A length (around 10 feet) of tygon tubing
3. A hot water bottle (rubber bladder type)
4. A hose barb
5. A board of wood about 8”x15”
6. A tape measure (12 ft)

This demonstration shows how a column of water can be used to levitate someone via hydraulics. In preparation, the plug to the hot water bottle is drilled out to accept the hose barb (either glued in or tapped and screwed in – but it has to be able to take a significant pressure without leaking!). The water bottle is connected to the milk jug via the tygon tubing and air is eliminated from the entire system. The board is placed on the water bottle (when deflated) and the effective contact area is measured.

The system is used for two types of demonstrations. First a relatively lightweight volunteer is asked to step on the board on the deflated bladder. The jug is then raised to about 5 feet or so while talking to the class. As the bladder fills the board becomes more and more unstable (visualized by the wobbling of the student volunteer), showing that simply raising the milk jug is able to levitate the much heavier person. In the second demonstration the bladder is deflated a bit until it is fairly stable – but still fully supporting the student. The end of the tygon tubing is then pulled out of the milk jug cap and the height of the column of water in the tube is measured by another volunteer (it dances around a bit as the student wobbles, so this is a little tricky!). A clip partially restricting the flow in the tube is useful to reduce fluctuations. Using hydrostatics and the contact area between the board and the bladder, the weight of the student is calculated. You can do the same experiment with a beefier student (or instructor), but you would need to stand on a chair to get the height of the column of water – and risk making a fountain! Note that it is important to have a very rigid board on the bladder: if the board bends and contacts the ground the force (and pressure) supported by the liquid is greatly reduced and yields significant underestimation of the weight.

The principles involved in this experiment are hydrostatics and the difference between force (e.g., the weight of the student, Mg) and pressure (force/area = ρgh). The largest source of error is determining the exact area over which the pressure is exerted onto the bladder.

Archimedes' Law

Materials:

1. A 500 ml beaker half-filled with water.
2. A number of different types of materials with known densities
3. A loop of dental floss.
4. A scale.

The ancient science behind Archimedes Law is often miss-described in the popular literature. As do many investigators (e.g., Galileo, 1586), I think it's pretty unlikely that water sloshing out of bathtubs ever factored into it, despite the writings of Vitruvius two centuries after Archimedes. The key, of course, is that the force on a submerged object is equal to the weight of the fluid displaced as described in the surviving parts of Archimedes' fragmentary text "On Floating Bodies". The mechanically simplest way of determining the relative density of two objects is to balance them dangling from a lever (stick) in air, and then lower the two objects into water (a pair of beakers suffices for this). If they are of the same density, the buoyant force will be proportional to their weight and they will remain in balance. If they are of different densities, the less dense one will displace more water (proportionally) and thus be displaced upwards. Note that the objects don't need to be the same weight, as they can be fastened at different distances along the lever arm. This is the method suggested by Galileo. It is likely that this is the way Archimedes demonstrated the gold content of the crown of legend. The crown could even have been checked against a permissible amount of alloying by hanging appropriate amounts of pure gold and silver at the same point on the lever.

While the above approach is mechanically simple, you can more easily quantitatively measure the density of an irregular object by placing the beaker of water on a scale, taring it, dangling the object on a thread so that it is both submerged in the water and above the bottom (recording this weight) and then letting the thread go and recording the full weight of the object. The density (relative to water) is the ratio of the two measured weights. Such a measurement could also have been done easily by Archimedes using a pan balance, although the "up or down" result of the simple lever test may have made for better theatre.

In demonstration I use a variety of minerals I have on hand: a block of fluorite, pyrite, silicon, a selenite egg, and a cluster of neodymium magnetic balls. The measured values are compared to literature, and are remarkably accurate.

This demonstration is used in concert with a derivation of the pressure distribution in a static fluid, the equation of hydrostatics, and the use of the divergence theorem to convert surface integrals (e.g., the net force on the object due to pressure) to volume integrals (the weight of the fluid displaced).

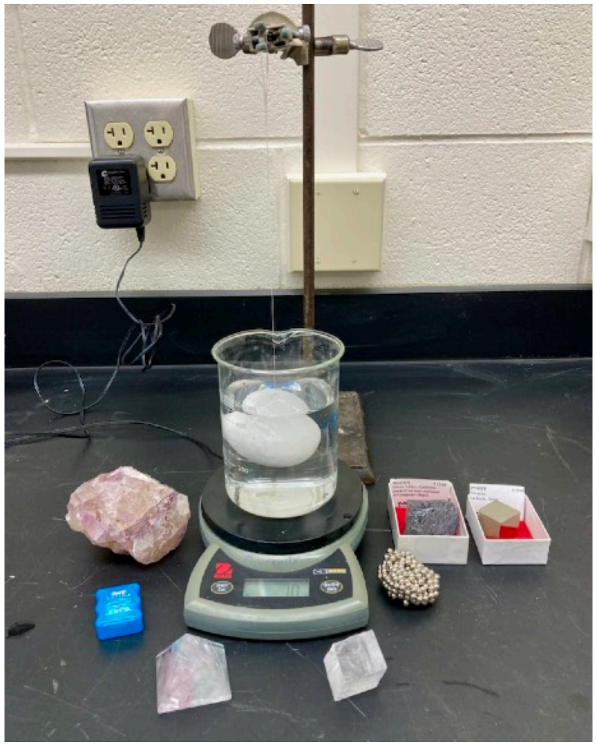

References:

Archimedes "On Floating Bodies", ca250BC
https://archive.org/details/worksofarchimede00arch/page/256/mode/2up?view=theater

Marcus Vitruvius Pollio: de Architectura, Book IX, ca40BC.
https://penelope.uchicago.edu/Thayer/E/Roman/Texts/Vitruvius/9*.html

Rorres, Chris, "The Golden Crown".
https://math.nyu.edu/Archimedes/Crown/CrownIntro.html

Galileu Galilei, La Bilancetta, (1586).
https://math.nyu.edu/Archimedes/Crown/bilancetta.html

Hero’s Fountain

Materials:

1. Two 1/2 gallon Nalgene bottles (narrow mouth)
2. Two corks (to fit the bottles) with two holes each
3. A medium size funnel
4. A small diameter rigid (curved) tube
5. Tygon tubing
6. A stand to elevate one of the bottles
7. A small beaker
8. A ruler

Hero’s Fountain goes back to Hero (or Heron) of Alexandria around 200BC. It is described in his book Pneumatics (available for free on the web) along with a lot of other interesting examples. The geometry is topologically similar to example 23 of that text. In this demonstration the funnel is inserted into one of the corks, and tygon tubing is attached to it so that it makes a tail to the bottom of the bottle. The rigid (curved) tube is inserted into the other cork, and again it has a tygon tube tail going to the bottom of its bottle. The other two holes are connected via tygon tubing to make an air pressure equalization between the two bottles. Initially the bottle with the curved tube (which will be the fountain outlet) is filled with (colored) water and the other is empty. The bottle with the water in it is placed on a stand (a small box or inverted 2 liter beaker works well for this). The fountain is started by pouring a little water (reserved in the small beaker) into the funnel in the empty bottle. This pressurizes the system, the water flows out of the curved tube and it is adjusted so that the stream arcs into the funnel – making what appears to be a continuous process.

While it looks like a perpetual motion machine, of course it runs down as one bottle empties and the other fills. The flow is unaffected by the relative height of the two bottles (I usually raise or lower the one with the fountain to demonstrate this), but it will stop when the distance between the fluid level in the funnel and the fluid in the bottle below it matches the distance between the tip of the curved tube and the fluid level in the bottle below. Dribbling at the end stage is avoided by tilting the bottle with the curved tube, reducing that distance. Once the end stage is achieved (and the fountain stops flowing) the distance between the fluid level in the curved tube and that of the bottle below is measured and shown to match the height difference in the other bottle.

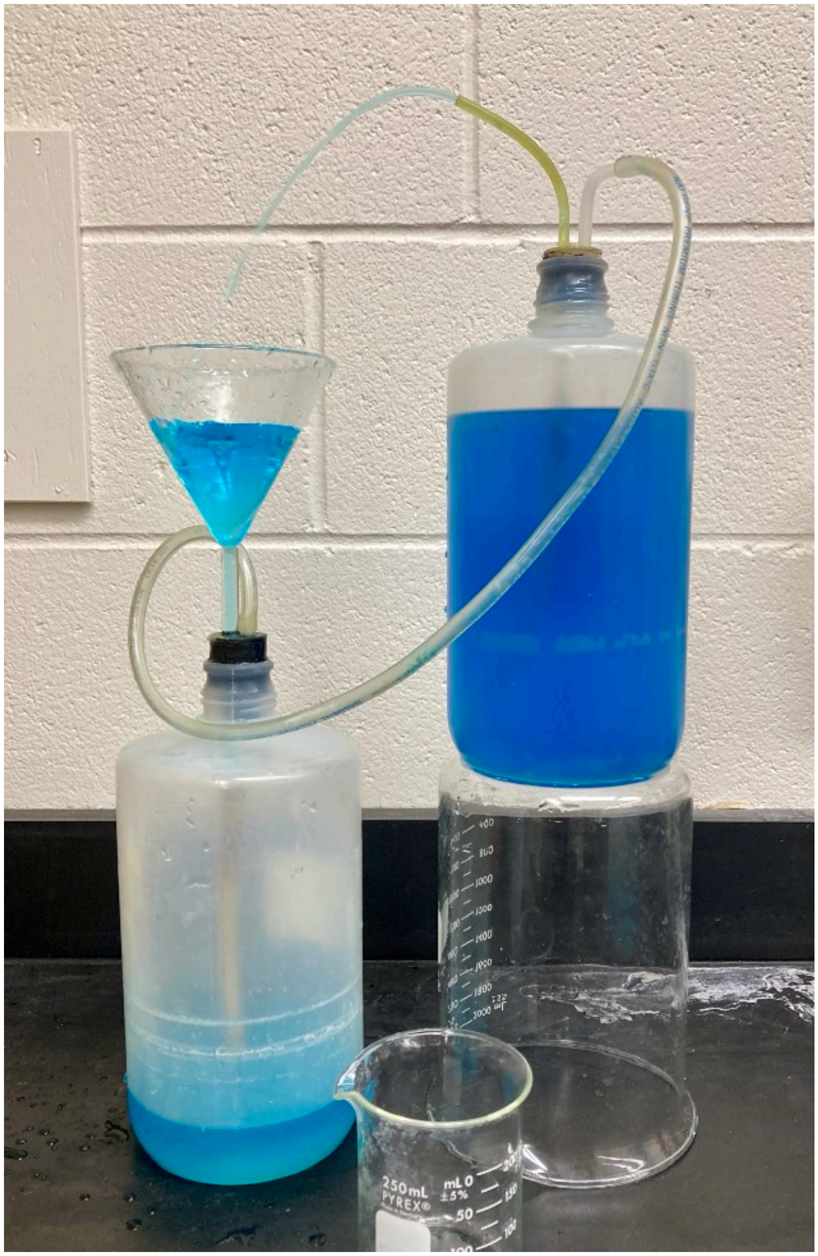

The fountain is also useful for doing quantitative analysis, answering questions such as estimating the fluid velocity and how long it should last before running down. The driving force is $\rho g h$ where h is the net height difference. If losses are ignored, from Bernoulli's equation this is balanced by the acceleration of the fluid, thus the fluid velocity is $U = \lambda \left(2gh\right)^{1/2}$ where λ is an effective discharge coefficient accounting for losses. In general, the discharge coefficient must be less than 1, and would be a function of the Reynolds number and other losses in the system (e.g., losses in the funnel side of the fountain and frictional losses in the thin curved tube producing the fountain). As the fountain slows down, frictional losses will increase (relative to inertia) and the discharge coefficient will decrease, so it will not be independent of time. Ignoring this variation, however, if the cross-sectional area of each bottle is A_b and that of the fountain pipe is A_f, then the flow yields a simple mass balance:

$$A_b \frac{dh}{dt} = -2A_f \lambda \left(2gh\right)^{1/2}$$

The factor of 2 arises because one bottle fills as the other empties. Scaling the height difference with its initial value h_0 and the time with some unknown scaling t_c, the dimensionless equation governing the height is:

$$\frac{dh^*}{dt^*} = -h^{*1/2} \quad ; \quad h^*|_{t^*=0} = 1$$

where the time scale is simply:

$$t_c = \frac{A_b}{A_f} \frac{{h_0}^{1/2}}{2\lambda\sqrt{2g}}$$

The dimensionless differential equation is solved via inversion to yield:

$$h^* = \left(1 - \frac{1}{2}t^*\right)^2$$

thus the fountain ceases at a dimensionless time of 2. Note that at a dimensionless time of 0.6 the driving height has already been reduced by a factor of two and at a dimensionless time of 1 the horizontal projection is reduced by a bit more than a factor of 2. Thus, for the last half of the possible operating time the fountain is much less impressive. For the system depicted above the fountain pipe has an ID of 0.33cm and the bottles an ID of 11.9 cm. For an initial height of $h_0 = 16$ cm, the characteristic time (taking $\lambda = 1$) is 58 s, so the fountain would be predicted to run down after a minute or so.

In order to get a better estimate of the operating time it is necessary to determine the discharge coefficient. This can be done by measuring the exiting fluid velocity U for some driving force, most easily accomplished by analyzing the parabolic arc described by the exiting stream of water. We take the origin to be the end of the curved fountain pipe, and the emergence angle of the stream (relative to horizontal) to be θ. The horizontal and vertical locations of fluid elements in the stream at a time t after emergence are just:

$$x = Ut\,cos\theta \quad ; \quad z = Ut\,sin\theta - \frac{1}{2}gt^2$$

which yields the parabolic arc:

$$z = x\,tan\theta - \frac{1}{2}g\frac{x^2}{U^2\,cos^2\theta}$$

There are three distances which are easy to measure with reasonable accuracy for this system: the horizontal and vertical location where the stream lands in the funnel x_f and z_f (the latter is negative), and the horizontal location where the stream reaches its highest point x_m. Solving the equations yields the relations:

$$tan\theta = \frac{z_f}{x_f - \frac{1}{2}\frac{x_f^2}{x_m}} \quad \text{and} \quad U^2 = \frac{x_m g}{cos\theta\,sin\theta}$$

For the Hero's fountain depicted above we have (at h = 16 cm) x_m = 1.7 cm, x_f = 17, and z_f = -16 cm. For small θ the calculated velocity is insensitive to x_m (useful, as it is the most difficult to estimate accurately). The above expression yields an emergence angle of $\theta = 13^o$, a velocity of 86 cm/s and an effective discharge coefficient of $\lambda = .49$, reasonable values which provide a better estimate of the duration of the fountain.

References:

The Pneumatics of Hero Von Alexandria from the Original Greek: Translated for and Edited by Bennet Woodcroft (1851).
https://www.google.com/books/edition/The_Pneumatics_of_Hero_of_Alexandria/O8PVAAAAMAAJ?hl=en&gbpv=1&printsec=frontcover

Torricelli's Fountain

Materials:

1. A rectangular plastic storage bin
2. A small submersible pump (396 GPH or equivalent)
3. PVC piping (1.5”) with elbows and connectors
4. Wire to hold the pipe vertical
5. Shield and clamps to catch the splashes
6. A ruler
7. A towel

A nice demonstration of both hydrostatics and Bernoulli's equation is Torricelli's Law (or Torricelli's Fountain). Evangeliste Torricelli (1608-1647) was an Italian mathematician and physicist, credited with the invention of the mercury barometer and demonstration that “a sea of air” exerts pressure, resolving why it was impossible to suck water up a pipe a vertical distance greater than 10m. It was because of this work that the unit of pressure (1 torr = 1mm Hg = 133.3 Pa) is named in his honor. A colleague of Galileo, Torricelli was interested in many problems, among them the analysis of “water clocks” in which time is kept by determining how fast a water container drains out of a hole. One of Torricelli's observations in his text *Opera Geometrica* (1644) was the trajectory of streams of water emerging horizontally from a filled bucket of water. Here we demonstrate this phenomenon.

Rather than use a bucket (which runs down all too quickly) in this demonstration I use a small submersible pump (ECO-396), which is connected to a vertical 1.5” PVC pipe as depicted below. 3/8” holes are drilled along the vertical length of the pipe, and these can be covered up with electrical tape as desired. In operation the pump fills the vertical pipe (overflowing if sufficient holes are covered), however the inertia of the vertical velocity of water in the pipe is negligible due to the large pipe diameter. The water emerges horizontally from the open holes, and forms a series of parabolic arcs. Torricelli showed that the envelope of these arcs corresponds to a 45° angle, and the maximum lateral distance occurs for the stream emerging from half-way up the pipe. In operation the shield is necessary to catch the splashes (a fun part of the demonstration, if a bit messy), and the towel is useful to clean things up!

Derivation of the maximum distance of each stream is a straightforward application of Bernoulli's equation and the vector nature of velocity. If the height of fluid in the (overflowing) vertical pipe is H and the height at which the stream emerges is h, then in the absence of losses the water has a horizontal velocity U governed by:

$$\frac{1}{2}\rho U^2 = \rho g(H-h)$$

which yields $U=(2g\,(H-h))^{1/2}$. Once the water emerges, it undergoes free-fall in the vertical direction (the horizontal velocity is assumed unaffected) and impacts the surface of the water after a time $t = (2h/g)^{1/2}$. The horizontal distance traveled in this time is just $L = U\,t = 2\,(h\,(H-h))^{1/2}$ which is a maximum $L_{max} = H$ for $h = H/2$. In fact, however, the distance traveled is just a bit less than this due to frictional losses. The decrease in L_{max}/H equals the discharge coefficient of the orifice, about 0.9 for these drilled holes. Because of the splashes it is easiest to measure the (almost) 45° locus of streams and compare the length of the hypotenuse S to the height of fluid in the vertical pipe H. The discharge coefficient is just $(S^2/H^2 - 1)^{1/2}$.

References:

E. Torricelli, "De motv aqvarvm" in Opera Geometrica, Libri Dvo (Amatoris Maffe & Laurentij de Landis, Florentiae, 1644), pp. 191–203
http://archive.org/stream/operageometrica00torrgoog#page/n212/mode/2up

Milena D. Davidović; Tatjana Marković-Topalović; Josip Sliško; Mirjana Božić, "Visualizing Properties of a Quadratic Function Using Torricelli's Fountain", Phys. Teach. 58, 263–267 (2020).
https://doi.org/10.1119/1.5145475

The Persian Water Clock

Materials:

1. A tall cylindrical vase
2. A tennis ball can
3. A 3 oz fishing weight
4. Rubber bands and thread
5. Food coloring

Accurate measurement of the passage of time has played a critical role in the history of civilization. While sun dials are quite effective, they don't work on a cloudy day - and certainly don't work at night! One approach which has been developed in many cultures is the water clock, or clepsydra (the name derives from Ancient Greek "water thief"). This relies on the inflow or outflow of water through a small hole. As the water level changed, clever artisans connected floats to gears and indicators indicating the passage of time. The simplest of such clepsydras was employed in ancient Persia, where a clay bowl with a small hole in the bottom was floated in a reservoir. The bowl was supported by hydrostatics, and the difference in water levels inside and outside the bowl drove water flow into the bowl. When the bowl filled to the point where it could no longer be supported by hydrostatics it abruptly sank, indicating the passage of a unit of time.

Here we demonstrate a slightly more sophisticated version of the inflow clepsydra. A 1/16" hole is drilled into the bottom of a tennis ball can (chosen for its size and relatively light weight). A lead fishing weight is secured to the bottom of the can. Because, at least initially, most of the empty can is above the water level, the weight needs to be secured in such a way that the can floats upright. There are many ways to do this, but rubber bands and thread allow the weight to be properly centered. A few drops of food coloring are added to the bottom of the empty can to aid in visualization. The tall vase is filled with water and the weighted can is inserted. As the water flows into the can, the food coloring makes the water inside clearly visible, and the difference in height between the fluid inside and outside the can is measured. If the weight of the can is negligible in comparison to the fishing weight (not a bad approximation) the rate of inflow and sinking is nearly constant. The side of the can may be marked to indicate shorter intervals of time. Once the water outside the can flows over the open top, the can immediately sinks.

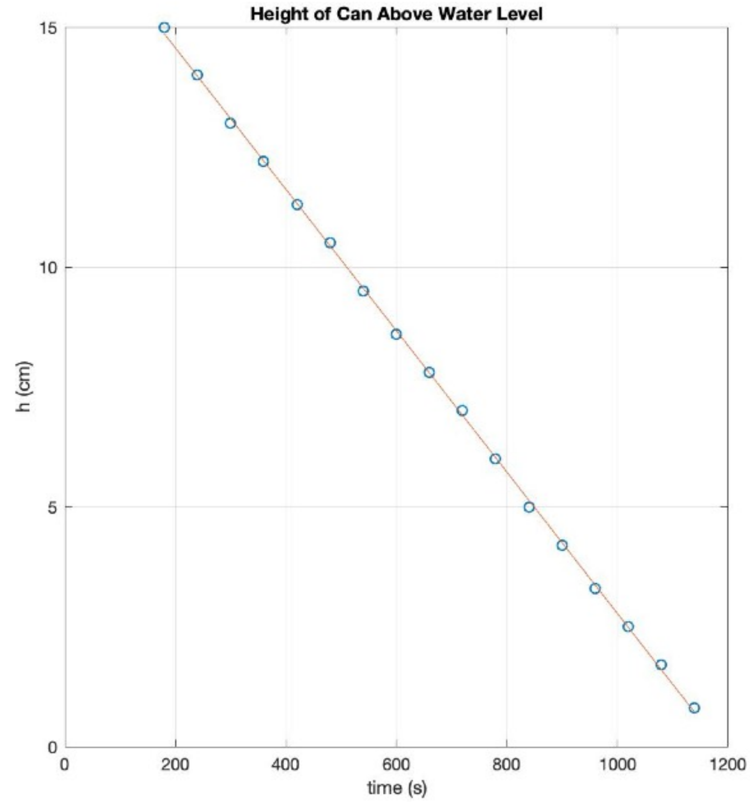

An idealized version of this clepsydra is easily analyzed. The can is taken to be a massless cylinder of height H and radius R with a hole in the bottom of radius R_0. The cylinder is dragged downward by the fishing weight of mass $M_w = \rho_w V_w$ of density ρ_w and volume V_w. The net force exerted by the mass is reduced by the buoyant force due to the density of the displaced water. We take the height of the can above the waterline in the vase to be h and the difference in the height of the water inside and outside of the can to be Δh. If the velocity of the water entering the hole is U, then via a mass balance the change in the height of the can above the external water level is just:

$$\frac{d\left(h + \Delta h\right)}{dt} = -\,U\frac{R_0^2}{R^2} \approx \frac{dh}{dt}$$

where, from the assumptions, Δh is approximately constant. From Bernoulli's equation, the velocity is related to the hydrostatic driving force Δh by:

$$\frac{1}{2}\rho U^2 = \rho g \Delta h$$

Finally, the net weight of the system is supported by the displaced water, yielding (via Archimedes Law):

$$V_w\left(\rho_w-\rho\right)g=\rho g\Delta h\pi R^2$$

Note that if the can isn't massless (as assumed above), Δh would change during the filling process (the additional weight of the can above the waterline in the vase would lead to increased Δh), also changing the velocity and filling rate. With the simplifying assumptions, however, the rate of change in height h is constant, and is given by:

$$\frac{dh}{dt}=-\frac{R_0^2}{R^2}\left[2g\frac{V_w\left(\rho_w-\rho\right)}{\pi R^2\rho}\right]^{1/2}$$

The total time before sinking (e.g., when h = 0) is given by:

$$T=\frac{H-\Delta h}{\frac{R_0^2}{R^2}\left[2g\frac{V_w\left(\rho_w-\rho\right)}{\pi R^2\rho}\right]^{1/2}}$$

Note that at t = 0 the can starts at a depth Δh even when empty. Losses can be accounted for by increasing the sinking time by the inverse of the orifice discharge coefficient C_d. For the depicted system R = 3.7 cm, R_0 = 0.079 cm, M_w = 73 g (measured weight of a nominally 3oz sinker), $\left(\rho_w-\rho\right)=10.35$ g/cm³, and H = 20.5 cm. The above expressions yield Δh = 1.7 cm, U = 55 cm/s, an orifice Reynolds number of 870, and T = 745 s. A plot of h vs. t revealed the expected linear relationship, with a velocity of -0.0147 cm/s. The measured sinking time, however, was 1218 s. The discrepancy is primarily due to the discharge coefficient (a typical value at this Reynolds number and orifice aspect ratio is C_d = 0.6; Iverson, 1956) as well as errors in the hole diameter and the non-negligible weight of the can itself above the waterline (approximately 15 g half way through the sinking). In addition the final sinking is delayed by about 20 seconds due to surface tension effects. The above expressions can be used to adjust the parameters to achieve the drainage time desired for the demonstration, for example increasing the hole size from 1/16" to 3/32" should decrease the sinking time by more than a factor of two.

References:

Wikipedia contributors. Water clock. Wikipedia, The Free Encyclopedia. September 8, 2024, 21:04 UTC
https://en.wikipedia.org/w/index.php?title=Water_clock&oldid=1244731800

Iversen, H. W. "Orifice Coefficients for Reynolds Numbers from 4 to 50,000." ASME. Trans. ASME. February 1956; 78(2): 359–364.
https://doi.org/10.1115/1.4013677

Conservation of Momentum: Crooke's Radiometer

Materials:

1. Crooke's Radiometer (available on-line)
2. A strong light source.

Crooke's radiometer is a very useful demonstration of conservation of momentum in many different ways. In class it is used when talking about momentum conservation when a jet of water is directed at a flat vane or a curved bucket (e.g., a Pelton wheel), and the discussion then moves to the concept of a light sail, now being investigated for space transport. The idea, of course, is that light is reflected off the white side of the vanes and absorbed on the black, thus the vanes should turn – which they do. The surprise is that they turn in the wrong direction… Students are directed to a nice discussion of what the actual mechanism is (as shown by Reynolds it is thermal transpiration at the edges of the vanes producing a "jet" from cold to hot), as well as the interesting backstory of the conflict between Reynolds and Maxwell. The website is found at https://math.ucr.edu/home/baez/physics/General/LightMill/light-mill.html

Reynolds identified the thermal transpiration mechanism and submitted a paper explaining the phenomenon. Maxwell (who had recently developed the theory that light had momentum) was a reviewer on the paper, and (critiquing some of the derivation, while recognizing that it was essentially correct) held it up in the review process. In the interim Maxwell published his own version, where proper credit to Reynolds was relegated to the appendix added in a year after original publication (and

after Reynolds' paper finally came out). Reynolds wrote a letter to the journal (PRS) complaining of this treatment, however they declined to publish it: Maxwell had died in the interim.

There are interesting variations on how to demonstrate the radiometer. If exposed to bright uniform light the vanes will always turn rapidly away from the black side. If you use a high intensity light source (a focusing tactical flashlight works well and can be purchased for under $10) then you get different behavior depending on which way the light shines. If you focus it on the black vanes (so that the white sides are in shadow) then the vanes spin rapidly. If you focus on the white sides, the vanes slow down and stop. This is evidence that the effect is (as was shown) due to temperature differentials, as the black side would be heating up while the white side wouldn't be absorbing enough energy to make it turn, even though the black side is in shadow.

References:

James Clerk Maxwell "VII. On stresses in rarified gases arising from inequalities of temperature" Royal Society Phil. Trans. (1879).
https://doi.org/10.1098/rstl.1879.0067

Osborne Reynolds "On certain dimensional properties of matter in the gaseous state." Proc. R. Soc. Lond. 28:303–321 (1879).
https://doi.org/10.1098/rspl.1878.0134

Gibbs, Philip (1996). "How does a light-mill work?"
https://math.ucr.edu/home/baez/physics/General/LightMill/light-mill.html

Wikipedia contributors. (2024, June 10). Crookes radiometer. In Wikipedia, The Free Encyclopedia. Web, June 19, 2024
https://en.wikipedia.org/w/index.php?title=Crookes_radiometer&oldid=1228203343

Can Crushing

Materials:

1. Aluminum soda cans
2. Water
3. Bowl with ice water
4. Gloves and eye protection
5. Hot plate

A very popular demonstration is the use of atmospheric pressure to crush a soda can. This is particularly true after interest generated by the collapse of the Titan submersible in 2023 while exploring the Titanic. The procedure is simple: put a little water into an empty soda can, boil the water on a hot plate, and then using tongs or insulating gloves flip the can upside down and immerse it in the ice water. The implosion is essentially instantaneous as the water vapor filling the can rapidly condenses and forms a near vacuum.

There are many aspects to this demonstration. The key to forming a pressure low enough inside the can is rapid condensation of the vapor as well as the inertia of the fluid (water) that is filling the can through the hole. If the volume of the can is V and the condensation time is T, then (for a given opening area A) the velocity of the water entering scales as U = V/AT. From Bernoulli's equation, the pressure differential required to produce this is:

$$\Delta P \approx \frac{1}{2}\rho U^2 \approx \frac{1}{2}\rho\left(\frac{V}{AT}\right)^2$$

The volume of a soda can is about $355cm^3$ and the area of the opening is about $3cm^2$. Examination of slow motion videos of the implosion process suggests that there is about a 0.025s delay between first contact and the initial buckling, followed by complete implosion in another 0.010s. About $30cm^3$ of water is drawn into the can during the implosion process. If we associate the volume of the inflow of water with, say, 0.025s we get a pressure of about 0.08 atm. The vertical cross section of the can is approximately 12.3x6.6 = $81cm^2$, so the crushing force (once the cylindrical symmetry is broken) is equivalent to about 66 N applied to the side of the can. These numbers are, of course, very rough but are the correct order of magnitude.

We can also look at the heat transfer process necessary to condense the water vapor to learn more about the mechanisms involved. The latent heat of vaporization of water at boiling is 2.25×10^6 J/kg. The density of water vapor at boiling is 5.98×10^{-4} g/cm^3, thus the energy associated with the condensation of all the water vapor in the can of volume 355cm^3 is 477 J. The surface area of the can in contact with the ice water is about 28cm^2, so the heat transfer coefficient for condensation to occur in 0.025s is about 70,000 W/m^2°K (assuming a temperature difference of 100°C). This is actually much too high – typical condensing steam heat transfer coefficients are an order of magnitude less than this, and of course there are other sources of heat transfer resistance. What is occurring instead is that as water sprays into the can through the opening it greatly increases the surface area available for heat transfer and condensation. The 477 joules (114 calories) of cooling required can easily be supplied by a spray of 30ml of ice water.

This interpretation of the condensation process can be demonstrated by preparing a can with a very small hole in the top (1/8 inch drill bit), where the pressure of the soda is used to remove all but a small amount of the liquid (to avoid messes, chill before you drill!). After bringing this residue to a boil and displacing all the air out of the can, the small hole is covered with a bit of vinyl tape which seals under suction. When the top of the can is immersed into the bath in the same manner as before, the can crushes – but only rather slowly, rather than with a sharp "bang". This is associated with the much smaller heat transfer coefficient in the absence of the spray of water getting inside. In a laboratory test a can with a 1/8" uncovered hole had about 15ml of water in it prior to implosion, and had an additional 30ml of water in it after implosion (which made a nice "bang"). A can prepared in the same manner, but with the hole plugged with vinyl tape, collapsed slowly, remained fairly warm, and did not import any water (as expected).

Additional variations on this demonstration are dunking the can without inversion (nothing happens as the density and heat capacity of the displacing air are too low to generate a significant pressure differential) and enlarging the hole (increasing the area, so reducing the velocity and pressure). It is also useful to project a slow motion video of the can crushing that can be found on-line.

References:

Wikipedia contributors. (2024, June 21). Titan submersible implosion. In Wikipedia, The Free Encyclopedia. Retrieved 23:56, June 23, 2024.
https://en.wikipedia.org/w/index.php?title=Titan_submersible_implosion&oldid=1230294582

Imploding Can Crusher - TB#1
https://youtu.be/mS8ZIrDetJM?si=E1osRyBtxpAQNQSD

Gravity Driven Flow Down an Incline

Materials:

1. A flat bottomed rectangular tray
2. Ruler
3. Corn syrup
4. Cardboard “dots”
5. Stopwatch

A classic problem in unidirectional flows is gravity driven flow down an incline. While the viscous problem is solved in class, the inertial analog (pyroclastic flows and landslides) is also introduced. In particular, the many lahars in the Mt Rainier area have devastated wide areas in the past and are certain to do so again. In class the unidirectional gravity driven flow down an incline is solved.

The flow down an incline is very simple to visualize. Two parallel lines 10 cm apart are drawn on the bottom of a rectangular tray. A known quantity of corn syrup is poured onto the tray (of known area) so that a known uniform depth is achieved. A “dot” is dropped onto the surface of the syrup a few cm above one of the lines, and then the tray is tilted to a known angle by propping one end on a block. The time for the dot to travel the 10 cm between the two lines is measured, and the velocity is used to calculate the viscosity of the fluid. The surface velocity is given by:

$$U = \frac{1}{2}\frac{g\delta^2}{\nu} sin(\theta)$$

where ν is the kinematic viscosity, g is the acceleration due to gravity, and δ is the film thickness (determined from the volume and area of the film). θ is the angle of inclination of the tray.

Because of the strong dependence on film depth, this is the largest source of error in the demonstration. Also, for corn syrup the kinematic viscosity is a very strong function of temperature, varying about 7% per degree C. Thus, quantitative agreement is sometimes lacking.

The letter tray depicted below was 36.5cm by 13.7cm at the base (500cm^2 area), and 225 ml corn syrup (311g, density 1.38 g/cm^3) was added yielding a depth of 0.45 cm. The tray was propped up on one end by a 2.54cm block, thus the angle was 0.0696 radians.

The “dot” traversed the 10 cm between the lines in 38 seconds, yielding a calculated kinematic viscosity of 26 cm^2/s, close to the expected value for corn syrup.

It is also useful to extend the demonstration by adding an additional known quantity of corn syrup (I used 100ml or 138g) to demonstrate the effect of depth on velocity. This amount only increases the depth to 0.65cm, but increases the velocity (decreases the transit time) by a factor of 2.1.

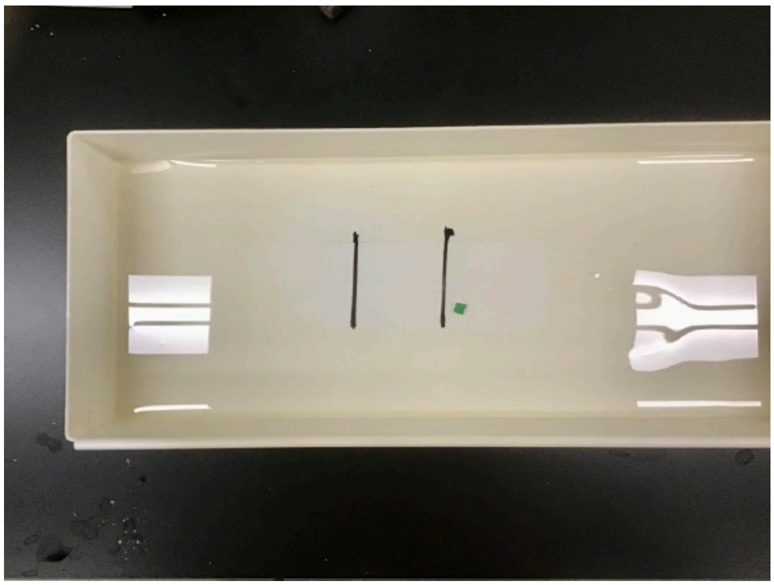

While this demonstration is not a very practical way to measure viscosity, flow down an incline actually does have application to the measurement of the rheology of more complex materials. In very innovative work, Roger Tanner’s group showed that when a suspension of particles flowed down a semicircular trough the surface would be deformed into a triangle, the magnitude of which is proportional to the second normal stress difference (the difference in the normal stress in the velocity gradient and vorticity directions for a simple shear flow). This is actually the most sensitive way to measure this important rheological quantity and provided insight into suspension dynamics at volume fractions as low as 10%. Images of the deformed surface from the paper are projected for the class.

An interesting extension of this demonstration is to examine the initial transient as an example of experimental design. Initially the tray is horizontal, and then at time t = 0 it is raised to the desired angle. By scaling the transient equation (not solving it) you obtain both the scaling for the velocity as well as the characteristic time t_c (just the diffusion time). Thus, we have:

$$U_c = \frac{g\delta^2}{\nu} sin(\theta) \ ; \ t_c = \frac{\delta^2}{\nu}$$

For a tray of characteristic length L we require the product of U_c and t_c to be much less than this value. This yields the design constraint:

$$\delta << \left(\frac{L\nu^2}{g\, sin(\theta)}\right)^{1/4}$$

So the demonstration will only match the expected behavior for sufficiently thin layers of sufficiently viscous fluids, not a problem for corn syrup but definitely a problem for water! Note that the complete problem can be easily solved via separation of variables and the resulting Sturm-Liouville eigenvalue problem (it is mathematically identical to start-up flow in a slit of width 2δ), however scaling alone is sufficient for the purpose of experimental design. I have used this scaling analysis as an exam question.

References:

https://www.usgs.gov/programs/VHP/lahars-move-rapidly-down-valleys-rivers-concrete

Bird, Stewart & Lightfoot, *Transport Phenomena*, rev 2nd ed., Wiley, 2007. Sec 2.2, p. 42-47.

Shao-Cong Dai; Erwan Bertevas; Fuzhong Qi; Roger I. Tanner; Viscometric functions for noncolloidal sphere suspensions with Newtonian matrices. J. Rheol. 57, 493–510 (2013).
https://doi.org/10.1122/1.4774325

Tears of Wine

Materials:

1. Wine glass
2. Cooking sherry
3. Strong light source
4. White board or screen

The tears of wine (or legs of wine) is a classic surface tension driven flow, having been studied for over 150 years. The sherry or port (more easily visualized than red wine) is poured into the wine glass and swirled to wet the inner surface. It is important to have the glass very clean so that the wine wets the surface well. After a short period of time a rim of fluid forms which drips down to the pool of wine below. The process is sustained by the surface tension driven flow up the (invisible) thin layer of wine on the glass surface, only the rim of fluid and the tears or legs are thick enough to see. By projecting a strong light source through the glass onto a screen, the legs can be more easily visualized. In my demonstration I use a small tactical flashlight and a white three ring binder as a screen. The resulting images are projected onto the main screen via an iPod and zoom. The process is driven by the surface tension gradient in the film resulting from the preferential evaporation of alcohol. A second wine glass can be passed around the class during the demonstration so that students can see it “up close”. In order to avoid students “sipping” from the glass, I now use cooking sherry.

The details of this process are quite complex (a very useful discussion is provided in the paper by Venerus and Simavilla, 2015), however the thickness of the prewetted film can be estimated from a simple balance between gravity driven flow downwards and surface tension gradient flow upwards. The maximum thickness would occur where the net flow due to these two mechanisms is zero, and the thickness leading to the maximum upward flow rate is also of interest. This demonstration is used in conjunction with a lecture on gravity driven flow down an incline and is a nice example of how scaling the boundary conditions leads to a simplified differential equation and solution.

The flow in the thin film is proportional to the Marangoni stress (surface tension gradient), which depends on the evaporation rate of the alcohol. This means that it is a complex coupled mass, momentum, and energy transport problem, and is further complicated by the surface tension effects at the curved interface between the film and the pool of wine below. To avoid this complexity for the demonstration, film depths for a "pre-swirled" film are calculated by simply assuming a surface tension gradient. Far from the pool at the base of the film and the ring of tears at the top, the film is flat. The velocity profile under these assumptions is governed by:

$$\mu \frac{\partial^2 u_x}{\partial y^2} = \rho g sin(\theta) \ ; \ u_x|_{y=0} = 0 \ ; \ \mu \frac{\partial u_x}{\partial y}|_{y=\delta} = \Gamma'$$

where Γ' is the surface tension gradient, ρ is the density, and μ is the viscosity. Rendering the equations dimensionless by $u_x * = \frac{u_x}{U_c}$, $y * = \frac{y}{\delta_c}$, and $\delta * = \frac{\delta}{\delta_c}$ yields the scalings $U_c = \frac{\Gamma'^2}{\mu \rho g sin(\theta)}$ and $\delta_c = \frac{\Gamma'}{\rho g sin(\theta)}$. The dimensionless equations are now just:

$$\frac{\partial^2 u_x *}{\partial y *^2} = 1 \ ; \ u_x * |_{y*=0} = 0 \ ; \ \frac{\partial u_x *}{\partial y *}|_{y*=\delta*} = 1$$

which has the simple quadratic solution

$$u_x * = y * - \delta * y * + \frac{1}{2} y *^2$$

The dimensionless flow rate per unit width is

$$\frac{Q}{W U_c \delta_c} = \frac{1}{2}\delta *^2 - \frac{1}{3}\delta *^3$$

This reaches a maximum at $\delta * = 1$ and is zero at $\delta * = 3/2$, so the scaling δ_c is a good measure of the appropriate film thickness. The dimensionless velocity at the surface of the film is just $u_x * |_{y*=\delta*} = \delta * - \frac{1}{2}\delta *^2$ so the dimensional surface velocity would be $U_c/2$ at the maximum film flow rate and $3/8\ U_c$ when the flow rate is zero.

To get quantitative estimates we would need to know the surface tension gradient. For a 15% by volume ethanol/water solution (the concentration of cooking sherry) the surface tension is approximately 45 dynes/cm. This is 25 dynes/cm less than that of pure water, thus (if the height of the film is 1cm) the maximum surface tension gradient could be 25 dynes/cm^2. This is an overestimation because additional components in the sherry would reduce the tension regardless of ethanol content, and not all the alcohol evaporates. Indeed, Venerus and Simavilla suggest that the typical change in ethanol content is much smaller, only around 1% by weight. This would yield a lower Marangoni stress of about 1.1 dynes/cm^2. The film depth scaling for this smaller value is only of order 10μm which is why the film itself is too thin to see. The visible ring is the result of the upward flow "piling up" and the legs or tears are attributed to the

Rayleigh-Plateau instability of this ring, the same mechanism that causes a stream of water to break up into drops.

Although it is beyond the scope of this demonstration, scaling can also be used to “close the loop” and estimate the surface tension gradient from the relationship between the gas film mass transfer coefficient, the characteristic velocity U_c, the film depth δ_c, and the dependence of surface tension on alcohol concentration. The effect of the mass transfer coefficient on the Marangoni stress is easily demonstrated, however: gently blowing on the wetted film causes a rapid increase in the film flow, sometimes even leading to a second ring of tears forming above the first.

References:

J. Thomson. On certain curious motions observable at the surfaces of wine and other alcoholic liquors. Phil. Mag. 10, 330–333 (1855).
https://doi.org/10.1080/14786445508641982

Venerus, D., Simavilla, D. Tears of wine: new insights on an old phenomenon. Sci Rep 5, 16162 (2015).
https://doi.org/10.1038/srep16162

A Rainbow of Skittles

Materials

1. A white or glass plate, flat or slightly depressed in the center
2. A bag of Skittles
3. A pushpin and a bit of carpet tape
4. A 400ml beaker or crystallizing dish
5. Distilled water

A classic children's demonstration is the pretty pattern that you can form from brightly colored Skittles dissolving on a plate. There are innumerable YouTube videos of the phenomenon. The procedure is simple: arrange the Skittles around the edges of the plate (with an appropriate color pattern) and then slowly add water to the center of the plate. As the water reaches the Skittles, they begin to dissolve, releasing their sugar and dye into the liquid. These form bands that flow toward the center of the plate.

The explanation of the effect is usually miss-described on the web as being solely due to diffusion. In fact, for this problem diffusion is principally important only in a very thin boundary layer adjacent to the candies. The correct explanation is that as the candies dissolve, releasing sugar into the water, the local density increases. This produces a buoyancy driven flow both around the candies and towards the center of the plate. The dye (which is at a concentration too low to affect the buoyancy) simply travels along with the sugar laden fluid. The bands remain separate because diffusion over the length scale of the band width is very slow: diffusion only plays a role over very short length scales in this problem.

There are a number of different demonstrations which can be done to illustrate this effect. Many plates are actually slightly concave up in the center. For such a plate the pattern initially forms regularly (in the downward sloped region) and then as it reaches near the center becomes unstable (and the motion greatly slows down). If the plate is inverted, the center is now convex and the pattern remains regular to the center and proceeds much more rapidly. A flat dish (such as a petri dish, below) also yields a regular pattern. A purely diffusive process would be relatively unaffected by such slight changes in geometry.

The dynamics of the dissolution process can be imaged by looking at a single skittle after immersion. This is easily done by pinning a Skittle with a pushpin and attaching it to the bottom of a crystallizing dish (useful because of the larger aspect ratio and flat

  

bottom) with a bit of carpet tape. Although it does not appear to greatly affect the dissolution process, fracture of the hard shell can be avoided by briefly heating the tip of the pushpin in a candle flame before insertion. The pinned Skittle is covered with an inverted small beaker, distilled water is added to the crystallizing dish sufficient to cover the candy, and the small beaker is carefully removed. This procedure is desirable to allow the initial swirls from adding the water to damp out as much as possible. Distilled water is used as tap water appears to cause micro bubbles to form once the sugar coat is breached, affecting the buoyancy driven flow. The dissolving layer is imaged from the side showing the flow of the dye around the Skittle, followed by the clear sugar solution after the dye coat is removed. The dissolving clear sugar is visible via refractive index variations showing the flow pattern. It is important to adjust the camera so that the area at the base of the Skittle is visible (e.g., observing it a bit from below) as it is the lower part of the pattern which is of greatest interest. A movie of this dissolution process is remarkable.

Quantitative calculations are also of use. The rate with which the Skittles dissolve is quite closely related to the classic problem of a dissolving spherical particle, important in pharmaceutical applications among others (e.g., Assunção et al., 2024). If the dissolution at the surface is “fast” (not kinetically limited), the solute is dilute, and the viscosity of the fluid is not significantly affected by the dissolving material, then this problem is actually identical to heat transfer from a heated sphere into a quiescent fluid. In that problem the Nusselt number (dimensionless heat transfer coefficient) is a function of the Rayleigh number and the Prandtl number. For mass transfer the Sherwood number (dimensionless mass transfer coefficient k_m) is the same function of the Rayleigh number analog $Ra_s = \dfrac{D^3 g \Delta\rho}{D_s \mu}$ and the Schmidt number $Sc = \nu / D_s$ rather than the Prandtl number (Churchill, 1983). The Rayleigh number analog is equivalent to that for heat transfer, where the thermal expansion driving force $\rho\beta\Delta T$ is replaced by $\Delta\rho$ (the difference between the solution density at the surface from that far away) and the thermal diffusivity is replaced by the molecular diffusivity D_s. This is also termed in the literature as the product of the Grashoff number and Schmidt number. The dimensionless mass transfer correlation defined in this way is, by analogy to heat transfer, given by:

$$Sh = \frac{k_m D}{D_s} = 2 + \frac{0.589\left[\frac{D^3 g \Delta\rho}{D_s \mu}\right]^{1/4}}{\left(1+\left(\frac{0.43}{Sc}\right)^{9/16}\right)^{4/9}}$$

Application of this to the dissolution of sugar is complicated by the very high solubility of sugar in water (about 200g of sugar in 100g of water), so it is hardly dilute. Finite concentration effects have been shown to modify mass transfer rates due to convection normal to the surface in the boundary layer (e.g., Acrivos, 1962). At high concentrations the viscosity is greatly increased as well, with the diffusivity similarly decreasing. For purposes of estimation, we shall take the surface concentration to be about 20% (the point where viscosity and diffusivity begin to diverge significantly from the dilute result) yielding a density difference at the surface of 0.08 g/cm^3. The diffusivity of sugar in water is 5x10^{-6} cm^2/s, so the Schmidt number is about 2000 for a dilute solution. Since the laminar momentum and mass transfer boundary layers scale as the square root of Sc, the velocity profile is some 40 times thicker than the solute profile - most of the convected fluid is actually sugar and dye free for laminar flow. For a candy with diameter of 1cm, the modified Rayleigh number is approximately 10^9, close to the point where the flow transitions from laminar to turbulent (e.g., Maestre, et al., 2021). Inserting these values into the Churchill correlation for the Sherwood number yields Sh ~ 10^2, so the steady-state mass transfer rate is some 50 times what would be expected from diffusion alone.

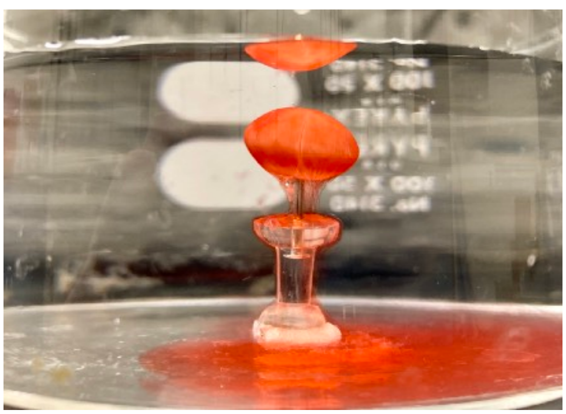

Quantitative application to dissolving Skittles is even more challenging. The candy is an oblate spheroid with major diameter of 1.27cm and minor diameter of 0.85cm. It consists of a thin hard sugar shell (approximately 700μm thick) surrounding the chewy core. The dye itself is confined to an even thinner layer on the surface of the shell, and there is a further insoluble protective coating on top of this on which the "S" is printed. The compositions and thicknesses of these layers are unfortunately proprietary. If a

Skittle is simply dropped into a beaker of water, the dyed layer appears to dissolve away in about a minute, with a visible downward flow at the base of the candy and the removed dye confined to a thin layer on the bottom of the beaker.

More specific information about the dissolution process may be obtained from close examination of the movie of the dissolving Skittle. Within 6 seconds of immersion the protective outer coat is disrupted, and after about 30s the insoluble coat has completely sloughed off. This is followed by dispersion of the dye and dissolution of the hard sugar shell. From images it is apparent that the Rayleigh number is indeed high enough to induce fluid instabilities in the wake region. The observed behavior and pattern is remarkably similar to studies of boundary layer separation and instability for natural convection around spheres (e.g., Schütz, 1963; Kitamura et al., 2015; and Lee & Chung, 2017). As in these experiments, at high Rayleigh numbers the boundary layer separates below the equator and the separated layer breaks into vortices which significantly increase the mass transfer coefficient in the wake region. For the Skittles, the time for the dye to locally vanish is roughly inversely proportional to the local mass transfer coefficient. Examination of the images suggests that the mass transfer coefficient is highest in the wake region and a minimum (longest dye persistence) near the separation region just below the equator in agreement with the measurements of Schütz at comparable Ra. While complicated by the sloughing of the protective coat, it appears that the ratio of the mass transfer coefficient in the wake region to that just below the equator is approximately a factor of 2. Comparison of this ratio to the measurements of Schütz for mass transfer from a sphere suggests that the equivalent Rayleigh number is approximately 1.5×10^9.

The separated sheet of dense, sugar laden fluid is unstable to a transverse disturbance with a wavelength of approximately 500μm. These vortices then form rivulets which further interact in the wake region and give rise to the higher mass transfer rate at the bottom (where the dye first disappears). Although more difficult to see, the rivulets persist in number and location even after the dye coat has completely vanished. While the rivulet formation mechanism and wavelength selection is less well described in the literature, it appears that the breakup of the sheet is a gravitational Rayleigh-Taylor type instability (e.g., Limat et al., 1992) rather than a Kelvin-Helmholtz shear instability, as the latter would lead to a vorticity axis perpendicular to the flow. The pattern formed closely matches what was observed by Kitamura et al. (2015) for heat transfer in water at a Rayleigh number of 1.7×10^9 (e.g., Figure 2.d of that paper). It is remarkable that this simple demonstration can qualitatively (and semi-quantitatively) capture such a complex phenomenon. In the class demonstration the dissolution of the Skittle is projected onto the screen and the observed behavior is compared to the flow pattern in Figure 2 of Kitamura and the dye disappearance rate to the spatially dependent Sherwood number measurements in Figure 6 of Schütz.

Whether the observed flow of the dye away from the Skittles on a plate is solely due to its own gravitational source of momentum or whether the subsequently dissolving sugar applies an additional stress to the surface of the dyed layer, dragging it towards the center of the plate or simply displacing it, is unclear as both processes likely play a role. In either case, however, the dye motion and pattern formation are primarily due to gravitationally driven flow rather than molecular diffusion as is often asserted. Diffusion is unimportant on the length scale of the Skittles for the short duration of the phenomenon.

In my class this demonstration is associated with a lecture on the derivation of the Prandtl boundary layer equations. I begin with the "rainbow" demonstration, and from scaling show that diffusion cannot lead to the pattern formation over the short duration of the experiment. This is followed with the demonstration of the dissolution of the Skittle on a pin. I then use scaling analysis of the mass and momentum transport equations in the boundary layer limit to obtain the dependence of boundary layer thickness on the Rayleigh number as well as an estimate of the fluid velocity in the boundary layer. At this point a recording of the same experiment is played for the class and the detailed features are discussed. A recording is particularly useful as it may be frozen at particular moments of the dissolution process and the recording also yields the time basis. These observations are compared to the results of Kitamura and Schutz, and the (very short) movie is played a final time.

References:

M. Assunção, M. Vynnycky, K. M. Moroney; Free-convective dissolution of a solid spherical particle. Physics of Fluids 1 April 2024; 36 (4): 043604.
https://doi.org/10.1063/5.0193605

Stuart W. Churchill (1983) "Comprehensive, theoretically based, correlating equations for free convection from isothermal spheres," Chemical Engineering Communications, 24:4-6, 339-352.
https://doi.org/10.1080/00986448308940090

Acrivos A. The asymptotic form of the laminar boundary-layer mass-transfer rate for large interfacial velocities. Journal of Fluid Mechanics. 1962;12(3):337-357.
https://doi.org/10.1017/S0022112062000257

Ismael Rodríguez Maestre, Juan José Gómez Sánchez, Francisco Javier González Gallero, Juan Luis Foncubierta Blázquez, Performance analysis of natural convection correlations for spheres at high Rayleigh numbers, International Journal of Thermal Sciences, Volume 168, 2021, 107061.
https://doi.org/10.1016/j.ijthermalsci.2021.107061

G. Schütz, Natural convection mass-transfer measurements on spheres and horizontal cylinders by an electrochemical method, International Journal of Heat and Mass Transfer, Volume 6, Issue 10, 1963, Pages 873-879, https://doi.org/10.1016/0017-9310(63)90078-4

K. Kitamura, A. Mitsuishi, T. Suzuki, T. Misumi, Fluid flow and heat transfer of high-Rayleigh-number natural convection around heated spheres, International Journal of Heat and Mass Transfer, Volume 86, 2015, Pages 149-157, https://doi.org/10.1016/j.ijheatmasstransfer.2015.02.081

Lee, DY., Chung, BJ. Visualization of natural convection heat transfer on a sphere. Heat Mass Transfer 53, 3613–3620 (2017). https://doi.org/10.1007/s00231-017-2097-1

L. Limat, P. Jenffer, B. Dagens, E. Touron, M. Fermigier, J.E. Wesfreid, "Gravitational instabilities of thin liquid layers: dynamics of pattern selection," Physica D: Nonlinear Phenomena, Volume 61, Issues 1–4, 1992, Pages 166-182. https://doi.org/10.1016/0167-2789(92)90160-O

Poiseuille's Law: A Funnel Viscometer

Materials

1. A small 60° glass funnel with long stem
2. A ring stand/clamp
3. Beakers for fluid
4. 90% by volume glycerin/water solution
5. A 25ml syringe
6. A stopwatch
7. A ruler

One of the most fundamental results in fluid mechanics is the relationship between pressure drop and flow rate for laminar flow in a circular tube, e.g., Poiseuille's Law. This is the basis for capillary viscometers, for example. In this demonstration it is shown how you can quantitatively measure the viscosity of a relatively viscous fluid using an ordinary funnel. The idea is to first pre-fill the stem of the funnel with the fluid to be measured, and then (with the flow stopped with a finger) inject a known volume into the top of the funnel. It is helpful to get a student volunteer to do this. The stopwatch is started by another volunteer when the flow is released and the time for the bowl at the top of the funnel to drain is measured.

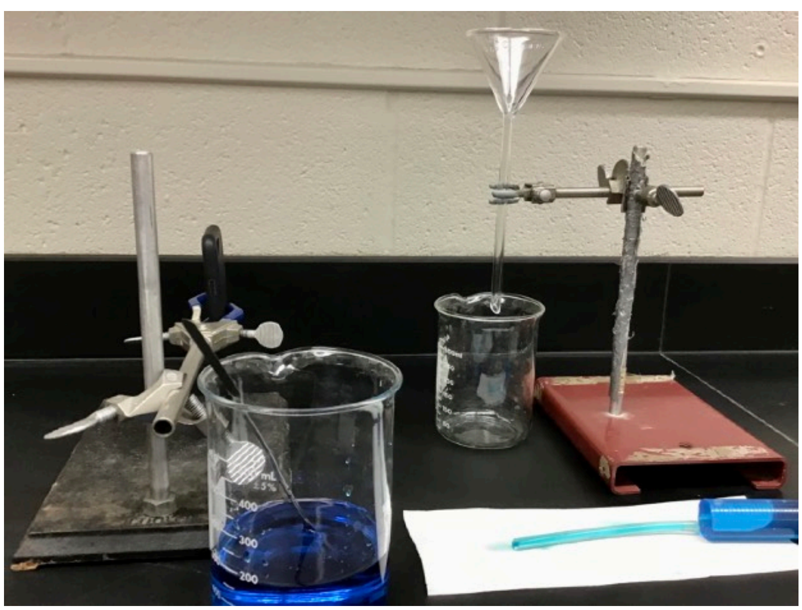

The drainage time depends on the fluid kinematic viscosity and the geometry of the system. Because the stem is of much smaller radius than the conical bowl, to a good approximation all the losses occur in the stem. If the height in the bowl is h and the stem length is L, then the head driving the flow is (h + L) which is a function of time. If this is dissipated over the stem of length L and radius R, then via Poiseuille's law the flow rate is just:

$$Q = \frac{\pi}{8}\frac{R^4 g}{\nu}\left(1 + \frac{h}{L}\right)$$

where ν is the kinematic viscosity. The filled volume of the conical bowl (with 60° cone angle) is $V = \frac{\pi}{9}h^3$ or initially $h_0 = \left(\frac{9V_0}{\pi}\right)^{1/3}$.

Thus we have a first order equation for the variation in filled height with time:

$$\frac{dh}{dt} = -\frac{3}{8}\frac{R^4 g}{\nu}\frac{1}{h^2}\left(1 + \frac{h}{L}\right)$$

Scaling h with the initial height h_0 (determined from the volume V_0) and t with an unknown scaling parameter t_c yields:

$$\frac{dh^*}{dt^*} = -\frac{\left(1 + \lambda h^*\right)}{h^{*2}} \;\; ; \;\; h^*|_{t^*=0} = 1$$

where $t_c = \frac{8}{3}\frac{\nu h_0^3}{gR^4}$ and $\lambda = \frac{h_0}{L}$.

The dimensionless drainage time t_d/t_c is just:

$$t_d^* = \frac{t_d}{t_c} = \int_0^1 \frac{h^{*2}}{\left(1 + \lambda h^*\right)} dh^* = \frac{\lambda(\lambda - 2) + 2ln(1 + \lambda)}{2\lambda^3}$$

The asymptotic value of this expression as $\lambda \sim 0$ is just 1/3 which is what would be obtained by ignoring the additional head produced by the fluid in the conical bowl. Combining this with t_c yields a simple way of calculating the kinematic viscosity ν from the drainage time t_d:

$$\nu = \frac{\pi}{24}\frac{t_d R^4 g}{t_d^* V_0}$$

For the thin stemmed funnel used in my demonstration (R = 0.219cm measured by volume and L = 14.3cm yielding t_d^* = 0.274 for V_0 = 25ml) with a 90% by volume glycerin and water solution (91.3 wt%) yielded a drainage time of 48.5s. This corresponded to a kinematic viscosity of 2.09 cm^2/s, fortuitously close to the expected value of 2.13 at 22°C for this concentration, particularly considering that the viscosity varies by about 7% per degree C and the temperature is not controlled. Because of the heat of mixing of glycerin/water solutions, the solution should be prepared well in advance of the demonstration so that it cools to room temperature. Also note that the calculated behavior is critically dependent on the measured stem radius. This is most accurately determined in the laboratory ahead of time by measuring the weight of water necessary to fill the stem.

It is useful to compare the behavior to what occurs if water is used instead of the more viscous glycerin/water solution. The calculated drainage time should be about 1/4 s based on the above expressions and the viscosity of water, however the measured drainage time is an order of magnitude greater (about 3 s). The reason for the discrepancy is that Poiseuille's law is not valid for the Reynolds number of the flow of the less viscous fluid, and in fact drainage is completely dominated by inertial effects. Ignoring viscosity entirely yields a characteristic drainage time of:

$$t_d \approx \frac{V_0}{Q} \approx \frac{V_0}{\pi R^2 (2gL)^{1/2}}$$

which is about a second for my funnel. Losses (initial transient, entrance effects, stem pipe friction factor, etc.) further increase this value.

References:

Bird, Stewart & Lightfoot, *Transport Phenomena*, rev 2nd ed., Wiley, 2007. Sec 2.3, p. 48-53.

Poiseuille's Law and the Milkshake

Materials

1. At least five small transparent plastic cups
2. Straws of varying length and diameters
3. A ruler
4. A large milkshake

In any transport course one problem is always done: laminar flow through a tube with circular cross-section. This, of course, results in Poiseuille's Law (or the Hagen-Poiseuille equation) relating pressure drop to flow rate for tubes of different geometries.

A class favorite is the demonstration of the very strong dependence of Poiseuille's Law on tube radius, and to a lesser extent on length. In this demo a large milkshake is divided evenly into about five cups, and student volunteers are paired up with other students who have a stopwatch (usually their iPhone). The goal, of course, is to see how long it takes each student to empty their cup. Before class it is necessary to measure the ID of the different types of straws being used. This is best done by a volume method: fill the straw with water, drain it out and measure the volume (or weight) of fluid. For the coffee straw (a fan favorite) it is necessary to do this a number of times to get a good measurement.

The suction pressure provided by each student is unknown, and the exact milkshake volume used is uncertain (although each cup is filled to the same amount), so quantitative calculation of the viscosity of the milkshake isn't practical. Instead I define a dimensional "Hunger Index" HI based on Poiseuille's Law:

$$HI = \frac{L}{R^4 \, t_d}$$

where t_d is the drainage time for each student.

There are quite a few limitations to the experiment, of course. The milkshake is prepared by freezing it overnight and then "warming it up" for about 20s in a microwave just before class, however it isn't clear that the milkshake is well approximated by a viscous Newtonian liquid. Corn syrup would be more reliable, but student volunteers would be scarce. It is also not clear that inertial effects are negligible. If dominated by inertia (for example, if it is too liquid), then there wouldn't be any dependence on straw length and the "Hunger Index" (essentially the suction pressure) should vary as $1/(R^4 t_d^2)$. Still, the strong dependence on radius (demonstrated by the struggles of the student with the coffee straw) is very clear.

References:

Bird, Stewart & Lightfoot, *Transport Phenomena*, rev 2nd ed., Wiley, 2007. Sec 2.3, p. 48-53.

Squeeze Flow

Materials:

1. Two circular 1/4″ glass plates, 9″ in diameter (obtainable from a commercial window dealer)
2. A small amount of glycerin
3. Food coloring
4. 5ml syringe
5. Light table
6. A transparent sheet marked with concentric circles.
7. A stopwatch

A classic demonstration of lubrication flows is the squeeze flow of a fluid between two glass disks. The diameter of the plates and thicknesses are not critical, but the weight of the top disk should be known. One of the disks is placed on the light box. Three ml of glycerin, dyed with food coloring, is deposited on the center of the lower disk using a syringe to precisely control the volume. A small amount of this fluid is "touched" to the center of the upper plate (this reduces bubble formation) and the upper plate is placed on the lower. Blocks are placed at the edges of the sandwich to prevent the upper plate from sliding sideways. Students are asked to record the time at which the expanding ring of fluid crosses each of the concentric rings. From lubrication theory, the radius of the expanding fluid should vary such that R^8 grows linearly in time. The observed behavior can be quantitatively compared to the results of a lubrication calculation.

This demonstration is very useful in communicating scaling analysis to students. In the lubrication limit the velocity profile is governed by the continuity equation and the viscous terms of the radial component of the Navier-Stokes equations in cylindrical coordinates:

$$0 = -\frac{\partial p}{\partial r} + \mu \frac{\partial^2 u_r}{\partial z^2} \quad ; \quad \frac{1}{r}\frac{\partial (r u_r)}{\partial r} + \frac{\partial u_z}{\partial z} = 0$$

The boundary conditions are:

$$u_r|_{z=0,H} = 0 \ ; \ u_z|_{z=0} = 0 \ ; \ u_z|_{z=H} = \frac{dH}{dt} \ ; \ p|_{r=R} = p_0$$

and the integral conditions:

$$\frac{dR}{dt} = \frac{1}{H}\int_0^H u_r|_{r=R}dz \ ; \ Mg = \int_0^R (p - p_0)\, 2\pi r dr \ ; \ V_0 = \pi R^2 H = \pi R_0^2 H_0$$

Scaling begins by equating the derivative of the fluid radius R with respect to time to the radial velocity at the outer edge of the fluid, averaged over the gap width. The force Mg on the fluid due to the upper plate is equated to the integral of the fluid pressure due to viscous fluid flow, and the gap width and radius are related to the volume of fluid deposited between the plates. Using this and scaling the continuity equation and radial component of the Navier-Stokes equations (in the thin gap limit), scaling alone determines the characteristic time. Solving the simplified equations yields the complete expression (and the constant).

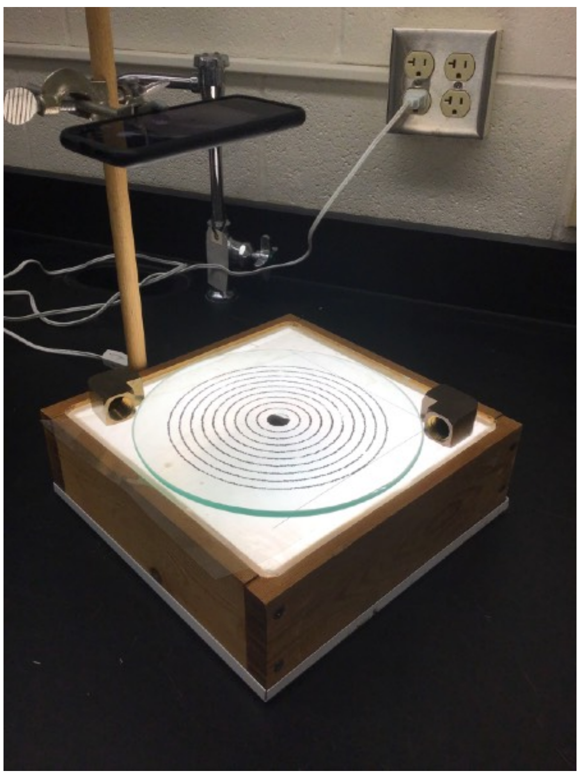

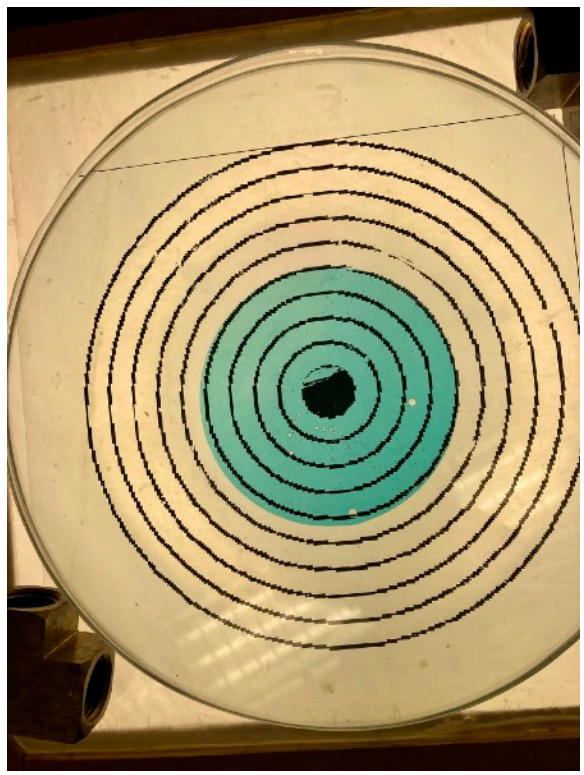

The exact relationship is:

$$R^{*8} = 1 + \frac{8}{3}t^* \quad \text{where } R^* = \frac{R}{R_0} \quad \text{and} \quad t^* = \left(\frac{V_0^2 Mg}{\pi^3 R_0^8 \mu}\right) t$$

This can be compared graphically to the data acquired in class using a short computer program. I have found that the R^8 dependence is accurately captured, however the constant is sometimes a bit off. This has been attributed to the warming produced by the light box and the high dependence of the viscosity of glycerin on temperature.

References:

Bird, Stewart & Lightfoot, *Transport Phenomena*, rev 2nd ed., Wiley, 2007. Example 3C.1, p. 110-111.

Detachment of a Disk Under a Constant Force

Materials:

1. A smooth glass or plastic disk with a paperclip attached to the center

2. Two large rubber bands

3. A ring stand with two horizontal bars

4. A flat glass or plastic plate.

5. A small quantity of glycerin.

5. A stopwatch

6. Particles 50μm, 100μm, and 325μm in diameter

This demonstration is closely related to the squeeze flow between two disks. Instead of having a ring of fluid expand, however, the detachment of a disk under constant force is examined as a function of initial separation. The demonstration is set up by attaching the rubber bands to the disk and threading them over the horizontal bars as depicted below (the lower bar is to limit motion when the disk "pops off"). A small quantity of glycerin is poured onto the glass or plastic plate, and a few particles of appropriate size are added. The disk is pressed into the fluid, stretching the rubber bands, until contact between the disk and the plate through the glass spheres is achieved. Contact can be felt by an increase in friction as the disk is pressed downwards and takes awhile for the smallest particles. The disk is then released, and the time necessary for the disk to "pop off" is measured. The weight of the lower plate must be greater than the force provided by the rubber bands (or the lower plate needs to be clamped). Lubrication theory shows that the time to detach is given by

$$t_\infty = \frac{3\pi}{4}\frac{\mu R^4}{H_0^2}\frac{1}{F}$$

where μ is the fluid viscosity, R is the disk radius, H_0 is the initial separation (determined by the particle size) and F is the force supplied by the rubber bands.

While the magnitude of the force can be measured (for a known stretch), it is much simpler to demonstrate the change in the detachment time for different size particles (and thus initial separations) for a constant force. Depending on the amount of stretch and disk radius, the 50μm initial separation will lead to a "popping off" in about 4 minutes, the 100μm separation will pop off in about a minute, and the 325μm spheres lead to detachment in a matter of seconds. Other diameter spheres can be used, of course, but 50μm is about the minimum practical - otherwise detachment with glycerin as the working fluid takes too long! This demonstration is useful to reinforce the scaling laws associated with lubrication flow, as everything except for the constant $3\pi/4$ can be determined from scaling alone. It also brings home the idea that small separations are critical in lubrication problems.

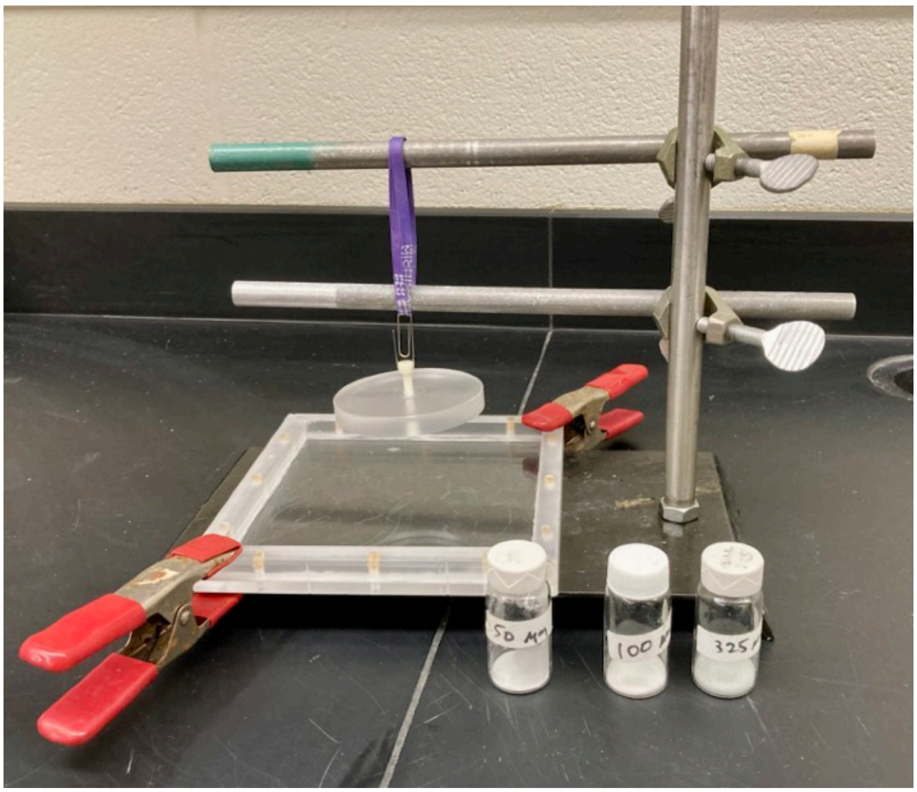

References:

Bird, Stewart & Lightfoot, *Transport Phenomena*, rev 2nd ed., Wiley, 2007. Example 3C.1, p. 110-111.

Squeeze Flow of a Non-Newtonian Fluid

Materials:

1. The glass plates and other materials in the previous demonstration.
2. About 100 g of 50μm glass spheres

In this demonstration the squeeze flow is repeated, but with a non-Newtonian suspension of glass spheres in glycerin. The 50μm glass spheres (typical density 2.5 g/cm^3) are added to the (dyed) glycerin to prepare a 40% by volume suspension (this should be done well in advance to allow bubbles to leave the suspension). The same experiment is performed. A number of key phenomena are observed. First, because of shear-induced migration the particles migrate away from the high shear stress regions at the plate surfaces and concentrate in the center of the gap (z direction) between the two plates. This, combined with the initially quadratic (in z) radial velocity profile, causes the flow average concentration of the outward flowing mixture to be higher than the volume average concentration, leading to an accumulation of particles at the advancing meniscus. This meniscus (visible as a colorless band around the expanding red fluid layer) is more viscous than the suspension in the interior, leading to the viscous fingering instability. The interface between the "colorless" meniscus layer and the interior fluid becomes very wavy, while the outer air/suspension interface (which is stable) remains fairly smooth.

There are many aspects of this demonstration that can be described to the students. The radius at which the meniscus layer first forms is the result of the shear-induced migration leading to the non-uniform concentration across the gap. The shear-induced diffusivity scales as $\dot{\gamma}a^2$ where $\dot{\gamma}$ is the characteristic shear rate and a is the particle radius. The dimensionless shear induced diffusivity for a 40% concentration suspension is about 1. The shear rate scales as U/b where U is the radial velocity and 2b is the gap width between the plates. The diffusion time t_D scales as $b^2/\dot{\gamma}a^2$, and the radius scales as Ut_D. Putting this all together, scaling analysis suggests that the radius at which the packed meniscus layer is first observable should be of order

$$R \approx \left(\frac{V_0^3}{(2\pi)^3 a^2} \right)^{\frac{1}{7}}$$

which agrees reasonably well with the experiment. The formation of the packed meniscus layer is the same phenomenon which has been shown to cause "capillary failure" for imbibing whole blood into very small capillaries via capillary wetting if the diameter of the capillary is too small (Zhou & Chang, 2005). The visually appealing instability of the meniscus layer at the suspension/meniscus interface is the same viscous fingering instability problem that occurs in oil recovery operations via water displacement (Homsy, 1987).

Students are directed to the paper by Ramachandran & Leighton (2010) for further details of the phenomenon.

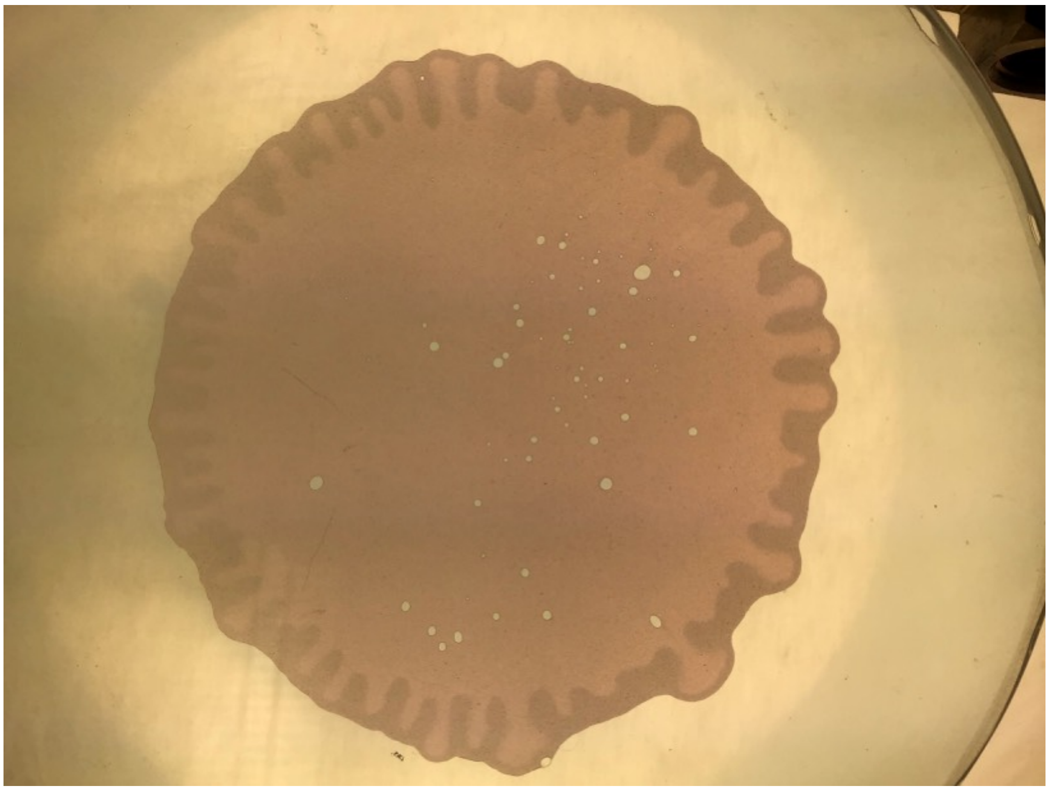

References:

Arun Ramachandran, David T. Leighton; Particle migration in concentrated suspensions undergoing squeeze flow. J. Rheol. 1 May 2010; 54 (3): 563–589. https://doi.org/10.1122/1.3372837

Ronghui Zhou, Hsueh-Chia Chang; Capillary penetration failure of blood suspensions. Journal of Colloid and Interface Science 287 (2005) 647–656. https://doi.org/10.1016/j.jcis.2005.02.023

G. M. Homsy; Viscous fingering in porous media. Ann. Rev. Fluid Mech. (1987) 19: 271-311. https://doi.org/10.1146/annurev.fl.19.010187.001415

Reynolds Dilatancy

Materials:

1. 9 inch balloon
2. 200 μm glass spheres
3. Tubing & rubber band
4. Water
5. Food coloring

Reynolds dilatancy is an important phenomenon in granular flow and an interesting demonstration of non-Newtonian behavior in suspensions. We have all experienced it when stepping on glistening sand at the beach: rather than the water bubbling up around your foot, instead the sand dries out. The explanation is that as a suspension is sheared, the particles exert a normal stress in order to pass over one another. Thus, it exhibits a normal stress difference with the normal stress being higher in the gradient direction than the vorticity direction (negative second normal stress differences). In granular flow this expansion leads to a decrease in the effective viscosity with shear and has a large impact on geophysical flows such as landslides.

In this demonstration Reynolds dilatancy is revealed with a simple balloon. Using a funnel the glass spheres are poured (dry) into a 9″ deflated balloon. It is useful to use glass in the 200-300μm range so that they are fairly fine but easy to remove bubbles from. Ordinary sand works too. After completely filling it up, water is added and the balloon is periodically squeezed to get the air bubbles out. A little food coloring is added to the water in the neck of the balloon and a short tube (I use ¼″ tygon tubing) is attached with a rubber band. Additional colored water is added to the tube via a syringe, and a wire is used to encourage the colored water to settle down the tube to the bottom. In demonstration students are asked what should happen to the level of water in the tube when you pinch the balloon – and they say that it should go up (as it does for a Newtonian fluid). Instead, of course, it goes down due to Reynolds dilatancy. The assembly is then passed around the class, and it continues to perform for a while before the glass spheres get squeezed into the tube (caused by squeezing too hard, which will usually occur).

References:

Osborne Reynolds (1885) LVII. On the dilatancy of media composed of rigid particles in contact. With experimental illustrations , The London, Edinburgh, and Dublin Philosophical Magazine and Journal of Science, 20:127, 469-481. https://doi.org/10.1080/14786448508627791

W. J. Mead, The Geologic Role of Dilatancy, J. Geology, Vol. 33, No. 7 (1925) p. 685. https://doi.org/10.1086/623241

Iverson, R. M. (2005), Regulation of landslide motion by dilatancy and pore pressure feedback, J. Geophys. Res., 110, F02015
https://doi:10.1029/2004JF000268

Dynamic Similarity of Vortices

Materials:

1. Stirring bars of different sizes
2. Beakers of different sizes
3. Glycerin
4. Water
5. A stirring plate with rotational speed indicator

The concept of preservation of dimensionless groups in scale up is core to many problems in chemical engineering. For strict dynamic similarity all dimensionless groups involved in a problem need to be preserved. For approximate dynamic similarity "key" dimensionless groups are preserved and others are kept in an appropriate range. For fluid mechanics problems involving a free surface (but where surface tension is unimportant) the dimensionless groups involved are the Reynolds number and the Froude number. Thus, if both are preserved the flow patterns should be identical. In this demonstration it is shown how a vortex produced by an impeller can be made identical at different length scales by preserving both of these dimensionless groups.

The characteristic velocity and length scale are based on the impeller angular velocity Ω and length L. The Reynolds and Froude numbers are thus:

$$Re = \frac{\Omega L^2}{\nu} \quad ; \quad Fr = \frac{\Omega^2 L}{g}$$

where ν is the kinematic viscosity. To preserve strict dynamic similarity angular velocities and kinematic viscosities of the two systems must scale as:

$$\Omega_2 = \Omega_1 \left(\frac{L_1}{L_2} \right)^{1/2} \quad ; \quad \nu_2 = \nu_1 \left(\frac{L_2}{L_1} \right)^{3/2}$$

It is convenient to choose water as the working fluid in the small beaker. The geometric ratios are preserved (as best possible), so the ratio of the stirring bar lengths to beaker diameters is kept constant. The exact choices depend on what stirring bars are available. For my demonstration I have bars of dimension 1.5cm x 0.5cm (3.0 aspect ratio) and 4.1cm x 0.8cm (5.1 aspect ratio). These aspect ratios aren't the same, but it is the best that I have been able to do with commercially available stirring bars. The small

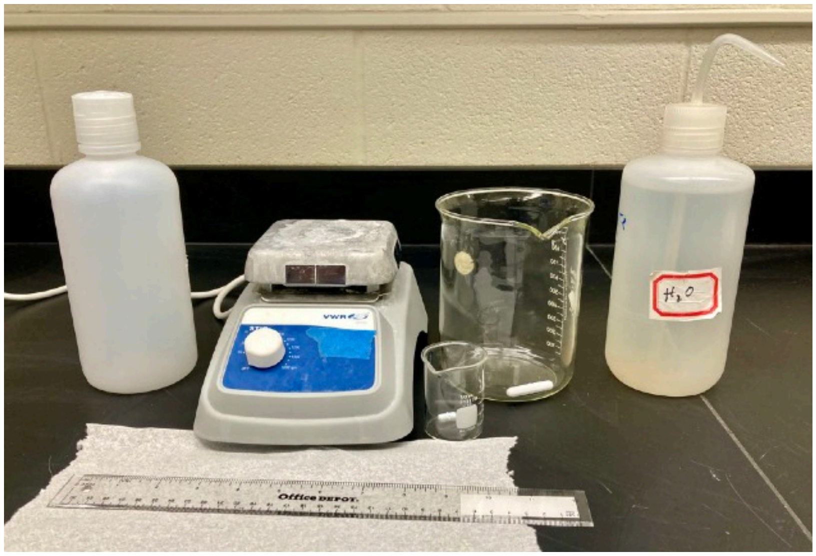

bar is used in a 50ml beaker (diameter 3.9cm, ratio to bar length 2.6) and the large bar is used in a 1000ml beaker (diameter 10.2cm, ratio to bar length 2.5). Water is used in the small beaker (ν = 1cs, volume = 40ml) and a 42% by volume glycerin/water solution is used in the large beaker (ν = 4.2cs, volume = 750ml). A rotation rate of 1280 rpm in the small beaker causes the vortex to reach half-way to the stirring bar, and corresponds to a rotation rate in the large beaker of 775 rpm for strict dynamic similarity based on the stirring bar lengths. Note that because the bar aspect ratio isn't kept perfectly constant, mixing would likely be a little bit stronger with the smaller scale beaker (a slightly thicker bar). This again illustrates one of the experimental challenges with strict dynamic similarity.

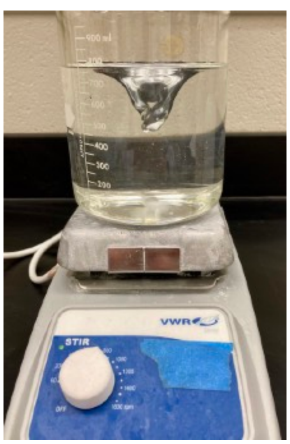

4.2 cs fluid
Fr = 13.8, Re = 8120

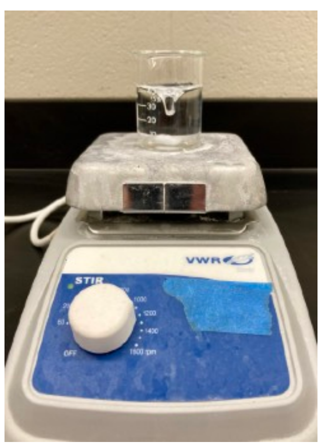

1.0 cs fluid
Fr = 13.7, Re = 7540

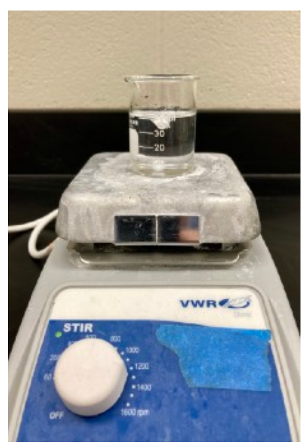

4.2 cs fluid
Fr = 13.7, Re = 1800

4.2 cs fluid
Fr = 18.8, Re = 2100

After demonstrating strict dynamic similarity, it is useful to explore approximate dynamic similarity. This is done by replacing the water in the small beaker with the glycerin/water solution from the large beaker. At the same rotation speed the Reynolds number would decrease by a factor of $(L_1/L_2)^{3/2} = 4.2$, but the Froude number would remain unchanged. The slight difference in behavior illustrates the effect of Re on the vortex, and (since Re is still "high") the concept of approximate dynamic similarity (preserving Fr but keeping Re "high", as is done in ship design for example). In the original case (for our conditions) Re = 7540 and Fr = 13.7 based on the bar half-length (e.g., impeller tip speed and radius), thus the vortex behavior is dominated by the Froude number. With the more viscous fluid, however, the Reynolds number decreased to 1800 which is apparently low enough that it is no longer "sufficiently high": the dimple of the vortex only reached a quarter of the way to the impeller. The rotation rate needed to be increased to 1500RPM (Fr = 18.8) to achieve the original vortex depth.

References:

Bird, Stewart & Lightfoot, *Transport Phenomena*, rev 2nd ed., Wiley, 2007. Ex. 3.7-2, p. 101-103.

Enzo O. Macagno, "Historico-critical review of dimensional analysis," Journal of the Franklin Institute, Volume 292, Issue 6, 1971, Pages 391-402, https://doi.org/10.1016/0016-0032(71)90160-8

Formation and Breakup of a Toroidal Drop

Materials

1. 500ml graduated cylinder
2. 1 liter bottle for mixing
3. 1ml plastic syringe
4. Glycerin and water
5. Food coloring
6. Several 50ml beakers

A visually appealing demonstration is the formation of a torus and its subsequent breakup when a miscible drop falls through a viscous fluid. Originally described by Thomson (1886), this phenomenon has more recently been studied by Kojima et al. (1984), Machu et al. (2001) and Pignatel et al. (2011) among others. The demonstration is quite simple: a 500ml graduated cylinder is filled with a glycerin/water mixture, and a small amount of this with a slightly higher glycerin concentration is dyed with food coloring and placed in the 50ml beaker. A 1 ml plastic syringe (with the tip cut off and plunger removed) is dipped into the dyed solution and filled to a desired volume, and it is then dripped into the cylinder from a height of 3cm. The resulting drop initially deforms into a torus, which subsequently expands and eventually breaks up via the Rayleigh-Taylor instability to form two (or more) daughter drops. These form additional tori and the process is repeated in a cascade. The key is to determine the combination of fluids which will result in the desired behavior in the 500 ml graduated cylinder that is easily used in the classroom.

The mechanism which produces an expanding torus from an initially spherical drop is generally associated with inertia (finite Re effects) as, for a symmetric torus, Stokes flow reversibility shows that it cannot expand or contract. Machu et al., however, showed that if there is initial asymmetry in the torus as a result of the injection procedure, then expansion is not forbidden even at zero Re. The experiments described in the literature are generally done with a much larger system (total height) than could be accommodated in a classroom demonstration, so it is necessary to determine how the expansion and breakup height depends on fluid and drop properties. Reexamination of the data of Kojima et al., and Pignatel et al., provide an interesting example of how dimensional analysis alone can be used to collapse experimental data and make useful predictions.

To perform the dimensional analysis we shall assume that surface tension effects are absent (appropriate for the suspension drop experiments of Pignatel, although Kojima argues that for liquid drops there is a transient surface tension despite miscibility), and that the breakup height H is a function of the undeformed drop radius a, the drop and fluid densities and viscosities, and gravity. The diameter of the cylinder is taken to be sufficiently large that it does not affect the breakup height. For these simplifying assumptions we obtain:

$$H = f^n \left(a, \rho_d, \rho_f, \mu_d, \mu_f, g \right)$$

There are three independent fundamental units, thus from the Buckingham ∏ theorem we obtain:

$$\frac{H}{a} = f^n \left(\frac{\rho_d}{\rho_f}, \frac{\mu_d}{\mu_f}, Re_c \right)$$

where $Re_c = \frac{\left(\rho_d - \rho_f\right) g a^2}{\mu_f} \frac{a \rho_f}{\mu_f}$ is the characteristic Reynolds number of the falling drop based on the Stokes sedimentation velocity. This is also known as the Archimedes number Ar and is used in the analysis of fluidized beds. If the difference in drop and fluid densities is small, then the drop density only appears in the buoyancy term. Thus, we may strengthen the result:

$$\frac{H}{a} = f^n \left(Re_c , \frac{\mu_d}{\mu_f} \right)$$

The experiments of Kojima were conducted with miscible drops in a corn syrup/water solution, and reported a ring expansion rate and torus sedimentation velocity. The experiments of Pignatel were conducted with drops composed of dilute suspensions of microparticles in the same fluid as the base fluid, and reported a ring breakup time (defined as when the tori were observed to have a significant bend). Using an average of the tori velocities reported by Kojima and that of an undeformed drop (to approximate the evolution) it is possible to convert both of these times to the desired heights, which were not reported in either study. Plotting up the data of Kojima and Pignatel in this manner (and ignoring the effect of viscosity ratio) it is observed that the breakup height is a decreasing function of Re_c (as would be expected from an inertial expansion mechanism) but that intriguingly it is fit by an approximate $Re_c^{-1/3}$ relationship over the range of experiments from $0.02 < Re_c < 2$. Like many such power-law empiricisms (e.g., the Blasius correlation for the dependence of pipe friction factors on Reynolds numbers), this approximate relationship is valid only over the range of

Reynolds numbers supported by the data. The $Re_c^{-1/3}$ relationship is very useful, however, because it suggests that the breakup height is insensitive to the drop size. Empirically, then, we observe that:

$$H \approx 136 \left(\frac{\mu_f^2}{\Delta\rho g \rho_f} \right)^{1/3}$$

provided that the drop viscosity ratio is close to unity. Note that the parameter range of these experiments and empirical curve fit is quite different from more recent work on droplet fracture (e.g., Nakajima and Hayashi, 2022) which focuses on Re_c of O(100) and thus would not be applicable to those results. It would also not be applicable to the zero Re calculations of Machu, et al.

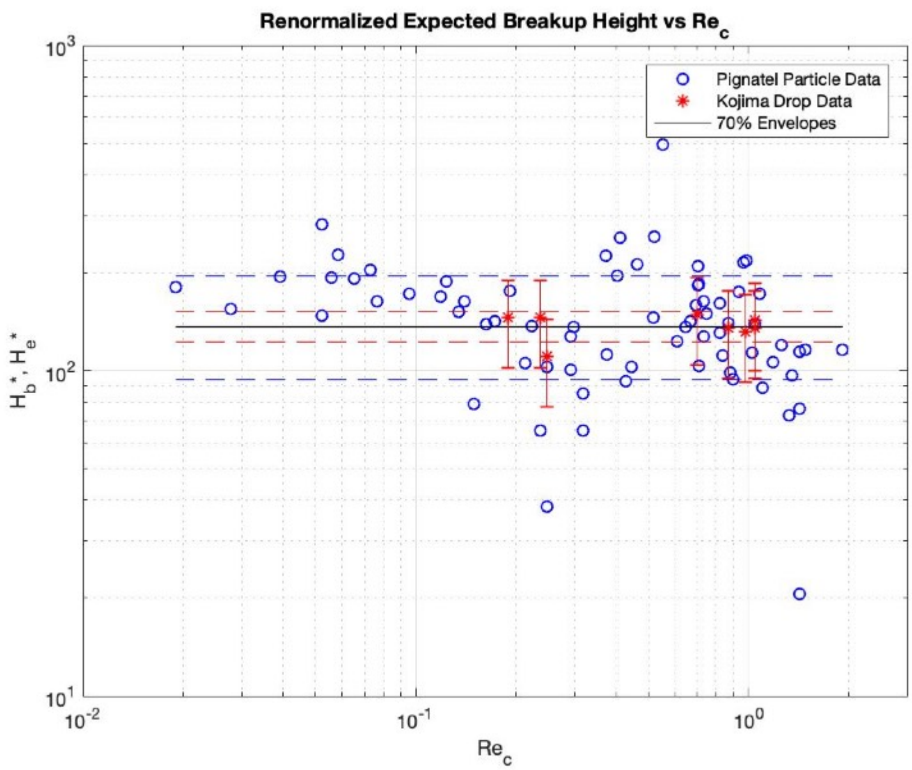

It is now possible to use the results of the dimensional analysis and empirical fit to the data to design the demonstration. It is desirable to have a breakup height great enough so that the transition is clearly visible, yet short enough that a cascade of breakups is also visible. For a 500ml graduated cylinder with a working height of 34 cm an attractive fluid is a 75% by mass glycerin/water solution yielding a viscosity of 0.28 poise. The concentration of the drop phase would need to be higher, up to about 90% for a viscosity ratio of 5. Predicted breakup heights based on this combination range from 16 to 30 cm. In laboratory tests of the demonstration it was found that this simple empirical relationship worked quite well for base fluids ranging from 70% to 80% and drop fluids from 75% to 85% glycerine. It was observed that higher viscosity ratios (resulting from drop concentrations of 90% and above) did not greatly affect the ring expansion, but did appear to delay the Rayleigh-Taylor instability which requires drainage along the ring. This led to large, thin rings at breakup and somewhat greater breakup heights than predicted. In a student-led follow-on demonstration, drops of the base fluid with salt added to yield the density (but not the viscosity) of a 95% glycerin solution were found to match the empirical prediction.

A fluid composition of 75wt% (70.4% by volume) and a droplet composition of 85wt% is an optimal combination for a classroom demonstration, yielding a viscosity ratio of 2.8 (not too large) and a density difference of 0.027 g/cm^3, with a predicted breakup height of 18 cm. Observed breakup heights ranged from 15 to 21 cm. This droplet composition can be easily prepared by combining 20g of the base fluid with 13.3g of glycerin. In contrast, if a somewhat higher glycerin composition for the base fluid is used (e.g., a mass fraction of 0.85, yielding a viscosity of 0.79 poise), then the predicted breakup height would exceed the height of a 500ml cylinder for all drop glycerin concentrations. A lower base fluid glycerin concentration of 65wt% (viscosity of 0.12 poise) would yield very short breakup heights and times, to the point where visualization of transitions would be difficult to distinguish from drop entrance effects.

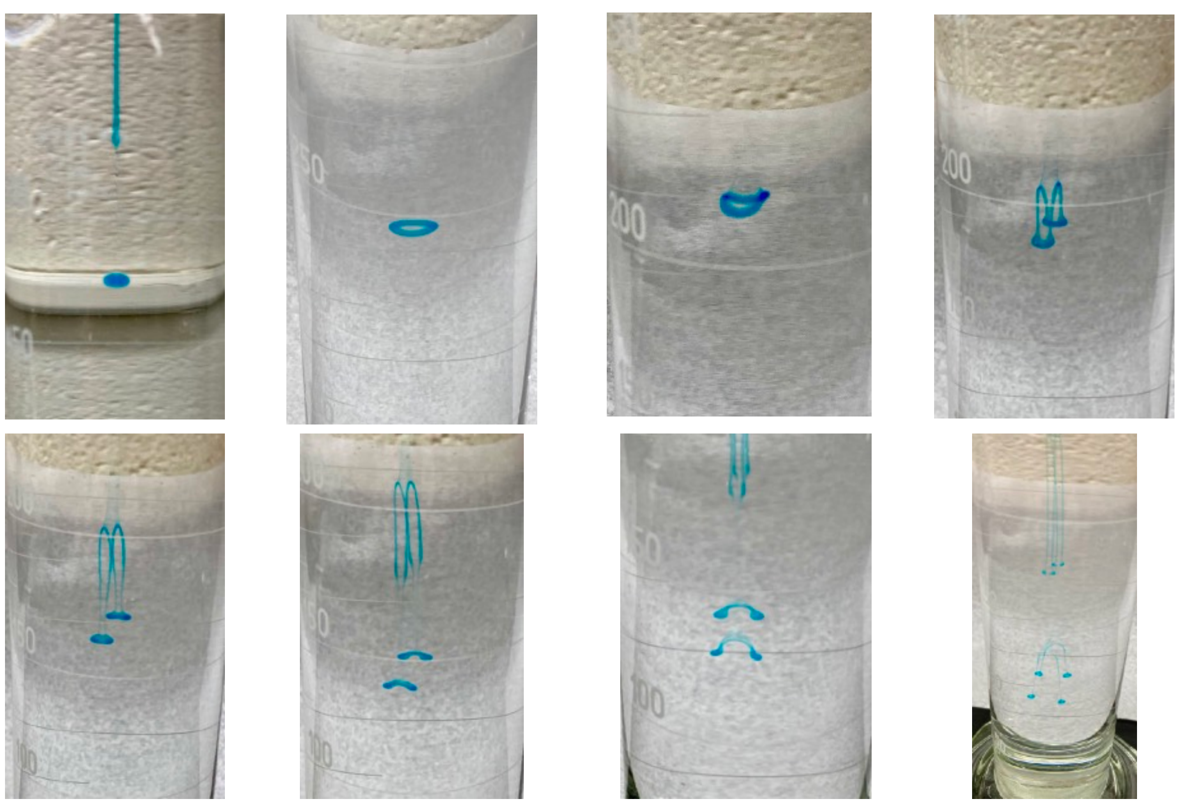

For this choice of fluid and drop compositions, a 0.1 ml drop has a diameter of 0.58 cm, a spherical drop Stokes velocity of 1.9 cm/s, and a Re_c of 2.5. The latter is somewhat greater than the values explored by Kojima, and just a bit larger than suspension drops (in what they termed the macro-inertial range where inertia is insignificant at particle length scales) examined by Pignatel. It would be expected to break up in about 12 seconds, all reasonable values for a demonstration. A 500ml graduated cylinder is of sufficient height to observe a secondary breakup cascade as well. A smaller drop would put it in the same Re_c range as those of Kojima, who used drops as small as 0.03 ml, however too small a drop becomes both difficult to see in a demonstration and to administer in a controlled manner without more extensive equipment than simply dripping from a tube. More viscous base fluids such as employed by Kojima would reduce the Reynolds number as well, but at the cost of increasing the height required for breakup.

It is important to note that the breakup height is quite sensitive to the fluid viscosity, varying approximately as $\mu_f^{2/3}$, which in turn is sensitive to the temperature. Because of the heat of mixing of glycerin/water solutions, mixing alone results in a temperature increase of 4°C. Thus, a freshly mixed solution may yield a different breakup height than one which has been cooled overnight in the laboratory. If the temperature decreases by 5°C, for example, the predicted height to breakup would increase by over 20%. Since classroom temperature often varies, it is a good idea to bring a bit of water. If the breakup is found to occur too far down the graduated cylinder, simply pour the base fluid solution into the mixing bottle, add a small amount of water (about 20 ml is sufficient) and then pour it back in. The decrease in viscosity due to the increase in water content and a small temperature rise due to heat of mixing significantly shortens the breakup height and should allow the secondary cascade to be observed.

In the demonstration it is possible to test some of the aspects of the predictions obtained from dimensional analysis. The insensitivity to drop size can be verified by using larger and smaller drops. Larger drops travel more quickly, but break up at about the same height (a larger diameter dropper is useful here). The dependence on the density difference is demonstrated by combining 10ml of the dyed drop fluid with 30ml of the base fluid in a second 50ml beaker yielding a 77.5wt% solution. This would be predicted to break up only close to the bottom of the cylinder due to the lower Reynolds number, and the difference is observable - although there is a lot of scatter in the experiment! Other things can be tried as well, such as adding drops in succession and observing their interaction (e.g., Lim, 1997). This is a good demonstration for student volunteers to try out, and the results are projected onto the classroom screen.

References:

Thomson, J.J. and Newall, H.F., 1886. V. "On the formation of vortex rings by drops falling into liquids, and some allied phenomena." Proceedings of the Royal Society of London, 39(239-241), pp.417-436.
https://doi.org/10.1098/rspl.1885.0034

Masami Kojima, E. J. Hinch, Andreas Acrivos; "The formation and expansion of a toroidal drop moving in a viscous fluid." Phys. Fluids 1 January 1984; 27 (1): 19–32.
https://doi.org/10.1063/1.864511

Machu G, Meile W, Nitsche L, Schaflinger U. "Coalescence, torus formation and breakup of sedimenting drops: experiments and computer simulations." Journal of Fluid Mechanics. 2001; 447:299-336.
https://doi.org/10.1017/S0022112001005882

Pignatel F, Nicolas M, Guazzelli É. "A falling cloud of particles at a small but finite Reynolds number." Journal of Fluid Mechanics. 2011; 671:34-51.
https://doi.org/10.1017/S0022112010005501

Rina Nakajima, Kosuke Hayashi, "Fragmentation of drops falling through a miscible liquid with and without drop–drop interactions," International Journal of Multiphase Flow, 2022; 153:104134.
https://doi.org/10.1016/j.ijmultiphaseflow.2022.104134

T. T. Lim; "A note on the leapfrogging between two coaxial vortex rings at low Reynolds numbers." Physics of Fluids 1 January 1997; 9 (1): 239–241.
https://doi.org/10.1063/1.869160

Bubbles and Antibubbles

Materials:

1. 1 liter beaker
2. 400ml beaker
3. 50ml beaker
4. Dawn dishwashing liquid
5. Sugar packets
6. 1ml disposable syringe
7. Spatula
8. Water
9. Food coloring
10. Soap bubble kit and tape measure

Soap bubbles – where a thin liquid separates air inside and out – are, of course, common childhood toys. What this demonstration does is look at the opposite: where an air sheath forms a spherical shell around water. The fascinating part is that the "antibubble" looks nearly identical to an ordinary bubble in water, but it is (nearly) neutrally buoyant and when it pops the air bubbles produced are of very small volume - it essentially disappears.

The basis for this demonstration is the paper by Kim & Stone (2008) who describe optimal conditions for the creation of antibubbles, as well as the reasons why such optimal conditions occur. The procedure is as follows. First, add 900ml of tap water to the 1 liter beaker and then using the 1ml syringe inject 1.8 ml of the dishwashing liquid (Dawn 50% less scrubbing) below the surface of the water. Note that the required amount depends on the detergent used. Kim & Stone recommend half this amount of Dawn Ultra, for example. Mix it thoroughly using a spatula, but endeavor not to create foam at the surface. Pour off 200ml into the 400ml beaker and add a packet (2.6g - although you need to check and adjust volumes accordingly, as this varies by manufacturer!) of sugar. Stir this solution well, and then pour a fraction of this mixture into the smallest beaker, using a paper towel to trap the foam. Rinse out the syringe (the residue in the 400ml beaker is good for this) and remove the plunger. Dip the syringe into the small beaker filling it to about 0.1 to 0.2ml, holding the liquid in by plugging the back with a finger. Carefully hold the syringe vertically over the large beaker so that the tip is about 1 cm above the surface and release the liquid. It takes a little practice, but after awhile about half the time you get an antibubble. The sugar is sufficient to make the larger antibubbles negatively buoyant, allowing them to sink to the bottom where they pop. Smaller antibubbles which are sometimes formed rise to the surface.

A useful way to begin this demonstration is to start with an ordinary soap bubble kit (waving the wand about to make big ones) and then proceed to the antibubbles. After demonstrating that the antibubbles look about the same as ordinary bubbles, one drop of food coloring can be added to the small beaker. The antibubbles now contain the dyed liquid (rather pretty) and produce interesting patterns when they pop. The bubbles are small, so the image of the beaker is projected onto the screen. Students should also be asked to come up and give it a try.

Because the sugar concentration (1.3 wt%, 0.005 g/cm^3 increase in density) is sufficient to make the 0.1ml bubbles approximately neutrally buoyant, it is possible to calculate the thickness of the air film. For a neutrally buoyant antibubble the thickness is related to the volume by:

$$\Delta\rho \frac{4\pi}{3} R^3 = \rho 4\pi R^2 \delta \;\text{ or }\; \delta = \frac{\Delta\rho}{\rho}\frac{R}{3} = \frac{1}{3}\frac{\Delta\rho}{\rho}\left(\frac{3V}{4\pi}\right)^{1/3}$$

For these bubbles (2.9mm radius) it works out to about 5μm.

Once the antibubble calculations are complete, it is useful to return to the ordinary soap bubbles and determine their thicknesses as well. While the soap films can be studied via interference patterns, they are also amenable to measurement via transport. Waving the wand in the air, have students determine the amount of time for a bubble to fall from a height of 2 meters to the ground. A typical bubble can also be captured on the wand and the diameter measured, and from this information and the kinematic viscosity of air (0.15 cm^2/s) the Reynolds number can be determined. A typical value is about 2000, placing it in the inertial regime with a drag coefficient of about 0.44 (e.g., Bird et al., 2007). From a force balance, the bubble film thickness can easily be calculated from the velocity. The force balance is:

$$\rho_{water} g \; 4\pi R^2 \delta = C_D \frac{1}{2} \rho_{air} U^2 \; \pi R^2$$

yielding:

$$\delta = \frac{C_D}{8} \frac{\rho_{air}}{\rho_{water}} \frac{U^2}{g}$$

The density ratio of air to water is about 0.0012. For the soap solution and wand used in my demonstration, the velocity (~50cm/s) and thickness (~1.6μm) were fairly large.

Note that it is important to make the air bubbles by waving the wand through the air (capturing room air) rather than blowing through the wand (capturing breath). This is because the exhaled density of breath is significantly different from room air due to higher temperature, humidity, and CO_2 content. The increased temperature and humidity decrease the density, while the higher CO_2 content increases it. Correcting for the buoyant force yields the modified force balance:

$$\left(\rho_{breath} - \rho_{air}\right) g \frac{4\pi}{3} R^3 + \rho_{water} g \; 4\pi R^2 \delta = C_D \frac{1}{2} \rho_{air} U^2 \; \pi R^2$$

or

$$\delta = \frac{C_D}{8} \frac{\rho_{air}}{\rho_{water}} \frac{U^2}{g} + \frac{\rho_{air} - \rho_{breath}}{\rho_{water}} \frac{R}{3}$$

Exhaled air has been reported to be saturated at a temperature of 34°C (Höppe, 1981) with a density of 1.15 kg/m^3 (Gao & Nu, 2006), about 5% less than inhaled air. For a bubble with radius R = 4 cm, this yields a correction to the film thickness of 0.8μm, comparable to the film thickness measured from the bubble velocity. In practice, the density of the air inside the bubble would lie somewhere between that of breath and room air due to entrainment, however the correction (while uncertain) is significant. In demonstration bubbles can be created both ways, and the ones produced by waving the wand fall noticeably faster, however the film thickness is also likely affected by the generating process.

References:

Kim, P. G., & Stone, H. A. (2008). Dynamics of the formation of antibubbles. EPL, 83(5), Article 54001.
https://doi.org/10.1209/0295-5075/83/54001

Bird, Stewart & Lightfoot, *Transport Phenomena*, rev 2nd ed., Wiley, 2007. Sec 6.3, p. 185-187.

Höppe, P. Temperatures of expired air under varying climatic conditions. Int J Biometeorol 25, 127–132 (1981).
https://doi.org/10.1007/BF02184460

Gao N, Niu J. Transient CFD simulation of the respiration process and inter-person exposure assessment. Build Environ. 2006 Sep;41(9):1214-1222.
https://doi.org/10.1016/j.buildenv.2005.05.014

Benard-Marangoni Instability

Materials:

1. Petri dish
2. Mineral Oil
3. 400μm dyed acrylic spheres
4. Small beaker
5. Hot plate

Marangoni instabilities driven by surface tension gradients arising from either solvent evaporation or temperature gradients are both interesting and industrially important. In this demonstration the flow pattern produced by the Benard-Marangoni instability is visualized using dyed acrylic spheres. In a small beaker a quantity of dyed acrylic spheres (the ones I use from my laboratory have been dyed by boiling in black RIT fabric dye and subsequently rinsed) is mixed with 20ml of mineral oil. The mixture is then poured into a petri dish (about 12 ml, yielding a depth of 1.8mm) and the particles settle to the bottom. The hot plate is turned on (a setting 3/10 worked for my heater) and the pattern quickly forms. The particles are drawn into the upwelling center of each circulation cell. After a short period the motion of most of the particles ceases, however if some of the particles have air bubbles in them (and thus are neutrally buoyant or positively buoyant) the fluid motion can still be observed.

The Benard-Marangoni instability has been studied for well over a century. It is susceptible to linear stability analysis much like the closely related Benard-Rayleigh instability, and it has been shown that the convective pattern will appear if the Marangoni number exceeds a critical value of 48 (Pearson, 1958) depending on the exact details of the thermal boundary condition at the upper surface. The Marangoni number is:

$$Ma = \frac{\frac{\partial \Gamma}{\partial T}\Delta T d}{\mu\alpha} = \left(\frac{d^2}{\alpha}\right)\left(\frac{\frac{\partial \Gamma}{\partial T}\Delta T}{\mu d}\right) = \frac{t_{dif}}{t_{conv}}$$

where Γ is the surface tension, ΔT is the temperature differential across the fluid, d is the film thickness, and μ and α are the dynamic viscosity and thermal diffusivity, respectively. The Marangoni number can be most easily understood as a ratio of the thermal diffusion time $t_{dif} = d^2/\alpha$ to the surface tension driven convective time scale

t_{conv} (the inverse of the characteristic shear rate at the surface). If the convection time scale is short relative to this diffusion time, the Marangoni number is large and convection sets in. If the thermal diffusion time is short, however, the temperature gradient (and resulting surface tension gradient) at the surface is suppressed and the fluid layer remains stable. For this demonstration the temperature is not well-controlled, thus quantitative analysis is not practical.

References:

Pearson JR (1958) On convection cells induced by surface tension. J Fluid Mech 4:489–500.
https://doi.org/10.1017/S0022112058000616

Double-Diffusive Convection Instability

Materials:

1. 600ml beaker
2. 400ml beaker
3. 3ml syringe
4. Funnel
5. Styrofoam block
6. Glycerin and water
7. Food coloring
8. Hot plate with gloves and eye protection

The double-diffusive convection instability arises due to the difference in the diffusion coefficient of energy and mass. In the ocean, for example, if a hot salty fluid overlays cold fresh water (usually caused by the intrusion of cold water from rivers or glacial melt) then the two layers are initially stably stratified. Because mass transfer is slow, however, as the salty fluid cools and the fresh water warms the densities are reversed and the interface between the two layers becomes unstable. This leads to salt fingers penetrating into the lower fluid, yielding much more rapid transport of mass (and nutrients) in the ocean than would otherwise occur. A good description of this phenomenon and its implications for geophysical systems is found in the article by Huppert & Turner (1981).

In this demonstration we use two glycerin-water solutions of slightly different densities to visualize the effect. The higher viscosity of the solutions slows things down enough to enable formation of the initial interface on the short length scale necessary for a classroom demonstration. In the 600ml beaker 300ml of glycerin and 100ml of water are combined. 300ml of the mixed solution is poured into the 400ml beaker and reserved (this will form the lower fluid). About 5 drops of food coloring are added to the remaining 100ml of fluid, which is then heated on the hot plate to about 50°C. While this is heating, 3ml of water is added to the reserved fluid and mixed. The colored fluid is removed from the heater, placed on the Styrofoam block, and the camera is adjusted to focus on the bottom of the beaker. Using the funnel, the reserved (cold) fluid is quickly added to the bottom of the colored layer, taking care to minimize the introduction of any bubbles. The instability shows up right away, however the plumes of the (now cooling) colored fluid are quite visible.

For this combination of fluids, the density difference at room temperature is 0.002 g/cm^3 with a viscosity of 0.48p. The coefficient of thermal expansion is $6x10^{-4}$ °C^{-1}, so a temperature difference of 28°C would yield an initial density difference an order of magnitude greater than that due to the concentration.

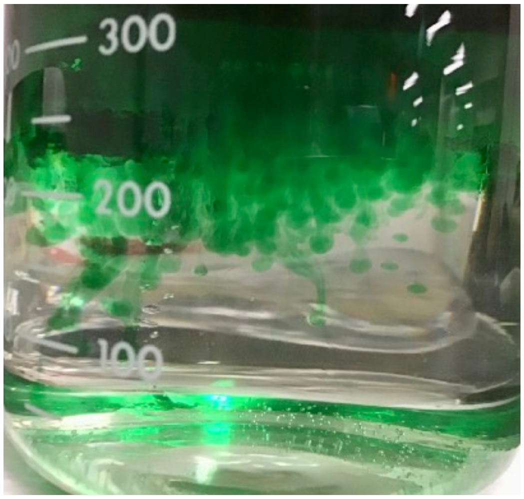

References:

Huppert HE, Turner JS. Double-diffusive convection. Journal of Fluid Mechanics. 1981;106:299-329.
https://doi:10.1017/S0022112081001614

Fractal Breakup of a Drop

Materials:

1. Triton X-100
2. Food coloring
3. Petri dish

Dendritic fractals are found in many examples in nature: the frost pattern which forms on a cold surface is a classic example. Here we have a very simple demonstration which produces a beautiful fractal dendrite in seconds. A small amount of Triton X-100 is put in a petri dish, and a drop of food coloring is dripped onto the surface. Initially the drop spreads out uniformly, however the interface rapidly becomes unstable leading to multiple generations of dendritic fractals. A second drop can be added, producing a rapidly cleared surrounding region before it too becomes unstable and forms dendrites.

The precise explanation for this effect is unclear, although it is obviously driven by surface tension gradients. Triton X-100 is slightly more dense than the dye, thus the dye floats as a disk on the surface. The two fluids are miscible, however the rheology of Triton/water solutions is complex. Notably, the addition of a small amount of water increases the viscosity of Triton, with the mixture forming a gel at a 50/50 ratio. Thus, at the interface below the drop disk the viscosity would be (at some point) very high. The pattern formed is similar to the phenomenon of "dendritic art" recently analyzed by Chan and Fried (2024) in which a painting is created by dripping an isopropyl alcohol and ink solution onto a diluted acrylic paint substrate, although in the case of

this demonstration the cleared regions suggest that the surface tension is undergoing a local minimum.

A note of caution regarding the use of Triton X-100: While it is still widely used in the United States, particularly in the pharmaceutical industry, breakdown products have recently been shown to be endocrine disruptors in environmental systems. Thus, in the European Union it is now only permitted for research purposes. The small amount of Triton used in this demonstration should be disposed of as hazardous waste.

References:

San To Chan, Eliot Fried, Marangoni spreading on liquid substrates in new media art, PNAS Nexus, Volume 3, Issue 2, February 2024, pgae059.
https://doi.org/10.1093/pnasnexus/pgae059

The Boycott Effect

Materials:

1. Glycerin and water
2. 24 g of 200μm glass spheres
3. 100 ml graduated cylinder with removable base
4. 800 ml beaker filled with water
5. 250 ml beaker for mixing

The Boycott Effect (named for Dr. A. E. Boycott, Nature 1920) is the result of the observation that red blood cells settle significantly faster when a tube of whole blood is tilted at an angle from vertical. In this demonstration a mixture of 107ml of glycerin and 43ml of water is prepared (mass fraction 0.76, density 1.195 g/cm^3, viscosity 0.34 poise), and the 24g of 200μm diameter glass spheres is added. When thoroughly mixed, the suspension (approximately 6% volume fraction) is poured into the cylinder and it is placed vertically in the beaker. The water in the beaker is sufficient to reduce the refraction caused by the curved graduated cylinder surface and allow particle motion at the interface to be seen. Visibility can be improved by inserting a black backing into the beaker behind the cylinder. The sedimentation rate can be measured by tracking the change in the particle free volume from the markings on the cylinder. After the suspension has settled it is poured out (some back-and-forth pouring is required to get the settled particles out) and the suspension is remixed. The suspension is poured back into the cylinder, but this time it is placed at an angle in the 800 ml beaker, yielding an inclination angle of $\theta = 30°$. The convection flow is imaged, and the new (greatly accelerated) rate of production of clarified fluid is recorded.

The mechanism leading to the enhanced sedimentation rate is most easily understood from the effect of inclination on the production of clear fluid. Particle-free fluid is produced when the particles in the suspension settle downwards, leaving the clear fluid behind. For a vertical tube of radius R with particle sedimentation velocity U_0, clear fluid is only produced at the upper interface at a rate $U_0\pi R^2$ (e.g., the sedimentation velocity times the horizontal cross-sectional area). For a tube at an angle, however, not only is the area of the still horizontal upper interface increased by a factor of $1/\cos(\theta)$, but clear fluid is also produced by particles falling away from the downward facing upper surface. Because this clear fluid has a lower density than the suspension, it rapidly flows upwards in a buoyancy driven convection process. In general the projected area of the downward facing upper tube surface is much greater than the somewhat enlarged horizontal cross-section, so the enhancement is dominated by the sedimentation from the inclined surface. From these simple kinematic arguments arises the Ponder-Nakamura-Kuroda (PNK) formula for the acceleration in the production of clarified fluid. Since it does not consider losses of clarified fluid due to remixing at the interface of the rapid buoyancy driven flow, the PNK formula is regarded as an upper limit to the increase in sedimentation rate. The details of the buoyancy driven flow are described in the classic paper by Acrivos and Herbolzheimer (1979).

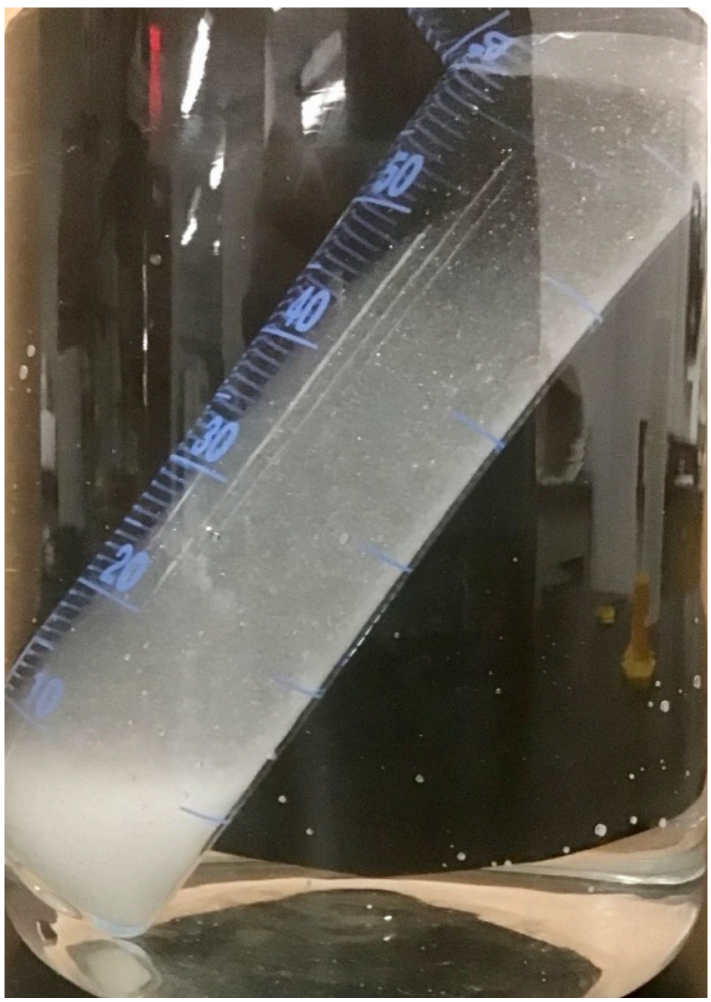

For a graduated cylinder of radius R and suspension-filled axial length L the PNK arguments yield (e.g., Oliver and Jensen, 1962) a rate of production of clarified fluid V of:

$$\frac{dV}{dt} = \pi R^2 U_0 \left(\frac{1}{cos\theta} + \frac{2L}{\pi R} \, sin\theta \right)$$

For a 100ml cylinder of radius R = 1.3cm, filled suspension length L = 10cm (e.g., about half-way through the process) and inclination angle of 30°, the two contributions are 1.15 + 2.45 = 3.60 vs. 1.0 for the vertical cylinder. Thus the enhancement in production of clarified fluid is dominated by sedimentation from the downward facing surface (the projected area of the horizontal upper interface increases only by 15% at this angle). The rate of enhancement also changes during the sedimentation process as the fraction of the upper cylinder wall exposed to the suspension decreases.

A number of useful calculations for this demonstration can be performed. The Stokes sedimentation velocity for the glass spheres is 0.077 cm/s, and the Richardson-Zaki hindered settling factor for this volume fraction is 0.73 (e.g., Davis and Birdsell, 1988), thus the front in the vertical cylinder should settle at U_0 = 0.057 cm/s. The Reynolds number is 0.0054 (based on the Stokes velocity and particle diameter) so inertial forces are negligible on the particle length scale. For a 100ml vertical graduated cylinder (radius R = 1.3cm) about 10 ml of clarified fluid is produced in 33s, so it is a slow process without enhancement. The production of clarified fluid is somewhat more difficult to observe for the inclined cylinder, however the time for the upper suspension interface to go from, say, the 60ml mark to the 50ml mark can be estimated and compared to that of the vertical tube and the PNK model.

An alternative approach to quantitative analysis can also be employed. Because the change in filled length is proportional to the production of clear fluid, the PNK formula can be rearranged to yield:

$$\frac{dL}{dt} = -\frac{1}{\pi R^2}\frac{dV}{dt} = -U_0\left(\frac{1}{cos\theta} + \frac{2L}{\pi R}\, sin\theta\right)$$

It is convenient to render L dimensionless with the initial fill length L_0 and time dimensionless with the vertical sedimentation time L_0/U_0. The dimensionless equation is thus:

$$\frac{dL^*}{dt^*} = -\left(\frac{1}{cos\theta} + L^*\frac{2L_0}{\pi R}\, sin\theta\right)$$

Neglecting the effect of settled particle buildup at the bottom (only a reasonable approximation for very dilute suspensions), the dimensionless sedimentation time t_f^* is:

$$t_f^* = \frac{ln\left(1 + \frac{2L_0}{\pi R}\, sin\theta cos\theta\right)}{\frac{2L_0}{\pi R}\, sin\theta}$$

which has a limiting value of unity for θ = 0 and is a function of both θ and the dimensionless ratio $2L_0/\pi R$. This latter quantity is about 10.1 for a 100ml cylinder filled to 110ml, so a 30° inclination yields a complete sedimentation time of $t_f^* = 0.33$, a factor of three speedup overall relative to the vertical tube. The end stage of the settling in the demonstration is somewhat uncertain due to sediment accumulation, however a ratio of 100s/315s =0.32 was observed, very close to the simple PNK prediction.

While a graduated cylinder in a water filled beaker is convenient and sufficient to observe the phenomenon, visibility of the flow at the interface can be improved by using a column of square cross-section, thereby avoiding refraction issues entirely. Such a column can be constructed from sheets of glass or acrylic, or from an acrylic square tube (available from online sources). By adjusting the angle of inclination it is also possible to visualize the instability of the upward flowing clear fluid layer that occurs under certain conditions. This implementation of the demonstration is identical to that performed by Professor Andreas Acrivos of Stanford in a number of invited seminars in the early 1980s.

Lamellar settlers which make use of this phenomenon are a standard industrial technique for increasing the throughput of settlers. Students interested in the theory describing this phenomenon are directed to the paper by Acrivos and Herbolzheimer, although the literature on the subject is quite extensive.

References:

Boycott, A. Sedimentation of Blood Corpuscles. Nature 104, 532 (1920). https://doi.org/10.1038/104532b0

Acrivos A, Herbolzheimer E. Enhanced sedimentation in settling tanks with inclined walls. Journal of Fluid Mechanics. 1979; 92(3):435-457. https://doi.org/10.1017/S0022112079000720

Oliver, D.R. and Jenson, V.G. (1964), The inclined settling of dispersed suspensions of spherical particles in square-section tubes. Can. J. Chem. Eng., 42: 191-195. https://doi.org/10.1002/cjce.5450420502

Davis, R.H. and Birdsell, K.H. (1988), Hindered settling of semidilute monodisperse and polydisperse suspensions. AIChE J., 34: 123-129. https://doi.org/10.1002/aic.690340114

K. Zhang, A. Acrivos, G. S. Triantafyllou; On the nature of the instability in buoyancy-driven flows in inclined settlers. Phys. Fluids 1 June 1992; 4 (6): 1156–1164. https://doi.org/10.1063/1.858234

The Tea Leaf Paradox

Materials:

1. 1 liter beaker
2. Lazy Susan
3. Clay
4. Tea

A classic demonstration is the "Tea Leaf Paradox", the observation that after stirring a tea cup with leaves on the bottom, the leaves will migrate to the center and accumulate in a puddle, the opposite of what would be expected from centrifugal forcing. The explanation is the very strong inertial secondary current resulting from centrifugal force along curved streamlines. This is the same effect which, for example, causes a river bed to meander (e.g., Einstein, 1926) and is found in very many systems. An interesting example of the effect of such meanders is the fate of Kaskaskia, the first state capitol of Illinois, which is now a ghost town on the west (Missouri) side of the Mississippi River.

In this demonstration I start with the classic tea leaf paradox: the beaker with water is affixed to the lazy susan (with clay to keep it centered) and tea leaves are added. The water should be cold and the tea leaves "pre-soaked" and dried to prevent the water from darkening. One used tea bag of jasmine green tea is ideal for a 1 liter beaker. After vigorous stirring with a spatula the tea leaves are observed to accumulate at the center as the flow slows down. The effect is due to both the no slip condition at the outer walls (reducing the centrifugal force on the fluid at the outer edge) and at the bottom. The fluid in the central core thus produces a vortex which goes up at the center and down at the outside. The negatively buoyant tea leaves accumulate at the center of the upwelling region.

Once the tea leaves have accumulated and the fluid is at rest, the lazy susan is rotated to explore the inverse start-up problem. The rotation of the bottom induces a boundary layer flow at the rotating surface which, again through centrifugal force, causes a very rapid radial outflow at the bottom. This is the same flow studied by von Karman (1921) and has practical application in rotating disk electrodes and rotating membranes, for example. The vortex now flows up at the outer edge and down at the center, thus the tea leaves are spread to the outside of the beaker. After a short period of time (if steady rotation is maintained, which is a little challenging to do by hand), the fluid in the beaker settles down to solid body rotation. If the rotation is stopped, the tea leaves again accumulate in the bottom center.

It is interesting to note the time scale for this flow to reach steady-state under rotation. If it were due to viscous diffusion over the 5cm radius of the beaker, the time scale would be of order $R^2/\nu \sim 42$ min where ν is the kinematic viscosity of water. Instead it reaches steady state much more quickly. This is because the fluid is accelerated in the narrow boundary layer at the bottom. The thickness of the boundary layer scales as $(\nu/\Omega)^{1/2}$, where Ω is the steady angular velocity of the beaker, the radial velocity is of order ΩR, and by scaling the continuity equation the vertical velocity is of order $(\nu\Omega)^{1/2}$. The time scale for reaching steady-state due to this secondary current for a height of fluid H is thus $t \sim H/(\nu\Omega)^{1/2}$ which, for water in the 1 liter beaker (at a rotation rate of about 4 radian/s) is of order 45 seconds, much faster than diffusion alone.

References:

Wikipedia contributors. (2024, January 25). Tea leaf paradox. In Wikipedia, The Free Encyclopedia. Retrieved 00:03, June 24, 2024.
https://en.wikipedia.org/w/index.php?title=Tea_leaf_paradox&oldid=1198972551

Einstein, A.(1926). "Über die Ursachen der Mäanderbildung der Flüsse und Baersschen Gesetzes." Naturwissenschaften, 14, 223–225.
https://doi.org/10.1007/BF01510300
https://www.ias.ac.in/article/fulltext/reso/005/03/0105-0108

von Kármán, T., Über laminare und turbulente Reibung, Zeitschrift für Angewandte Mathematik und Mechanik (ZAMM), Vol. 1, No. 4 (1921), pp 233-252.
https://doi.org/10.1002/zamm.19210010401

Suction From Rotation: the Parallel-Plate Viscometer

Materials:

1. A vertical stirrer with digital readout
2. Flat bottomed glass container
3. Portable scale
4. Plastic disk with rod in center
5. Glycerin and water

Inertial forces can cause surprising effects even when the Reynolds number is very low. One example of this is the negative normal force (essentially a suction) which occurs when a rapidly rotating disk is brought near another surface. This can cause problems in rotating machinery, however in fluid mechanics the classic example is in trying to measure normal stresses using a parallel-plate viscometer.

In such a system a polymer melt or suspension of particles is confined between two plates. One plate is rotated and the torque and normal force on the other plate is measured. In general, the normal force is either zero (for a Newtonian fluid) or positive for either polymers or suspensions. If you rotate the plate too fast, however, the measured force is negative - and has nothing to do with the rheology of the fluid being studied!

The magnitude of this erroneous normal force is easy to calculate from the Navier-Stokes equations in the limit that the gap width H between the plates is small. In this case, the θ velocity is just a radially increasing simple shear: $u_\theta = \Omega r \dfrac{z}{H}$. where Ω is the angular velocity of the upper plate at z = H. From scaling it is easy to show that the dominant terms in the radial component of the Navier-Stokes equations are just

$$-\rho \frac{u_\theta^2}{r} = -\frac{\partial p}{\partial r} + \mu \frac{\partial^2 u_r}{\partial z^2}$$

with boundary conditions:

$$p\,|_{r=R} = p_0 \;\; ; \;\; u_r|_{z=0} = u_r|_{z=H} = 0 \;\; ; \;\; \int_0^H u_r dz = 0$$

This problem admits the von Karman self-similar solution where both u_r and the radial pressure gradient are proportional to r. Thus we may define the dimensionless variables:

$$r^* = \frac{r}{R} \ , \ \ z^* = \frac{z}{H} \ , \ \ u_r^* = \frac{u_r}{U_c} = r^* f(z^*) \ , \ \ \frac{\partial p^*}{\partial r^*} = \frac{\partial p}{\partial r}\frac{R}{\Delta P_c} = \lambda r^*$$

The scalings are $U_c = \dfrac{\rho \Omega^2 R H^2}{\mu}$ and $\Delta P_c = \rho \Omega^2 R^2$. The normal force is just:

$$F = \int_0^R (p - p_0) 2\pi r dr = \pi \rho R^4 \Omega^2 \int_0^1 p^* 2 r^* dr^*$$

The dimensionless problem is thus:

$$\frac{d^2 f}{dz^{*2}} = \lambda - z^{*2} \ ; \ f\,|_{z^*=0} = f\,|_{z^*=1} = 0 \ ; \ \int_0^1 f dz^* = 0$$

The no-slip boundary conditions yield

$$f = \frac{1}{2}\lambda \left(z^{*2} - z^*\right) - \frac{1}{12}\left(z^{*4} - z^*\right)$$

The integral conservation condition results in $\lambda = \dfrac{3}{10}$. The pressure is just a quadratic function of r*, and when integrated the force is the classic result:

$$F = -\frac{3\pi}{40}\rho R^4 \Omega^2$$

In order for this solution to be valid, it is required that the boundary layer at the rotating surface (e.g., the Tea Leaf Problem) be sufficiently large that it spans the gap between the plates. This requires $H < (\nu/\Omega)^{1/2}$, although the force will only gradually diminish as this condition is no longer satisfied.

In class this effect is very simply demonstrated. I use a portable scale and a crystallizing dish (this has a flat bottom). The upper plate is a 3″ diameter acrylic disk with a screw in the center which is chucked up into a vertical stirring motor (minimum speed of 70RPM). The disk and stirrer are lowered until the gap is about 0.5 cm. The gap is tricky to set accurately, but is measured by pouring the liquid (84% by volume glycerin and water, density 1.22 g/cm^3 and kinematic viscosity 1 cm^2/s) until it fills the gap beneath the disk. By knowing the required volume and the surface area of the dish, the gap width is easily calculated. The fluid is added until it is about half way up the thickness of the disk, and the scale is tared. The disk is rotated at varying speeds (I go up to about 300RPM) and the (negative) weight is recorded. The force is just Mg. The results are plotted up - and the match with the theoretical prediction is precise.

It is interesting to compare the behavior for the viscous glycerin/water solution with that of pure water (kinematic viscosity of 0.01 cm^2/s). At 200RPM the boundary layer scaling for the 1 cm^2/s solution is 0.2 cm, which is large enough that the prediction described above holds. For water, however, the boundary layer is an order of magnitude thinner, and thus the magnitude of the force is substantially reduced, which can be demonstrated. In theory it would be possible to recover the thin gap prediction even for water, however it would be difficult to control such a small gap in this demonstration.

References:

R J Poole (2016), Measuring normal-stresses in torsional rheometers: a practical guide. The British Society of Rheology, Rheology Bulletin. 57(2) pp 36-46 https://www.researchgate.net/publication/309040563_Measuring_normal-stresses_in_torsional_rheometers_a_practical_guide

Walters, K. (1975). Rheometry. Chapman Hall

The Tornado Vortex

Materials:

1. 2 Large soda bottles
2. Water
3. A "tornado vortex" connector

This is a classic demonstration for grade school science classes, however it can be made much more sophisticated and illuminate a number of principles. The basics are simple: one bottle is filled with water, the second is left empty, and the two are connected using the "tornado vortex connector" which is $10 for a pack of 20 on Amazon. When the filled bottle is on top a little water drips through, but quickly stops. If swirl is imparted, however, a vortex forms providing a continuous channel for air to displace the descending water and the upper bottle drains out.

The tornado effect is a result of the coriolis effect in which the water, approaching the narrow throat of the bottle with swirl (e.g., a combination of both u_θ and u_r), accelerates in the θ direction due to conservation of angular momentum. This rotational velocity is sufficient that the centrifugal effect produces a "water free" tube allowing air to pass into the upper bottle. Thus, the phenomenon is a good demonstration of the two key "pseudo forces" which are produced in the coordinate transformation of the Navier-Stokes equations from rectilinear to curvilinear coordinates.

In many respects the most interesting aspect is why, in the absence of rotation, the water will not flow from the top to the bottom. Because water is incompressible (and air nearly so) the pressure is low at the top of the (inverted) bottle via hydrostatics, but the pressure at the connector is simply the pressure in the empty lower bottle. Thus, the driving force for the water to leak out depends only on local conditions. If the diameter of the hole is small enough, and the surface tension resisting the air exchange with the water high enough, then the interface is pulled flat and there is no flow. If the hole is very large, then the water-air interface at the connector will be unstable and the water and air will cross between the bottles.

The critical radius of the opening can be estimated from simple arguments. We take the local diameter of the hole to be D. For water to leak out, the surface must deform with a characteristic radius of curvature of $D/4$ (e.g., water bulging downwards in half the opening and air bulging upwards in the other half). This would lead to a restoring pressure from surface tension Γ of order $4\Gamma/D$. Gravity would tend to destabilize the interface, with a pressure differential which is of order $\rho g D/4$ (e.g., the same characteristic length scale). Thus, the critical diameter $D_c \sim 4(\Gamma/\rho g)^{1/2}$. For water-air systems, this yields $D_c \sim 1.1$cm. This value is, of course, approximate, but is a reasonable estimate. For the commercially available connectors, the hole size is 3/8" = 0.95cm, which is a bit less than this value. Thus, if the soda bottle walls are strong enough to support the low pressure produced by hydrostatics, the interface is stable and the water doesn't leak out. Interestingly, if the connector is removed the diameter is now about 7/8" = 2.2cm and the water empties out even without rotation and formation of the vortex. Once it starts, of course, the drainage process becomes complex with slugs of water passing through alternating with slugs of air and flexing of the bottle walls. The same sort of effect can be seen in a plugged vertical tube filled with air, but containing a slug of water. If the diameter is small enough, the slug of water will remain trapped (very annoying if you are trying to get rid of it!), but if the diameter is larger the water will fall out of the tube to the bottom. The inverse occurs for trapped air bubbles, depending on the wetability characteristics of the tube.

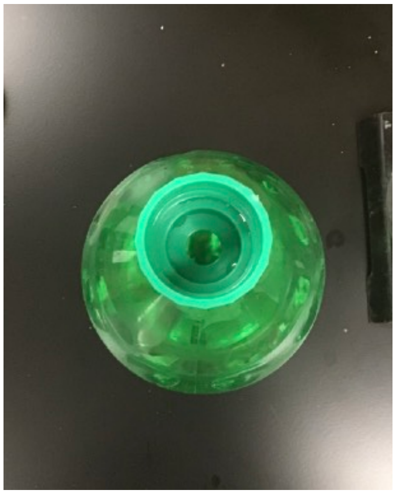

View from above filled bottle

View from below filled bottle (no rotation)

Bottle drainage with rotation

References:

C. W. Extrand, Spontaneous Draining of Liquids from Vertically Oriented Tubes, Langmuir 2017 33 (45), 12903-12907
https://doi.org/10.1021/acs.langmuir.7b03247

Bernoulli Suction

Materials:

1. A cylinder with a hole in the center
2. A piece of cardboard and paperclip

A common demonstration of high Reynolds number flows is the trick of a ping pong ball in a funnel: no matter how hard you blow, you can't blow it out. While interesting, it is a little hard to quantify the forces involved. Instead, I demonstrate the equivalent: that if you have a flat piece of cardboard (centered with a paperclip over a hole in the center of a cylinder), if you blow through the back you can't blow it off. In fact, the forces are sufficient to keep the cardboard attached to the cylinder (in my case a roll of adding machine tape) against the force of gravity. It only falls off when you run out of air.

The key to this demonstration is Bernoulli's equation and the decrease in radial velocity between the cylinder and the plane as the radius increases. By continuity, the radial velocity at any radial location r is just $u_r = u_e R/r$ where u_e is the exit velocity at the outer edge R. In the central core of radius R_0 the velocity is taken to be zero (resulting in stagnation pressure p_0). This will be a reasonable approximation if the core radius R_0 is much greater than the gap width H between the surfaces so that the volume of the central core is "large" and by continuity the local velocity in the core is small. Ignoring all losses (more questionable), the exit velocity u_e can also be calculated from the stagnation pressure via Bernoulli's equation. Thus, with these approximations the pressure under the cardboard decreases from atmospheric pressure at the outer edge until it experiences a jump at the center, and the overall force on the cardboard is just an integral of this pressure distribution, e.g.,

$$p = p_e + \frac{1}{2}\rho u_e^2 \left(1 - \frac{u^2}{u_e^2}\right)$$

or:

$$p = \begin{cases} p_e + \left(p_0 - p_e\right)\left(1 - \frac{R^2}{r^2}\right) & R_0 < r < R \\ p_0 & 0 < r < R_0 \end{cases}$$

and thus:

$$F = \int_0^R \left(p - p_e\right) 2\pi r dr = \left(p_0 - p_e\right) \pi R^2 \left(1 - 2ln(R/R_0)\right)$$

The cardboard will remain attached provided the radius ratio satisfies:

$$R/R_0 > e^{\frac{1}{2}} = 1.65$$

In demonstration, the adding tape and disk are first demonstrated to fall apart without flow, and then the students are asked what would happen if you blow on the back. Invariably, of course, the response is that it would blow off. After much huffing and puffing (with, of course, the disk sticking tight), the derivation of the pressure distribution is provided.

An interesting question is what the minimum separation should be. For smooth surfaces there would also be losses due to viscous effects: for sufficiently small gaps this could be calculated from lubrication approximations. The viscous flow between the cylinder surface and disk would lead to a negative radial pressure gradient, thus by scaling the radial momentum equations and balancing the inertial and viscous terms it is seen that the critical gap width H should scale as:

$$H \sim \left(\frac{R\mu}{\rho u_e}\right)^{1/2} \sim \left(\frac{R\mu}{\left(\rho\left(p_0 - p_e\right)\right)^{\frac{1}{2}}}\right)^{1/2}$$

For the specific demonstration used here, the surfaces are not smooth, thus the equilibrium gap width would be larger than this value.

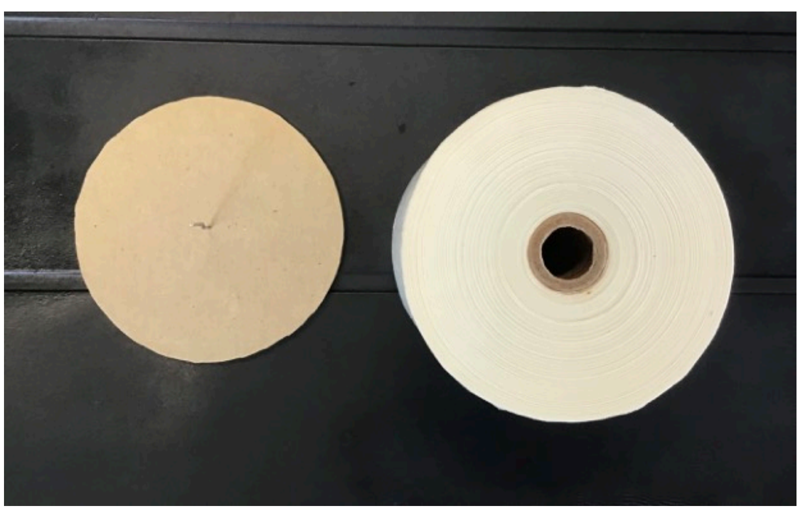

The principle behind this demonstration is, of course, well known. Industrially the same geometry is commercially available as a “Bernoulli suction cup” or “Bernoulli grip” that finds application in robotic movement of flat, fragile objects. The second reference below contains a movie of how such a gripper can rapidly assemble sandwiches from slices of bread!

References:

Wikipedia contributors. (2023, October 16). Bernoulli grip. In Wikipedia, The Free Encyclopedia. Retrieved July 11, 2024
https://en.wikipedia.org/w/index.php?title=Bernoulli_grip&oldid=1180462961

https://www.vacuumdaily.net/2019/01/bernoulli-suction-cups-its-not-magic-its-a-project/

Magnus Lift and the Coanda Effect

Materials:

1. Portable vacuum cleaner
2. Ring stand and clamp
3. Styrofoam balls of varying sizes

Both Magnus lift and the Coanda effect play important roles on lateral forces on objects in high Reynolds number flows. Magnus lift, of course, is what causes a golf ball to have a high arcing trajectory and land softly on a green (or in a pond, as is more usual in my experience). The Coanda effect is classically observed from the deflection of a laminar stream of water from a faucet by the back side of a spoon. Both are the result of the boundary layer interacting with a surface at high Re. In the case of the Coanda effect it "follows the curve" of the spoon, while in Magnus lift the backspin of the golf ball causes the boundary layer and wake to be deflected by the rotation. The Coanda effect is ascribed to the tendency of a jet to adhere to an adjacent surface, and thus if the surface is curved it is deflected leading to a lateral force by conservation of momentum. This is important in aircraft wing design, for example, particularly for VTOL aircraft. The Magnus effect is commonly seen in the deflection of balls in many sports, but also plays a role in transportation. Bulk cargo carriers (so-called Rotor Ships) use large vertical rotors to act as directional sails, reducing propulsion costs.

In this demonstration both effects are visualized by the motion of a large styrofoam ball in a stream of air produced by a vacuum cleaner. The hose is connected to the outflow, and the filter is removed to get a higher flow rate. Initially the ball (I have found a 5.5 inch diameter ball works best) is suspended vertically in the stream. Because the ball is larger in diameter than the jet, the stability relies on the Coanda effect as first observed by Reynolds in 1870. If the ball is displaced from the center of the stream, the Coanda effect causes the jet to follow the curve of the ball, deflecting the jet and, by conservation of momentum, causing a lateral force which draws the ball back into the center. Due to inertia, the ball will oscillate across the center of the jet with an amplitude that depends on the ratio of the ball diameter to jet diameter. For sufficiently small diameter balls the motion is unstable and the ball will be thrown out of the jet (e.g., Feng & Joseph, 1996). The most interesting part of the demonstration is when the jet is angled from the vertical. This initially causes the Coanda effect to keep the ball suspended, however the ball rapidly begins to rotate (the ball is marked to make the rotation visible). The Magnus lift further deflects the stream of air, greatly increasing the lateral force, and

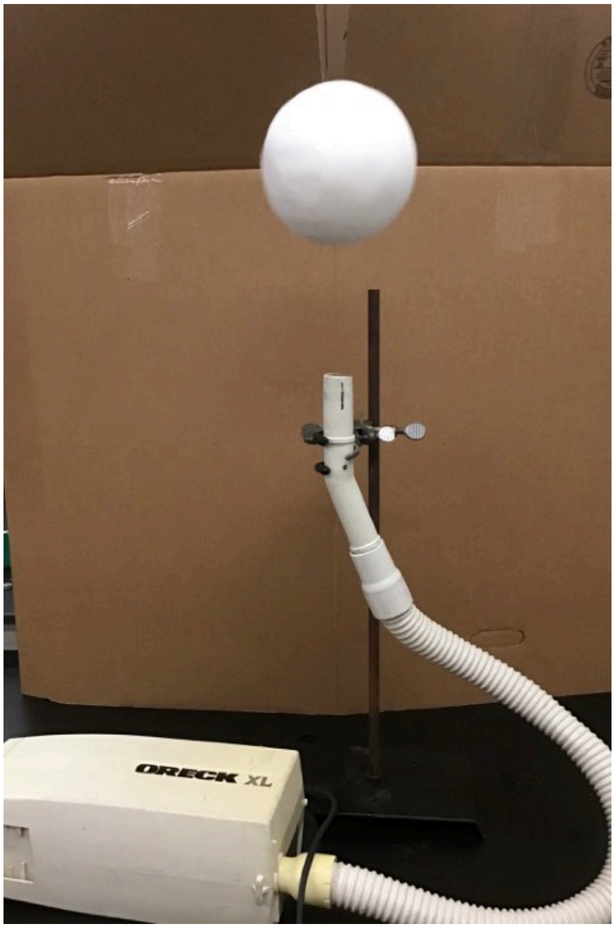

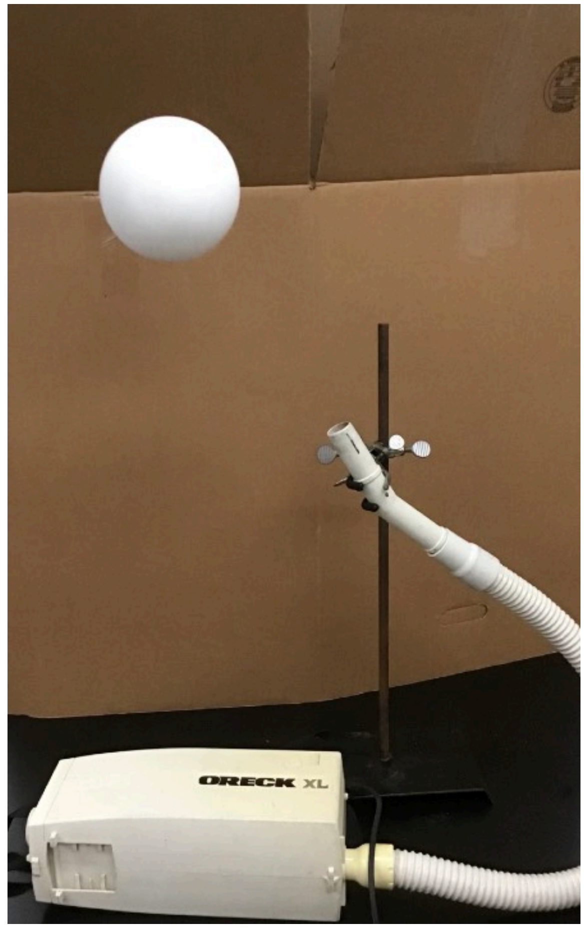

allowing the angle to be further increased. For the Oreck vacuum cleaner and styrofoam ball I employ an angle of more than 30° from vertical is achievable.

Quantitative measurements are also possible if an anemometer is used to measure wind speed at the ball locations. Measurements include the spread of the jet from the nozzle (described by Tollmien, 1926), the balance between the inertia of the jet stream and the weight of the ball, and a force balance in two directions when the ball is suspended at an angle.

For the Oreck vacuum cleaner depicted here, the centerline velocity of the jet can be measured as a function of distance from the nozzle. Because the convection of momentum through any plane is conserved, if the velocity profile of the jet is self-similar then the product $\rho U \left(\pi R_j^2 \; U \right)$ should be constant, where U is the local centerline velocity and R_j is the effective jet radius. For a linear spread of the jet with distance H as described by Tollmien, the product U H should likewise be constant. For this jet over the range of H from 0.3m to 1.0m this simple relationship actually works well, yielding an average value of 6.3 m^2/s for my vacuum cleaner. This is useful for determining the jet velocity at the height where the ball is at equilibrium H_{eq}. The drag coefficient can be defined as:

$$C_D = \frac{Mg}{\frac{1}{2}\rho U^2 \frac{\pi D^2}{4}} = \frac{8}{\pi}\frac{Mg}{\rho U^2 D^2} = \frac{8}{\pi}\frac{Mg}{\rho D^2}\left(\frac{H_{eq}}{6.3\ m^2/s}\right)^2$$

where $\rho = 1.22\ kg/m^3$ is the density of air. The Reynolds number can likewise be calculated as:

$$Re = \frac{UD}{\nu} = \frac{D}{H_{eq}}\left(\frac{6.3\ m^2/s}{\nu}\right)$$

where $\nu = 1.5x10^{-5}\ m^2/s$ is the kinematic viscosity of air. For the largest ball (M = 0.053kg, D = 0.14m, H_{eq} = 0.20m) C_D defined in this way is only 0.056, likely affected by the ball being much larger than the jet diameter at the equilibrium height. The drag coefficient would be much larger if it were based on the jet cross-sectional area rather than the ball cross-section. In addition, the Reynolds number based on the diameter and jet velocity is about $2.9x10^5$, close to the range where the drag coefficient drops due to boundary layer transition to turbulence. For the smallest ball (M = 0.004kg, D = 0.06m, H_{eq} = 1.0m - very difficult to measure due to instability!) the drag coefficient is about 0.58, close to the expected value of 0.5 for a uniform stream at its much lower Reynolds number of $2.5x10^4$. When the jet impinging on the largest ball was tilted to the maximum (yielding a very rapid rotation) the separation distance increased to over 0.30m (corresponding to a local jet velocity less than 2/3 of the initial value), indicating that the lift coefficient when enhanced by the Coanda and Magnus effects increased by more than a factor of two. The behavior of spheres in both vertical and inclined jets has been extensively studied by Feng and Joseph (1996). They found that under some conditions (generally smaller sphere diameter to jet diameter ratios) the rotation of the sphere could actually be backwards from what would be expected and is observed here.

References:

Wikipedia contributors. (2024, February 1). Coandă effect. In Wikipedia, The Free Encyclopedia. Web, June 24, 2024
https://en.wikipedia.org/w/index.php?title=Coand%C4%83_effect&oldid=1201980803

Wikipedia contributors. (2024, June 18). Magnus effect. In Wikipedia, The Free Encyclopedia. Web, June 24, 2024
https://en.wikipedia.org/w/index.php?title=Magnus_effect&oldid=1229751020

Wikipedia contributors. (2024, April 23). Rotor ship. In Wikipedia, The Free Encyclopedia. Web, June 25, 2024
https://en.wikipedia.org/w/index.php?title=Rotor_ship&oldid=1220385980

Feng J, Joseph DD. "The motion of a solid sphere suspended by a Newtonian or viscoelastic jet." Journal of Fluid Mechanics 315 (1996): 367-385.
https://doi.org/10.1017/S0022112096002467

Jackson, Derek, and Brian Launder. "Osborne Reynolds and the publication of his papers on turbulent flow." Annu. Rev. Fluid Mech. 39.1 (2007): 19-35.
https://doi.org/10.1146/annurev.fluid.39.050905.110241

Tollmien, W. (1926), Berechnung turbulenter Ausbreitungsvorgänge. Z. angew. Math. Mech., 6: 468-478.
https://doi.org/10.1002/zamm.19260060604

Hussein, Hussein J., Steven P. Capp, and William K. George. "Velocity measurements in a high-Reynolds-number, momentum-conserving, axisymmetric, turbulent jet." Journal of Fluid Mechanics 258 (1994): 31-75.
https://doi.org/10.1017/S002211209400323X

https://www1.grc.nasa.gov/beginners-guide-to-aeronautics/drag-of-a-sphere/

Transient Thermal Diffusion

Materials:

1. ½″ diameter steel and aluminum rods
2. Thermochromic paint
3. Hot water
4. Ice water
5. Flat bottomed glass or plastic container with lid
6. Stirring bar

An important process in heat transfer is the transient diffusion of energy due to conduction. This is mathematically identical to transient unidirectional fluid flow as well, thus visualization of the phenomenon applies to both heat and momentum transfer. In this experiment rods (I use steel and aluminum, but other metals would work as well) are coated with a thermochromic paint. Such thermochromic powder can be found inexpensively on-line and when mixed with a clear polyurethane lacquer makes a nice coating. Note that when combined with the lacquer the paint is much darker than the powder itself (which is quite pale), so it shows up well. I find that either the blue/clear or red/yellow combinations work well. Note that the rod needs to be shiny if the blue/clear dye is used, however, as the rod color will show through when above the transition temperature. After drying the rods are marked in 1cm increments for quantitative measurements. The transition temperature for both dyes is reported to be 82°F (although the transition is over a range in temperature and varies by manufacturer), so the rods are initially heated above this point in the hot water and then dried off. The rods are arranged so that the ends project through the lid of the ice water container, which is then rapidly stirred to maintain good thermal contact. The propagation of the color change up the rods is observed. Visibility of the transition region can be improved by illuminating with a strong light source (e.g., a flashlight). It is important to have rods of sufficiently large diameter that heat transfer through the surrounding air is negligible compared to conduction up the rods.

There are a number of aspects of this phenomenon which can be quantitatively analyzed. First, from dimensional analysis alone the time necessary to diffuse a given length x along the rod is proportional to $t_D \sim x^2/\alpha$ where α is the thermal diffusivity of the material. Thus, comparison of the time for the color to propagate half-way up the steel and aluminum rods yields the ratios of the thermal diffusivities of the two materials. The numbers will be a little off both because heat transfer resistance from the ice water to the base of the rods would play a greater role for the aluminum than for the steel, and because external heat transfer to/from the air would play a greater role for the steel than for the aluminum. Both effects would reduce the difference in propagation times, however the propagation in the aluminum is clearly much faster than for the steel due to its higher thermal diffusivity.

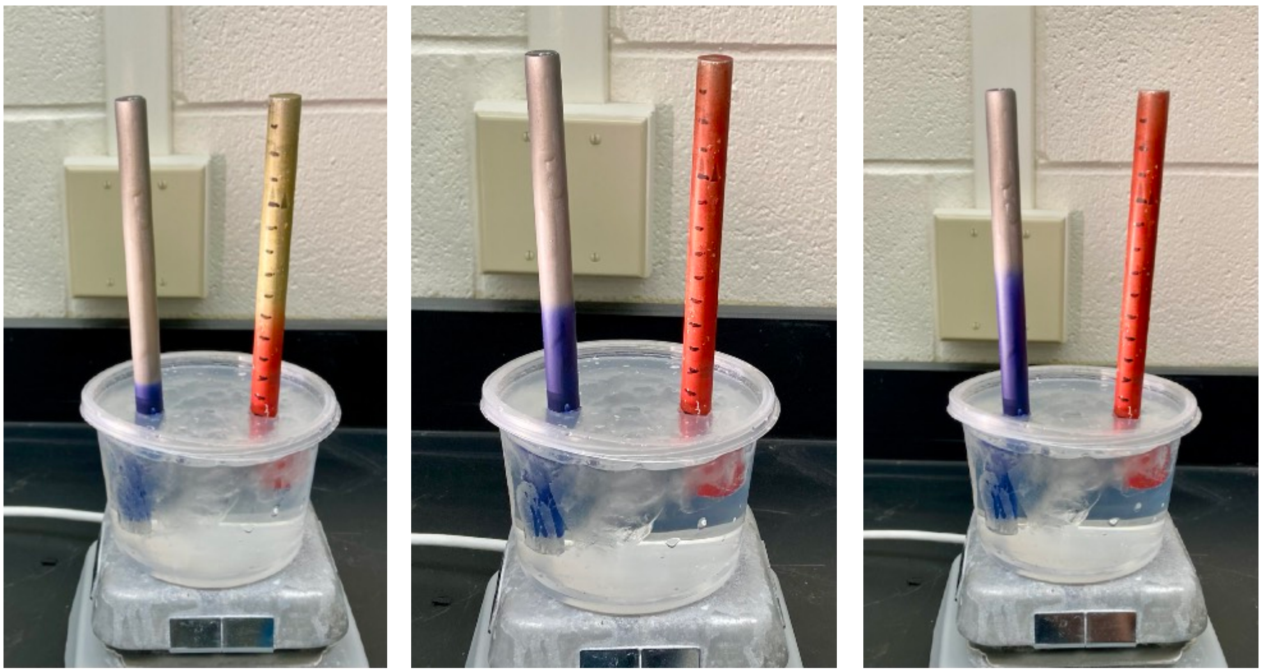

60 seconds 180 seconds 280 seconds

More sophisticated analysis can also be done, particularly for the aluminum rod. If we take the initial temperature of the rod to be T_0 and at time $t = 0$ set the temperature at the base of the rod $x = 0$ to T_1, then it is convenient to define a dimensionless temperature:

$$T^* = \frac{T - T_1}{T_0 - T_1}$$

If the propagation distance x is much less than the length of the rod L, then the temperature profile (and hence the transition point) is self-similar, where the dimensionless temperature is given by the well known error function solution:

$$T^* = erf\left(\frac{x}{\sqrt{4\alpha t}}\right)$$

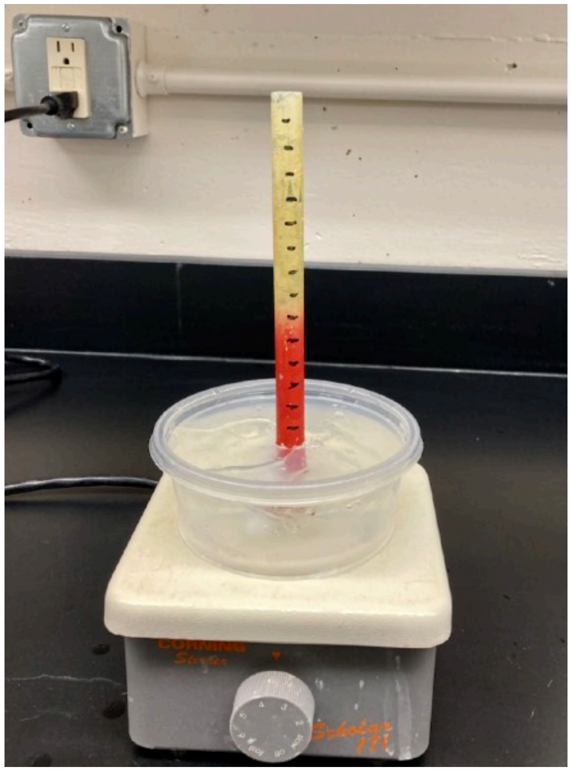

Transition location at 60s, Al-6061 rod.

This is convenient, as if the color transition temperature has a dimensionless value of T_c^*, then the location x_c at time t are related by:

$$x_c = \sqrt{4\alpha t}\ \ erfinv\left(T_c^*\right)$$

where erfinv is the error function inverse and is a defined function in Matlab and Wolfram Alpha.

The propagation wave, initially fairly fast, slows down as time increases and the distance the energy must diffuse becomes larger. Interestingly, as the end is approached the propagation wave actually speeds up again. Not captured by the short time solution, this is a consequence of the breakdown of the self-similar profile due to the boundary condition at the end of the rod. If the end of the rod is considered "insulated", then by reflection the solution is the same as if a rod of twice the length were subjected to a temperature change at both ends.

The complete solution is obtained via separation of variables and a Sturm-Liouville eigenvalue expansion. If we define the dimensionless time $t^* = \alpha t/L^2$ and position $x^* = x/L$ the series solution is just:

$$T^* = \sum_{n=0}^{\infty} \frac{2}{\sigma_n} e^{-\sigma_n^2 t^*} sin(\sigma_n x^*) \quad ; \quad \sigma_n = \left(n + \frac{1}{2}\right)\pi$$

As is true of most solutions of this type, the series converges very rapidly at larger times. For a dimensionless time $t^* > 0.1$ the solution is well approximated by the lead eigenvalue:

$$T^* = \frac{4}{\pi} sin\left(\frac{\pi x^*}{2}\right) e^{-\frac{\pi^2 t^*}{4}}$$

This expression can be inverted to yield the long-time asymptote for the location of the color wave (before it reaches the rod end):

$$x_c = \frac{2L}{\pi} sin^{-1}\left(T_c * \frac{\pi}{4} e^{\frac{\pi^2 \alpha t}{4L^2}}\right)$$

The long and short time asymptotes for the transition location match to within 4% at a dimensionless time of 0.15 (depending on the value of T_c*), although they do not quite overlap. These predictions can be compared to observations in the demonstration.

Most simply, it is useful to determine the time t_f when the color wave reaches the end of the rod as this is easily determined in the demonstration. This is given by:

$$t_f = \frac{L^2}{\alpha} \frac{4}{\pi^2} ln\left(\frac{4}{\pi T_c^*}\right)$$

or, rearranging, we can use this measurable t_f to determine the thermal diffusivity of the rod and compare it to literature values:

$$\alpha = \frac{L^2}{t_f} \frac{4}{\pi^2} ln\left(\frac{4}{\pi T_c^*}\right)$$

The thermal diffusivity depends on the alloy of aluminum used. Pure aluminum has a diffusivity of 0.97 cm^2/s at room temperature, while the alloy Aluminum-6061 (the composition of the rod from our laboratory) has a lower diffusivity of 0.64 cm^2/s. For the simple experiment depicted the initial rod temperature was 43.5°C, thus for the reported transition temperature of 27.8°C the dimensionless transition temperature is $T_c^* = 0.64$. The propagation wave reached the end of the rod (15 cm from the lid) after about 145s. Plugging this into the expression above yields a thermal diffusivity of 0.43 cm^2/s, not too far off from the correct value. The discrepancy is likely due to neglecting the finite heat transfer resistance between the base of the rod and the stirred ice water bath as well as uncertainty in the transition temperature.

Quantitative comparison between the aluminum and steel rods can also be done, however the thermal diffusivity of steel varies widely depending on the alloy used. In the demonstration depicted the transition front reached both the midway point and the rod end three times faster for the aluminum as for the steel. This is consistent with the ratio of the reported thermal diffusivities of Aluminum-6061 and low carbon steel.

This demonstration is very useful when discussing transient heat transfer as it illustrates many of the key concepts and solution approaches to these problems.

References:

Bird, Stewart & Lightfoot, *Transport Phenomena*, rev 2nd ed., Wiley, 2007. Sec 12.1, p. 374-378.

The Cooling Fin

Materials:

1. ½" diameter aluminum rod
2. Thermochromic paint
3. Ice water
4. Hair dryer with mounting
5. Anemometer with temperature scale
6. Flat bottomed glass or plastic container with lid
7. Stirring plate

Heat transfer due to forced convection is a core problem in energy transport. We have all experienced the cooling effect of a breeze on a hot day - particularly if that is combined with evaporative cooling! In this demonstration we look at the heat transfer associated with forced convection past a cylinder. A cylinder of aluminum is coated with thermochromic paint and inserted through the lid of a container of ice water. The container is placed on a stirring plate to ensure rapid mixing and good thermal contact. The rod will quickly change to its "cold color" via conduction. The hair dryer is then turned on at an appropriate distance (about 0.3m for my setup) and the wind speed and temperature at the rod are measured. The end of the rod will turn to the "hot color" and the location of the transition region between hot and cold is measured as a function of wind speed and temperature.

The temperature distribution in the rod is governed by a balance between axial conduction and a convective heat transfer coefficient h at the surface. The latter is described by the correlation suggested by Whitaker for perpendicular flow for cylinders in terms of the Reynolds and Prandtl numbers:

$$Nu = \frac{h(2R)}{k_{air}} = \left(0.4Re^{1/2} + 0.06Re^{2/3}\right) Pr^{0.4} \left(\frac{\mu_\infty}{\mu_0}\right)^{1/4}$$

The viscosity ratio correction is small for air due to the weak dependence on temperature.

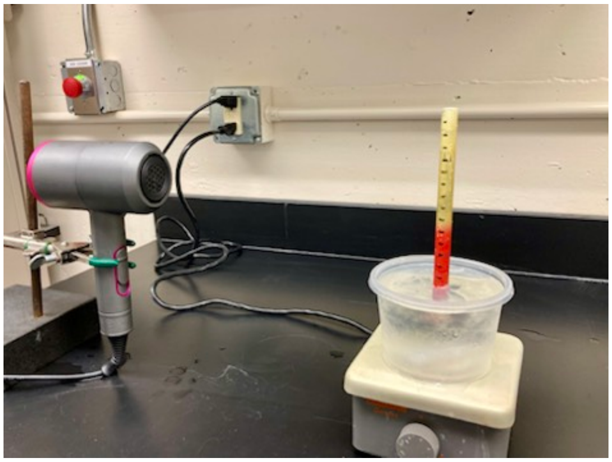

High Speed Setting

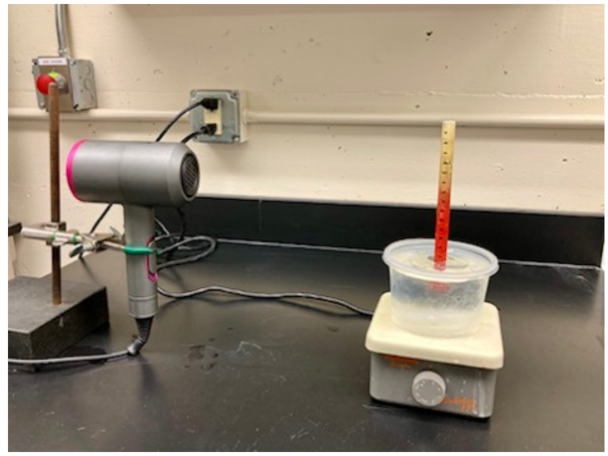

Low Speed Setting

Assuming that radial conduction in the rod is "fast" the energy equation is averaged over the cross-section of the rod. The radial average temperature distribution is governed by:

$$0 = \pi R^2 k_m \frac{\partial^2 T}{\partial z^2} - 2\pi R h \left(T - T_\infty\right)$$

where k_m is the thermal conductivity of the rod of radius R and length L. If the temperature at the base is T_0 and the temperature provided by the hair dryer is T_∞, then we may define the dimensionless quantities:

$$T^* = \frac{T - T_\infty}{T_0 - T_\infty} \quad ; \quad z^* = \frac{z}{L} \quad ; \quad \lambda^2 = \frac{2hL^2}{Rk_m}$$

The dimensionless differential equation and boundary conditions become:

$$\frac{\partial^2 T^*}{\partial z^{*2}} = \lambda^2 T^* \quad ; \quad T^* |_{z^*=0} = 1 \quad ; \quad \frac{\partial T^*}{\partial z^*} |_{z^*=1} = 0$$

The solution to this equation is well known, and is given by:

$$T^* = cosh(\lambda z^*) - \frac{sinh(\lambda)}{cosh(\lambda)} sinh(\lambda z^*)$$

For large values of λ (long rods), this expression reduces to a single exponential:

$$T^* = e^{-\lambda z^*} = e^{-\left(\frac{2hz^2}{Rk_m}\right)^{1/2}}$$

If the color transition is at a dimensionless temperature T_c^* and measured location z_c we have the relation:

$$h = \frac{Rk_m}{2}\frac{\left(lnT_c^*\right)^2}{z_c^2}$$

Or, in terms of the Nusselt number:

$$Nu = \frac{h(2R)}{k_{air}} = \frac{R^2}{z_c^2}\frac{k_m}{k_{air}}\left(lnT_c^*\right)^2$$

provided $Nu\frac{L^2}{R^2}\frac{k_{air}}{k_m} >> 1$ or, alternatively, $z_c << L$. The results of the measurements in the demonstration can be compared to the Whitaker correlation where the Reynolds number is calculated from the anemometer reading.

The kinematic viscosity of air is about 0.15 cm^2/s, and the Prandtl number is 0.71. The ratio of conductivities is more uncertain depending on the alloy of aluminum used in the rod. The conductivity of Al-6061 (our laboratory rod composition) is 152 W/m°K vs. pure aluminum of 237 W/m°K. The conductivity of air is 0.026 W/m°K. For the two cases depicted above the transition temperature was reported to be 27.8°C. At the high speed setting the air velocity was about 14 m/s and the air temperature was approximately 46°C. The transition point was at 5 cm, yielding a calculated Nu of 81. The Reynolds number for this air speed was $1.2\text{x}10^4$, so from the Whitaker correlation the expected Nu was 65, not too far off considering the non-uniformity of the flow and uncertainty of the measurements. Perhaps the largest source of the discrepancy is neglecting the finite heat transfer resistance between the base of the rod and the stirred ice water bath. The calculated Nu is also quite sensitive to errors in the relatively small deviation of the air temperature from the transition temperature.

At the lower speed setting the air velocity was approximately 10 m/s and the air temperature was 37°C. The transition point increased to about 8 cm yielding a calculated Nu of 71. For the lower Re of $8.5\text{x}10^3$ the Whitaker correlation yields an expected Nu of 54, again somewhat lower than that measured from the transition point. Perhaps the clearest part of the demonstration is to show how the transition location changes with air speed, going back and forth between the two settings and changing the distance between the hair dryer and the rod.

References:

Bird, Stewart & Lightfoot, *Transport Phenomena*, rev 2nd ed., Wiley, 2007. Sec 10.7, p. 307-310.

Whitaker, S. "Forced convection heat transfer correlations for flow in pipes, past flat plates, single cylinders, single spheres, and for flow in packed beds and tube bundles," AIChE Journal 18(2) 361-371, 1972.
https://doi.org/10.1002/aic.690180219

Zhang A, Li Y. Thermal Conductivity of Aluminum Alloys-A Review. Materials (Basel). 2023 Apr 8;16(8):2972.
https://doi.org/10.3390/ma16082972

Penetration Depth with Oscillatory Forcing

Materials:

1. Petri dish
2. Axle mounting
3. Cam for converting rotation to oscillation
4. Glycerin and water
5. Vertical stirring motor
6. 25ml syringe

The penetration depth of of an oscillating surface forcing is an important problem in heat transfer: the penetration depth of cold due to seasonal forcing determines required pipe depths to avoid freezing, for example. Heat transfer is difficult to visualize, however the problem is mathematically identical to unidirectional fluid flow. In this demonstration the penetration depth resulting from oscillatory motion is visualized, identical to the equivalent heat transfer problem.

This demonstration requires a bit of construction, as it is necessary to convert the rotation provided by a vertical stirring motor into oscillatory motion. This is done using the simple cam depicted below. A base plate is constructed with a central, short peg (a cut off aluminum nail, in this case). A thick disk (wood in my case) with a central hole is placed over the peg, and the petri dish is secured to the disk using carpet tape. A long bracket with holes is pinned to the edge of the disc with a screw. A second, much shorter bracket is attached to the end of a rod which can be chucked into the stirring motor, and the two brackets are pinned together (note: this connection must be free to rotate). If everything is put together correctly, when the rod is rotated by the stirring motor the disk holding the petri dish will be rotated back and forth with a frequency equal to the rotational frequency of the motor. The cam tends to "walk", so it it is necessary to firmly clamp the base to the stand holding the stirring motor. The stirring motor likewise needs to be firmly braced for smooth operation.

In operation, a known quantity of a glycerin/water solution is injected into the petri dish, resulting in a known depth of fluid. Starting with a small depth, it is shown that a small dot (a bit of paper punch out works well) floating on the surface of the fluid moves in phase and with the same amplitude as a dot marked underneath the fluid on the petri dish. As more fluid is added with the syringe, however, the floating dot experiences both a phase lag and decrease in amplitude. The amplitude further decreases if the rotational speed of the stirring motor increases, however in general the demonstration works best at low rotational speeds.

Both the heat transfer and unidirectional fluid flow problems are mathematically identical and are approached in the same way. If we impose an oscillating temperature at z = 0 of $T|_{z=0} = \Delta T cos(\omega t)$, and a "no flux" boundary condition at z = h, the temperature distribution is governed by the unsteady conduction equation:

$$\frac{\partial T}{\partial t} = \alpha \frac{\partial^2 T}{\partial z^2} \;\; ; \;\; T|_{z=0} = \Delta T cos(\omega t) \;\; ; \;\; \left(\frac{\partial T}{\partial z}\right)|_{z=h} = 0$$

where α is the thermal diffusivity. It is usual to define dimensionless quantities:

$$T^* = T/\Delta T \;\; ; \;\; t^* = \omega t \;\; ; \;\; z^* = z/\delta = z/(\alpha/\omega)^{1/2}$$

The dimensionless thickness of the layer is $\beta = h/(\alpha/\omega)^{1/2}$ which, for the corresponding fluid flow problem, is known as the Womersley number. The quantity $\delta = (\alpha/\omega)^{1/2}$ is the penetration depth for oscillation at angular frequency ω. The dimensionless problem becomes:

$$\frac{\partial T^*}{\partial t^*} = \frac{\partial^2 T^*}{\partial z^{*2}} \;\; ; \;\; T^*|_{z^*=0} = cos(t^*) \;\; ; \;\; \left(\frac{\partial T^*}{\partial z^*}\right)|_{z^*=\beta} = 0$$

These sorts of linear oscillatory problems are solved via analytic continuation into the complex plane. If we define a new problem with the same differential equation, but with the complex boundary condition $\hat{T}\,|_{z^*=0} = e^{it^*}$ then T* is just the real part of $\hat{T}$. Because it is linear, the solution to $\hat{T}$ is just

$$\hat{T} = e^{it} f(z^*)$$

where the spatial part obeys the ordinary differential equation:

$$\frac{d^2 f}{dz^{*2}} = if \;\; ; \;\; f(0) = 1 \;\; ; \;\; \left(\frac{df}{dz^*}\right)|_{z^*=\beta} = 0$$

This problem is very easy to solve for the unbounded system (large β). In that case, f is just the decaying exponential:

$$f = e^{-\sqrt{i}z^*}$$

and the complete solution for T* is

$$T^* = e^{-z^*/\sqrt{2}}\, cos\left(t^* - \frac{z^*}{\sqrt{2}}\right)$$

Thus, the temperature wave decays away from the oscillating boundary exponentially and experiences a phase lag as well. This solution determines the soil depth at which pipes could freeze in the winter, or alternatively the depth at which permafrost could melt in the summer. The required burial depth is thus a function of the yearly average temperature, the summer/winter average monthly temperature variation (shorter time scales do not matter as they decay away faster) and the thermal diffusivity of the local soil.

For the demonstration it is necessary to impose the boundary condition at β rather than at infinity. This yields the more complex solution in terms of hyperbolics:

$$\hat{T} = e^{it^*}\left(cosh\left(\sqrt{i}z^*\right) - \frac{sinh\left(\sqrt{i}\beta\right)}{cosh\left(\sqrt{i}\beta\right)} sinh\left(\sqrt{i}z^*\right)\right)$$

The temperature oscillation at the upper surface is somewhat simpler:

$$\hat{T}\,|_{z^*=\beta} = \frac{e^{it^*}}{cosh\left(\sqrt{i}\beta\right)}$$

which has a dimensionless amplitude:

$$Amplitude = \left| \frac{1}{cosh\left(\sqrt{i}\beta\right)} \right| = \frac{2\left(cos^2\left(\frac{\beta}{\sqrt{2}}\right) + sinh^2\left(\frac{\beta}{\sqrt{2}}\right)\right)^{1/2}}{cos\left(\sqrt{2}\beta\right) + cosh\left(\sqrt{2}\beta\right)}$$

Interestingly, this decays more slowly than the unbounded solution evaluated at $z^* = \beta$ for small β, reaches a value of 0.5 for $\beta = 2.04$, and asymptotically approaches twice the unbounded solution for $\beta > 3$. The discrepancy is due to the effect of the "extra material" for $z^* > \beta$ in the unbounded case decreasing the amplitude of oscillation.

The motion of the upper surface in the demonstration is identical to the temperature calculated above, so it is useful to look at values of β from 1 to 3. For $\beta = 1$ the amplitude of oscillation is 92.6% of the petri dish (virtually the same), while at $\beta = 2$ it rapidly decreases to 51.5%. For $\beta = 3$ it further decreases by a factor of two to 24.1%. For my stirrer with minimum rotational speed of 70RPM, a fluid with kinematic viscosity of 1 cm^2/s (84 % by volume glycerin) yields a penetration depth of 0.37 cm. Thus, fluid volume is injected to increase depth in stages by this amount.

In an undergraduate class the unbounded penetration depth process is derived and compared to literature values for required pipe depths in different climates. I also bring up the interesting problem with the Trans-Alaska Pipeline, where increases in average temperatures have led to the permafrost melting around the pipeline support foundations in some elevated sections over frozen peat bogs. This was actually solved by chilling the ground around the pillar foundations to locally reduce the average temperature.

References:

Bird, Stewart & Lightfoot, *Transport Phenomena*, rev 2nd ed., Wiley, 2007. Ex 12.1-3, p. 379.

David Hasemyer, "Trans-Alaska pipeline under threat from thawing permafrost," July 14, 2021. Web. https://www.hcn.org/articles/climate-change-trans-alaska-pipeline-under-threat-from-thawing-permafrost/

Stokes Flow Reversibility

Materials:

1. Large cylindrical jar with concave bottom and plastic lid
2. Straight sided wine bottle with concave bottom
3. 10 ml syringe
4. Tygon tubing
5. Corn syrup
6. Food coloring

This is essentially identical to the classic G. I. Taylor demonstration of Stokes flow reversibility at low Reynolds numbers. This video, as well as other sources available on the web, are referenced below. A Couette cell is prepared by machining a hole in the plastic lid to the jar of precisely the diameter of the wine bottle. The concave bottom of the wine bottle (filled with water and corked off) matches up with the concave bottom of the jar, so that between the bottom and the top the wine bottle is precisely centered in the gap. The jar is filled with corn syrup or glycerin (corn syrup is more viscous, but does tend to dry out on the threads of the lid, making removal difficult), and the same fluid (dyed) is loaded into the syringe. Attaching the tygon tubing to the tip of the syringe, a large drop is injected into the Couette gap (avoiding introducing air bubbles). When the wine bottle is rotated the drop is sheared into a band because portions are on different streamlines and thus move with different angular velocities. When the bottle is rotated back again, however, the un-deformed drop reappears. The starting point of the bottle can be marked with a bit of black tape aligned with a mark on the centering lid. About three bottle rotations are sufficient to smear out the drop before reversal. The assembly can be passed around the class for students to try it out, however the drop eventually loses its coherence.

References:

David Pine Hydrodynamic Reversibility web page
https://physics.nyu.edu/pine/hydrodynamic_reversibility.html

Complete G.I.Taylor Low Reynolds Numbers film:
https://youtu.be/51-6QCJTAjU?si=RlC-ywmHfWEm1bDw

Stokes Flow Reversibility part of Taylor film:
https://youtu.be/rA6T83FKuE8?si=EG7JUj0JtxjT2YoQ

All National Committee for Fluid Mechanics Films
https://web.mit.edu/hml/ncfmf.html

Moffatt Eddies

Materials:

1. Square tray with sharp internal corners
2. 3” plexiglas disk with mounting rod
3. Low speed stirring motor with chuck
4. Clamp
5. Corn syrup
6. Food coloring
7. 1 ml syringe with needle

One of the more mathematically advanced topics covered in undergraduate transport is the stream function ψ. While generally useful for any two-dimensional incompressible flow (e.g., boundary layer flow past a flat plate), it is particularly interesting for 2-D Stokes flows. That is because it is governed by the biharmonic equation, and (for certain geometries) has separable solutions. These problems are described in detail in Leal (2007), however the solution to problems in “corners” is particularly straightforward, as the stream function is separable in polar coordinates.

We may define ψ such that:

$$u_r = -\frac{1}{r}\frac{\partial \psi}{\partial \theta} \ ; \ u_\theta = \frac{\partial \psi}{\partial r} \ ; \ \nabla^4 \psi = 0$$

The separable solution in cylindrical coordinates is of the form:

$$\psi = \sum_{n=1}^{\infty} \psi_n = \sum_{n=1}^{\infty} r^{\lambda_n} f_{\lambda_n}(\theta)$$

In general, the radial dependence r^λ is forced by the boundary conditions, and is usually $\lambda = 1$ (the Taylor wiper problem), 2 (a collapsing wedge), or 0 (a draining trough). These problems lead to special cases for the function $f_\lambda(\theta)$, and are quite easy to solve to yield exact solutions. Moffatt eddies, however, occur for swirling 2-D flow in a corner with homogeneous boundary conditions. For such a swirling flow the velocity u_θ is symmetric in θ, thus the solution for the stream function is also symmetric in θ and becomes (by solving the biharmonic equation):

$$\psi_n = r^{\lambda_n}\left(A_n cos(\lambda_n \theta) + C_n cos((\lambda_n - 2)\theta)\right)$$

Sufficiently close to the corner, the higher eigenvalues decay away and we are left with just the λ_1 term. The homogeneous no-slip boundary conditions on the sides of the corner at $\theta = \pm\,\alpha$ require that the determinant of a 2x2 matrix vanish for a non-trivial solution to occur:

$$det\begin{vmatrix} cos\lambda_1\alpha & cos(\lambda_1 - 2)\alpha \\ \lambda_1 sin\lambda_1\alpha & (\lambda_1 - 2)sin(\lambda_1 - 2)\alpha \end{vmatrix} = 0$$

This can be rearranged to yield:

$$-(\lambda_1 - 1)sin2\alpha = sin[2(\lambda_1 - 1)\alpha]$$

The key result shown by Moffatt was that for values $2\alpha < 146°$ the solution for λ_1 must be complex. That means that if we take

$$\lambda_1 = 1 + p + i\ q$$

where p and q are real, the radial dependence is:

$$\psi \sim r^{\lambda_1} = r^{1+p}\ r^{i\ q} = r^{1+p}\ e^{iq\ ln(r)} = r^{1+p}\ \left(cos(q\ ln(r)) + i\ sin(q\ ln(r))\right)$$

which, since the log of r blows up as r -> 0, yields a periodic function with an infinite sequence of zeros. Since the stream function is also zero on the walls, this means that there is an infinite sequence of dividing streamlines corresponding to the boundaries of counter-rotating eddies for any viscous swirling flow as you move into the corner. As a practical matter, this is the explanation for why it is so difficult to clean out pockets or grooves at a surface: the external flow never gets into the corner to sweep it out.

The existence of Moffatt eddies is demonstrated by clamping a shallow, sharp cornered box to the base of the stirring motor ring stand. A shallow layer of corn syrup is poured into the box, and the plexiglas disk is chucked up to the stirring motor and lowered into the box until it is nearly in contact with the flat bottom. It is important not to get the disk too close to the corner as this will cause distortion of the surface of the corn syrup. Once everything has been set, you dye a bit of corn syrup and draw a thin line of dye between the corner and disk. This is done most conveniently by loading a 1ml syringe with dyed corn syrup and attaching a disposable needle. The dye line is injected below the surface of the corn syrup (it may be necessary to hold the needle onto the syringe to keep it from popping off due to the high viscosity). The stirring motor is turned on, and the deformation of the dye line is observed. The bounding streamline of the corner eddy is observable as a dyed line. Other lines can be drawn between the disk and the side wall as desired yielding a variety of patterns such as is depicted below where the recirculating corner eddy is clearly observable.

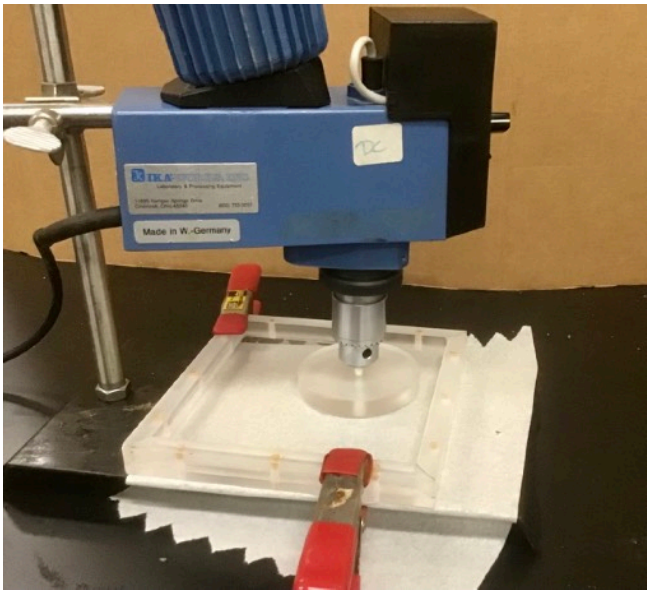

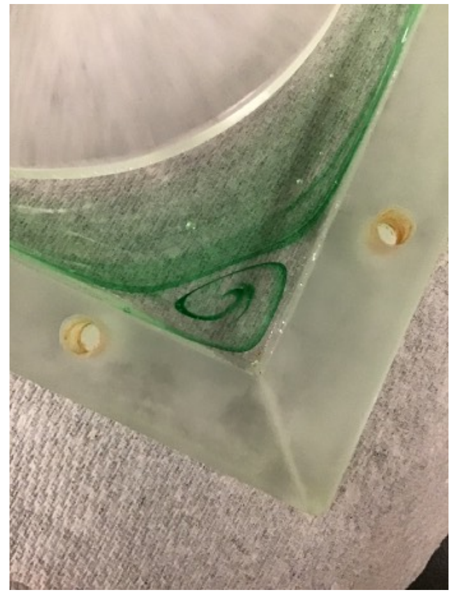

References:

Leal LG. Advanced Transport Phenomena: Fluid Mechanics and Convective Transport Processes. Cambridge University Press; 2007. p. 451-458

Taylor GI. "Deposition of a viscous fluid on a plane surface." Journal of Fluid Mechanics. 1960;9(2):218-224.
https://doi.org/10.1017/S0022112060001055

Moffatt HK. "Viscous and resistive eddies near a sharp corner." Journal of Fluid Mechanics. 1964;18(1):1-18.
https://doi.org/10.1017/S0022112064000015

Sedimentation of a Body of Revolution at Low Re

Materials:

1. 2 liter beaker (or comparable vessel with square cross-section)
2. Sheet with concentric rings
3. Small washers
4. Spatula and tweezers
5. 4 pints of corn syrup
6. Stopwatch
7. Flat plastic ruler with clips

This demonstration relies on the linearity of the Stokes flow equations to relate the sedimentation velocity of a body of revolution to its orientation. By measuring the time necessary for the object (in this case a small washer) to fall a fixed distance when both edge on and flat side on it is possible to calculate the sedimentation trajectory for arbitrary orientation. This is confirmed by dropping the washer at a 45° angle and determining its lateral drift. It is helpful to have a white background behind the beaker to improve visualization of the lateral motion, and the sheet with concentric rings below the beaker to measure the final lateral displacement.

The demonstration is closely related to that done in the classic film by G I Taylor, however here we use a washer rather than a rod and do the analysis using index notation rather than trigonometry and geometry. Two lines are drawn on the beaker about 8 cm apart (the distance is immaterial to the calculations), and students are asked to determine the times T_A and T_B taken for the washer to travel between the lines when edge on (director perpendicular to gravity) and flat side on (director parallel to gravity) respectively. Note that for an oblate object such as a washer $T_A < T_B$. The general mobility tensor as a function of the director p_i is given by:

$$u_i = \left(\lambda_1 \delta_{ij} + \lambda_2 p_i p_j\right) F_j$$

The "case A" selects out the isotropic part (λ_1) while the "case B" has contributions from both. Thus, the constants λ_1 and λ_2 are given by:

$$\lambda_1 = \frac{H}{T_A F} \quad ; \quad \lambda_2 = \frac{H}{T_B F} - \frac{H}{T_A F}$$

Now consider the trajectory of the washer when dropped at an angle θ (θ = 0 is flat-side on in this case). The velocity in the direction of gravity (taken to be u_1) is:

$$u_1 = \frac{H}{T_A} + \left(\frac{H}{T_B} - \frac{H}{T_A}\right) cos^2(\theta)$$

while the velocity in the transverse direction (e.g., u_2) is:

$$u_2 = \left(\frac{H}{T_B} - \frac{H}{T_A}\right) cos(\theta) sin(\theta)$$

The sideways drift after falling a height H is simply:

$$\Delta x_2 = H\frac{u_2}{u_1} = H\frac{\left(\frac{T_A}{T_B} - 1\right) cos(\theta) sin(\theta)}{1 + \left(\frac{T_A}{T_B} - 1\right) cos^2(\theta)}$$

This can be compared to the results of the demonstration, although dropping it at a 45° angle is a bit challenging!

While the above linear relationship is valid for any symmetric body of revolution, the problem has been studied quite extensively for specific shapes over the years. The mobilities for ellipsoids were solved by Oberbeck in the 19th century, and the relationship for general slender bodies (and specifically cylinders) was obtained by Batchelor over 50 years ago. It turns out that the maximum ratio for a long, slender body (both prolate spheroid and cylinder) is 2 (e.g., $T_A/T_B < 2$), while that for a thin disk is 1.5 (e.g., $T_A/T_B > 1/1.5$). The ratio for a washer (if sufficiently thin) is similar to this latter value, so it can be compared to the results of the experiment. The paper by Oberbeck is in German, so other more accessible citing references are also provided below.

An interesting extension of this demonstration is to look at the effect of boundaries on rotation (e.g., Yang & Leal, 1983; Russel, et al., 1977). For a body of revolution with fore-and-aft symmetry such as a washer, linearity shows that the object does not rotate when falling through an unbounded viscous liquid. This is observed for the washer dropped at an angle at the center of the beaker, for example. In the vicinity of a lateral boundary, however, the object does rotate due to the wall reflection of the disturbance velocity produced by the falling particle. Interestingly, when dropped at an appropriate grazing angle near the walls of the beaker, the object will drift toward the wall, “swoop”, and then after rotation will drift away. If the object is dropped at a sharper angle it will come into contact with the wall, and then “flip” and drift away. Using a spatula the washers dropped in the earlier phases of the demonstration can be scraped up and repositioned for demonstration of this effect. If a cylindrical beaker is used, this motion is most clearly observed from above due to refractive index issues near the curved wall, however a better side view can be obtained if you have a vessel with square or rectangular cross-section. The side view can also be used if a plate is inserted at the center of a beaker to provide the planar surface, although there is some distortion. The plate can be kept vertical using a couple of clips, allowing even a flat plastic ruler to be used as the planar surface.


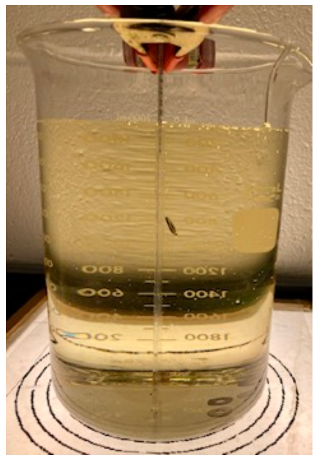


A corollary to this effect is that if a body of revolution is dropped along a plane slightly inclined from vertical, the combination of drift along and normal to the plane will cause it to acquire both a steady orientation and separation distance by the same mechanism. The small plane incline angle should exceed the maximum trajectory angle for the particle (11.5° for a disk, 19.5° for a long rod), so that no matter the starting separation or initial orientation it will eventually reach the vicinity of the plane and equilibrium separation and orientation (but if too far away at the start it may not get there fast enough before hitting the bottom of the beaker). The inclined plane can be produced by either just tilting the beaker, or (if an inserted plane is used) adjusting the clip to keep the plane at the desired angle. The motion is most easily seen by starting the washer off on the surface of the plane. At first it moves slowly due to lubrication resistance, but as it "swoops away" it accelerates, acquiring its steady angle and separation. At equilibrium the director of the particle lies in the plane of gravity and the plane normal regardless of starting orientation. The same is observed for prolate objects: in our laboratory we have taken advantage of this trick to orient O(600μm) diameter slightly prolate spheroids so that their aspect ratios could be accurately determined using a camera. Such small particles tend not to "lay flat" when dry making their eccentricity difficult to measure otherwise.

References:

Complete G.I.Taylor Low Reynolds Numbers film:
https://youtu.be/51-6QCJTAjU?si=RlC-ywmHfWEm1bDw

Oberbeck, A.. "Ueber stationäre Flüssigkeitsbewegungen mit Berücksichtigung der inneren Reibung." Journal für die reine und angewandte Mathematik, vol. 1876, no. 81, 1876, pp. 62-80.
https://doi.org/10.1515/crll.1876.81.62

Batchelor GK. "Slender-body theory for particles of arbitrary cross-section in Stokes flow." Journal of Fluid Mechanics. 1970;44(3):419-440.
https://doi.org/10.1017/S002211207000191X

Payne LE, Pell WH. "The Stokes flow problem for a class of axially symmetric bodies." Journal of Fluid Mechanics. 1960;7(4):529-549.
https://doi.org/10.1017/S002211206000027X

Trahan, J. F. "Stokes Drag on a Thin Circular Disk Moving Edgewise Midway Between Parallel Plane Boundaries." ASME. J. Fluids Eng. July 2006; 128(4): 887–889.
https://doi.org/10.1115/1.2201650

Yang S-M, Leal LG. "Particle motion in Stokes flow near a plane fluid-fluid interface. Part 1. Slender body in a quiescent fluid." Journal of Fluid Mechanics. 1983;136:393-421.
https://doi.org/10.1017/S0022112083002207

Russel WB, Hinch EJ, Leal LG, Tieffenbruck G. "Rods falling near a vertical wall." Journal of Fluid Mechanics. 1977;83(2):273-287.
https://doi.org/10.1017/S0022112077001190

Zarraga, Isidro E., and David T. Leighton Jr. "Measurement of an unexpectedly large shear-induced self-diffusivity in a dilute suspension of spheres." Physics of Fluids 14.7 (2002): 2194-2201.
https://doi.org/10.1063/1.1483304

Jeffery Orbits

Materials:

1. Large cylindrical jar with concave bottom and plastic lid
2. Straight sided wine bottle with concave bottom
3. Corn syrup
4. A ¼" acrylic (or PVC) sphere
5. Approximately 1cm long length of insulated bell wire, marked at one end
6. Paper tape measure
7. Calipers

A fundamental result in low Reynolds number hydrodynamics is the motion of a body of revolution in a shear flow. As was demonstrated by Jeffery (1922) the dynamics of such a particle can be described for arbitrary linear shear flows by a single scalar quantity, now known as the Jeffery Orbit constant. This is key, because it enables the description of the orientation distribution of (for example) a dilute suspension of fibers in any linear shear flow, as well as many other applications. The paper by Jeffery has been cited in excess of 5500 times.

To see how this works, consider a body of revolution with orientation specified by the director p_i. The particle is freely suspended in a linear shear flow specified by $u_j = A_{jk}x_k$. The particle will translate with the local velocity of the fluid, however the angular velocity Ω_i will be a function of the orientation and the shear tensor A_{jk}. From the linearity of the governing Stokes flow equations, the most general relationship is:

$$\Omega_i = B_{ijk}\, A_{jk}$$

Where B_{ijk} is a third order pseudotensor. There are four possible non-zero contributions to the tensor B_{ijk}:

$$\varepsilon_{ijk}, \quad p_i p_l \varepsilon_{ljk}, \quad \tfrac{1}{2}(p_j p_l \varepsilon_{ilk} - p_k p_l \varepsilon_{ilj}), \quad \tfrac{1}{2}(p_j p_l \varepsilon_{ilk} + p_k p_l \varepsilon_{ilj})$$

where ε_{ijk} is the third order alternating tensor. The first three of these are antisymmetric with respect to interchange of the indices j and k, while the last is the only symmetric contribution. Because of the double dot product with A_{jk}, the antisymmetric part of B_{ijk} acts only on the antisymmetric part of A_{jk}, and likewise the symmetric part of B_{ijk} selects out the symmetric part of A_{jk}. This is very useful, because for any linear shear flow tensor A_{jk} the anisotropic part is just the result of solid body rotation. Since any freely suspended object will rotate with the fluid, the antisymmetric contribution to B_{ijk} just reduces to the isotropic term with coefficient -½ (the terms which are a function of p_i can't contribute). Thus, the angular velocity reduces to:

$$\Omega_i = [-\tfrac{1}{2}\varepsilon_{ijk} + \tfrac{1}{2}\,\xi\,(p_j p_l \varepsilon_{ilk} + p_k p_l \varepsilon_{ilj})]\,A_{jk}$$

where ξ is the Jeffery's Orbit constant. The director evolution equation can be calculated from this angular velocity:

$$dp_i/dt = \varepsilon_{ijl}\,p_l\,\Omega_j = \varepsilon_{ijn} p_n\,[-\tfrac{1}{2}\varepsilon_{jkl} + \tfrac{1}{2}\,\xi\,(p_k p_m \varepsilon_{jml} + p_l p_m \varepsilon_{jmk})]\,A_{kl}$$

Using the identity $\varepsilon_{ijn}\,\varepsilon_{jkl} = \delta_{nk}\,\delta_{il} - \delta_{nl}\,\delta_{ik}$ the director evolution equation can also be expressed in terms of the symmetric and antisymmetric parts of the rate of strain tensor A_{ij}. If we let $E_{ij} = \tfrac{1}{2}(A_{ij}+A_{ji})$ and $W_{ij} = \tfrac{1}{2}(A_{ij}-A_{ji})$ then the director equation above reduces to:

$$dp_i/dt = W_{ij}\,p_j + \xi\,(E_{ij}\,p_j - E_{jk}\,p_i p_j p_k)$$

In a simple shear flow the dynamics are particularly straightforward. As demonstrated by Trevelyan and Mason (1951), a particle with large aspect ratio will spend most of its time with alignment close to the direction of fluid motion, and the dimensionless orbital period T^* is given by:

$$T^* = \frac{4\pi}{\sqrt{1-\xi^2}}$$

where T^* has been rendered dimensionless with respect to the shear rate. Note that this period is independent of any angle of the director out of the plane of shear. For an isotropic particle such as a sphere, $\xi = 0$, and thus the period is just $T^* = 4\pi$. If we measure the orbital period of a particle and normalize it with the orbital period of a sphere under the same conditions (e.g., $\hat{T} = T^*/4\pi$) then the Jeffery's Orbit constant is simply:

$$\xi = \left(1 - \frac{1}{\hat{T}^2}\right)^{1/2}$$

With knowledge of this quantity it is simple to predict the orientation distribution of a dilute suspension of particles with the same shape in *any* linear shear flow.

The orbit constant depends only on the shape of the object, however its calculation is very demanding mathematically. For a prolate spheroid it was shown by Jeffery to have a remarkably simple result:

$$\xi = \frac{r^{*2} - 1}{r^{*2} + 1}$$

where r* = a/b is the aspect ratio of the spheroid with major radius a and minor radius b. The dynamics of other shapes were studied in great detail by Bretherton (1962). For the specific case of a long cylinder (e.g., a fiber) there is no analytic solution. Cox (1971), however, showed via asymptotic analysis and comparison with experimental data that the orbit constant could be obtained from the Jeffery spheroid result by using an effective aspect ratio:

$$r_e = r^* \frac{1.24}{\left(ln\ r^*\right)^{1/2}}$$

where r* is the cylinder length/diameter ratio. The period of a cylinder normalized by that of a sphere in the same simple shear flow is thus:

$$\hat{T} = \frac{r_e^2 + 1}{2r_e}$$

In this demonstration the Couette device constructed for the Stokes reversibility demo is used. For corn syrup a short length of insulated bell wire is nearly neutrally buoyant. Examining its motion as the bottle is rotated reveals that the rotational velocity for such a large aspect ratio particle is not steady, but rather it spends most of its time aligned close to the direction of motion (theta direction in this case) as expected. It also rotates more slowly than a sphere in the same geometry, and always “flips” at the same point in the flow when the direction of rotation is reversed. The Jeffery orbit constant can be calculated by determining the ratio of the flipping strain for the rod to that of a marked sphere. This ratio can be determined by measuring the displacement of the inner cylinder using a paper tape measure which is attached to the wine bottle against a mark on the lid. It is important to place the sphere and the rod at the same radial location in the gap (mid point works best). This is because the shear rate varies significantly across the gap due to the finite cylinder diameter to gap width ratio (torque is preserved in Couette flow, so the shear rate varies as the inverse square of the radial position). An acrylic sphere will float in corn syrup (the density of PVC would be a closer match), however the free surface will not affect the rotational velocity of the sphere.

A quantitative comparison of the Jeffery Orbit constant or orbit period measured in this way to that calculated for a cylinder using the formula of Jeffery for ellipsoids and the modified aspect ratio proposed by Cox can be done (the aspect ratio of the rod is measured using calipers). For the device depicted below a rod with aspect ratio r^* = 1.4cm/0.157cm = 8.9 and equivalent ellipsoidal ratio r_e = 7.5 “flipped" after rotating the bottle 60cm, while the sphere “flipped” (half a period) after 15cm. This ratio of 4 is actually quite close to the expected ratio of 3.8 for this aspect ratio rod, although discrepancies are likely due to the finite gap width (e.g., the flow is not precisely a simple shear flow), as well as the proximity of the walls to the sphere and rod affecting the rotation.

After projecting the experiment for the whole class, the Couette cell can be passed around for students to try it themselves and observe it more closely.

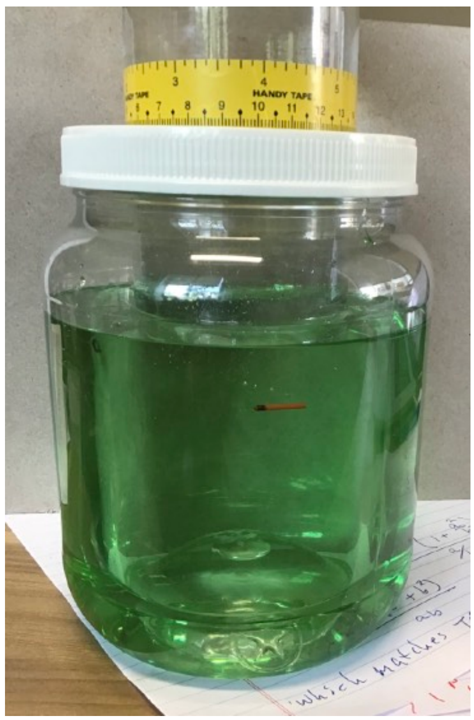

References:

Jeffery, G. B., "The motion of ellipsoidal particles immersed in a viscous fluid." Proc. R. Soc. Lond. A, November 1922; 102:161–179
https://doi.org/10.1098/rspa.1922.0078

Bretherton FP. The motion of rigid particles in a shear flow at low Reynolds number. Journal of Fluid Mechanics. 1962; 14(2):284-304.
https://doi.org/10.1017/S002211206200124X

B.J Trevelyan, S.G Mason, "Particle motions in sheared suspensions. I. Rotations," Journal of Colloid Science.1951; 6(4): 354-367
https://doi.org/10.1016/0095-8522(51)90005-0

Cox RG. The motion of long slender bodies in a viscous fluid. Part 2. Shear flow. Journal of Fluid Mechanics. 1971; 45(4):625-657. https://doi.org/10.1017/S0022112071000259

Afterword

Good classroom demonstrations have a way of turning abstract concepts into moments of insight and I hope that this collection has sparked some ideas for your own teaching.

Over the years, far more demonstrations have been used in my classroom than the three dozen included here, with many developed and led by students themselves.

In particular, recurring student favorites have included shear-thickening cornstarch and water mixtures—used to mold Oobleck by hand, create rudimentary "armor," or make it "dance" atop a speaker—as well as classics like the vacuum cannon, the Kaye effect, and the Cartesian diver.

Rather than students feeling limited by examples already tested, however, I encourage exploration: new demonstrations are often just a clever twist or novel combination away.

If your students are stuck for ideas, a quick consultation with ChatGPT or other AI tools can be surprisingly fruitful—although it's worth noting that an AI's first explanations of even simple effects are often incorrect, which can lead to some interesting detours.

Still, these tools serve as valuable starting points in the creative process, helping to shape and refine demonstration concepts.

Hopefully your own students will take inspiration and curiosity from these examples and perhaps surprise you with innovations of their own.

(With apologies to Bird, et al., and acknowledgement of an AI assist)